Development and Applications of Enhanced Multiplexing to Better Understand Aging, Infection, and Alzheimer's Disease

by

Christina Dee King

B.S. Chemistry, University of Houston, 2012

Submitted to the Graduate Faculty of the

Dietrich School of Arts and Sciences in partial fulfillment

of the requirements for the degree of

Doctor of Philosophy

University of Pittsburgh

2018

UNIVERSITY OF PITTSBURGH

Dietrich School of Arts and Sciences

This dissertation was presented

by

Christina Dee King

It was defended on

November 16, 2018

and approved by

Dr. Renã A. S. Robinson, Associate Professor, Department of Chemistry, Vanderbilt University, Adjunct Associate Professor, Department of Chemistry, University of Pittsburgh

Dr. Kabirul Islam, Assistant Professor, Department of Chemistry

Dr. Nathan Yates, Associate Professor, Departments of Cell Biology and Chemistry

Co-Advisor: Dr. Stephen G. Weber, Professor, Department of Chemistry

Dissertation Co-Advisor: Dr. Renã A. S. Robinson, Associate Professor, Department of Chemistry, Vanderbilt University, Adjunct Associate Professor, Department of Chemistry, University of Pittsburgh

Development and Applications of Enhanced Multiplexing to Better Understand Aging, Infection, and Alzheimer's Disease

Christina Dee King, Ph.D.

University of Pittsburgh, 2018

Proteomics is the wide – scale study of proteins, in which the proteome of an organism is studied. Proteomics experiments obtain both qualitative and quantitative information by using a combination of analytical techniques including liquid chromatography, ion mobility, and mass spectrometry (MS). In quantitative experiments, relative protein amounts are determined to gain a better understanding of biological problems related to disease-state, kinetic changes, and effects of pharmaceutical products. In many cases, multiple samples (e.g. 10s to 100s) are analyzed to obtain statistically – significant results, which requires ample time (on the order of several days to weeks). To reduce sample analysis time and potential experimental error, multiplexing strategies have been developed. Samples are labeled metabolically, enzymatically, or chemically during sample preparation, pooled together, and analyzed simultaneously in the mass spectrometer.

In this body of work, multiplexing strategies have been applied to study aging and response to infection in *C. elegans* and the involvement of the periphery in Alzheimer's disease. In addition, the development of analyzing multiplexed samples on Orbitrap MS platforms will be presented. These developments and applications contribute to science by providing insight to two conditions that affect the aging population.

TABLE OF CONTENTS

TABLE OF CONTENTS V

LIST OF TABLES XI

LIST OF FIGURES XII

ACKNOWLEDGEMENTS XV

1.0 INTRODUCTION 1

1.1 AGING AND IMMUNITY 1

1.1.1 Studying Aging and Host-Response to Infection in Model Organisms 2

1.1.2 Aging and Alzheimer's Disease 4

1.2 PROTEOMICS 5

1.2.1 Bottom-up Proteomics 6

1.2.2 Quantitative Proteomics 11

1.3 ENHANCED MULTIPLEXING TECHNIQUES 16

1.3.1 Combined Precursor Isotopic Labeling and Isobaric Tagging (cPILOT) 16

1.4 OVERVIEW OF DISSERTATION 20

2.0 PROTEOMICS ANALYSIS OF VIRULENCE-RELATED FACTORS IN YOUNG AND AGING C. *ELEGANS* EXPOSED TO *PSEUDOMONAS AERUGINOSA* PA01- PART 1 21

2.1 INTRODUCTION 21

2.2 EXPERIMENTAL PROCEDURES 24
2.2.1 Nematode and Bacterial Culture 24
2.2.2 Pathogenicity Assays 25
2.2.3 Sample Preparation for Proteomics Analysis 26
2.2.4 Protein Extraction 26
2.2.5 Protein Digestion 27
2.2.6 TMT Labeling 27
2.2.7 Dimethylation Labeling 28
2.2.8 Strong Cation Exchange (SCX) Fractionation 28
2.2.9 LC – MS Analyses 29
2.2.10 Data Analyses 30
2.2.11 Measurement of Protein Carbonylation Levels 32
2.3 RESULTS 33
2.3.1 C. elegans Resilience to P. aeruginosa PA01 Declines with Increasing Age 33
2.3.2 Mapping the C. elegans Proteome upon P. aeruginosa PA01 Exposure 35
2.3.3 Dimethylation Labeling Verifies TMT^6-based Identification of Proteins Whose Levels are Altered in PA01 Infection 38
2.3.4 Major Biological Pathways Influenced in C. elegans Proteome after Exposure to P. aeruginosa PA01 42
2.3.5 PA01 Exposure Elevated Protein Carbonylation in C. elegans 46
2.3.6 unc-60 Mutants Have Reduced Lifespan 48

2.3.7 Comparing C. elegans Host Response when Exposed to P. aeruginosa PA01 and Other Pathogens 50
2.4 DISCUSSION 53
2.4.1 Pathogen-induced Proteomic Changes in Day 1 and Day 5 Adults are Overlapping but Distinct 54
2.4.2 Mutations in unc-60 Reduce Lifespan 57
2.4.3 P. aeruginosa PA01 Exposure Causes Elevated Carbonylation of Worm Proteome 57
2.5 CONCLUSIONS 58
3.0 PROTEOMICS ANALYSIS OF VIRULENCE-RELATED FACTORS IN YOUNG AND AGING C. *ELEGANS* EXPOSED TO *PSEUDOMONAS AERUGINOSA* PA01- PART 2……...……...60
3.1 INTRODUCTION 60
3.2 EXPERIMENTAL PROCEDURES 61
3.2.1 Protein Digestion 61
3.2.2 TMT Labeling 62
3.2.3 Offline SCX Fractionation 62
3.2.4 LC – MS Analyses 63
3.2.5 Data Analyses 64
3.3 RESULTS AND DISCUSSION 64
3.4 CONCLUSIONS 68
4.0 EVALUATING CPILOT PERFORMANCE OF ORBITRAP INSTRUMENTS TO STUDY THE PERIPHERAL PROTEOME OF ALZHEIMER'S DISEASE 70

4.1 INTRODUCTION 70
4.2 EXPERIMENTAL PROCEDURES 74
4.2.1 Animal Husbandry and Ethical Statement 74
4.2.2 Tissue Homogenization, Protein Extraction, and Digestion 74
4.2.3 cPILOT Labeling 75
4.2.4 Offline SCX Fractionation 77
4.2.5 Liquid Chromatography and Mass Spectrometry Analyses 77
4.2.6 Data Analysis 80
4.3 RESULTS 81
4.3.1 Evaluation of LC Gradients and Precursor Isolation Windows (Experiments 1 and 2) 86
4.3.2 Dynamic Exclusion (Experiment 3) 92
4.3.3 Targeted Mass Analyses (Experiment 4) 94
4.3.4 Synchronous Precursor Selection (Experiment 5) 98
4.3.5 Comparisons of Samples Analyzed by Velos and Fusion Lumos Instrumentation 100
4.3.6 Differentially – Expressed Proteins in AD Brain, Heart, and Liver Tissues 106
4.4 DISCUSSION 110
4.4.1 cPILOT Method Optimization Experiments (Fusion Lumos) 110
4.4.2 AD Pathogenesis from Brain, Heart, and Liver Tissues 111
4.5 CONCLUSIONS 114

5.0 PROTEOMICS ANALYSIS OF HUMAN POSTMORTEM TISSUES IN ALZHEIMER'S DISEASE 115
5.1 INTRODUCTION 115
5.2 EXPERIMENTAL PROCEDURES 117
5.2.1 Tissue Harvesting and Ethical Statement 117
5.2.2 Tissue Homogenization, Protein Extraction, and Digestion 119
5.2.3 cPILOT Labeling 119
5.2.4 Offline SCX Fractionation 120
5.2.5 Liquid Chromatography and Mass Spectrometry Analyses 120
5.2.6 Data Analysis 122
5.3 RESULTS 123
5.3.1 Hierarchical Clustering Patterns of Quantified Brain, Heart, and Liver Tissues 126
5.3.2 Canonical pathways Associated with Differentially – Expressed Proteins 133
5.4 DISCUSSION 136
5.4.1 Protein Clustering Across Brain, Heart, and Liver Tissues 137
5.4.2 Differentially – Expressed Post-Mortem Brain and Peripheral Tissues 138
5.5 CONCLUSIONS 140
6.0 SUMMARY AND FUTURE DIRECTIONS 141
6.1 SUMMARY 141
6.2 FUTURE DIRECTIONS 142
APPENDIX A 148

APPENDIX B 151

APPENDIX C 152

APPENDIX D 153

REFERENCES 154

LIST OF TABLES

Table 2.1 Proteins Whose Levels are Altered in *C. elegans* upon *P. aeruginosa* PA01 Exposure 45

Table 4.1 Experimental Scheme of cPILOT 76

Table 4.2 Effects of Targeted Analyses on the Number of PSMs Quantified (Experiment 4). ... 96

Table 4.3 Effects of SPS Parameters on the Number of Protein IDs (Experiment 5). 99

Table 4.4 Effects of SCX Fractionation on the Number of Proteins and PSMs Identified. 101

Table 4.5 Differentially – Expressed Proteins in the Brain, Heart, and/or Liver. 108

Table 5.1 AD and CN Subject Clinical and Neuropathological Data. 118

Table 5.2 Experimental Scheme of cPILOT 120

Table 5.3 Differentially – Expressed Proteins in the Brain, Heart, and/or Liver. 132

Table 6.1 Protein and Peptide Results of a FPOP-cPILOT Experiment. 144

Appendix A Table A2.1 Pathogenicity Assays 150

LIST OF FIGURES

Figure 1.1 Bottom-up Proteomics Workflow 8

Figure 1.2 Potential Fragmentation Positions of Peptides 10

Figure 1.3 TMT Chemical Reaction 14

Figure 1.4 TMT^6-plex Labeling Strategy 14

Figure 1.5 Example Peptide after cPILOT Labeling 18

Figure 2.1 Survival Curves of Exposed and Control *C. elegans* 34

Figure 2.2 Proteomics Experiments and Mass Spectra of *C. elegans* Exposed to *P. aeruginosa* PA01 37

Figure 2.3 Proteomics Workflow using Dimethylation Labeling. 39

Figure 2.4 Comparisons of Proteins from TMT^6 and Dimethylated-Labeled Peptides. 41

Figure 2.5 Interactions of Statistically – Significant proteins in D1 *C. elegans* Exposed to *P. aeruginosa* PA01 43

Figure 2.6 Interactions of Statistically – Significant proteins in D5 *C. elegans* Exposed to *P. aeruginosa* PA01 44

Figure 2.7 Comparisons of Protein Carbonylation (PCO) Levels in Day 1 and Day 5 Adult *C. elegans* Exposed to *P. aeruginosa* PA01 and Aged – Matched Controls. 47

Figure 2.8 Survival Curves of Day 1 Adult *unc-60* Mutants and Control *C. elegans* 49

Figure 2.9 Comparison of Differentially – Expressed genes/proteins from this Study to other Pathogenicity Studies. 51

Figure 2.10 Scheme of Day 1 and Day 5 *C. elegans*' Response to *P. aeruginosa* PA01 Exposure. 56

Figure 3.1 Experimental Workflow of Young and Aging *C. elegans* Exposed to *P. aeruginosa* PA01. 66

Figure 3.2 a) Protein and b) Peptide Overlap across Orbitrap Velos and Orbitrap Elite Platforms. 66

Figure 4.1 Experimental Workflow of AD and WT Brain, Heart, and Liver Tissues. 83

Figure 4.2 Comparison of Reporter Ion Spectra from a) and c) Light and b) and d) Heavy Peptides Labeled by cPILOT Acquired on a) and b) an Orbitrap Fusion Lumos or c) and d) a LTQ Orbitrap Velos MS Platforms 85

Figure 4.3 Comparison of a) Protein and b) Peptide Identification, and c) Quantified Spectra at 105, 120, and 150 min 88

Figure 4.4 Effects of Dynamic Exclusion Times 0, 10, 20 s on Protein Identifications from a) Light and b) Heavy Dimethylated Peptides. 93

Figure 4.5 Comparison of a) and b) Protein and c) and d) Peptide Identifications of Light and b) Heavy Dimethylated Peptides using Targeted Analyses Methods. 95

Figure 4.6 Identification of a) Protein and b) Peptide Groups Identified Across Three MS Experiments. 102

Figure 4.7 Distribution of PSMs within Identified Proteins 103

Figure 4.8 Correlation of Reporter-Ion Intensities from Proteins Present in Both Fractionated Datasets 105

Figure 4.9 Volcano plots of Brain, Heart, and Liver Proteins as a Function of Disease. 107

Figure 4.10 Canonical Pathways of Statistically-Significant Proteins in a) Brain and b) Liver Tissues..... 109

Figure 4.11 Comparison of Quantified Brain, Heart, and Liver Proteins. 113

Figure 4.12 MA plots of Quantified Brain, Heart, and Liver Proteins. 113

Figure 5.1 Experimental Workflow of Human Post-Mortem AD and CN Brain, Heart, and Liver Tissues..... 124

Figure 5.2 Protein Quantification of Brain, Heart, and Liver Tissues a) across all and b) each Biological Replicate..... 125

Figure 5.3 Hierarchical Clustering Across CN and AD Brain, Heart, and Liver Tissues 128

Figure 5.4 Volcano Plots of Brain, Heart, and Liver Tissues 129

Figure 5.5 Trends of Statistically – Significant Proteins in Brain, Heart, and Liver Tissues.... 131

Figure 5.6 Canonical Pathways of Statistically – Significant Heart Proteins 134

Figure 5.7 Canonical Pathways of Statistically – Significant Liver Proteins 135

Figure 6.1 Proposed Experimental Workflow of Labeling *C. elegans* with *in vivo* FPOP and cPILOT. 147

ACKNOWLEDGEMENTS

First and foremost, I would like to thank Dr. Robinson for taking me on as a student. I still remember the first day I met her in separations class. I was so amazed to see a professor who looked like myself in such an esteemed place (as a tenure-track professor)! Her research group piqued my interests because they were studying conditions affecting the elderly population, a group near and dear to me. I was not very familiar with mass spectrometry, but I was eager to learn and start performing experiments. Over the years, Dr. Robinson has provided tremendous support and guidance in my efforts to learn how to develop and execute experiments, analyze data, and write effectively. Dr. Robinson truly cares for the well-being of her students and I am truly grateful for this. I know I can be extremely stubborn and difficult at times, but Dr. Robinson has been very patient with me and never gave up on me. Graduate school has been a very tough and stressful experience for me to endure, but I am really glad to have had Dr. Robinson as my advisor to help me navigate this journey. Her work-ethic and passion for aging-related disorders and life, in general, has really encouraged me to strive to do better as a graduate student. Lastly, I would like to thank Dr. Robinson for providing me with the opportunity to apply for a T32 training grant to work with Professor Angela Jefferson (Dept. of Neurology, Vanderbilt University) and her as a postdoctoral trainee. I just cannot thank her enough for the opportunities I have had in the RASR laboratory!

In addition to my advisor, I would like to thank my committee members, Dr. Kabirul Islam, Dr. Stephen Weber, and Dr. Nathan Yates for taking out the time to listen to my projects. Both Dr. Islam and Dr. Weber have provided me with ideas and tips to move my work forward from my comprehensive exam and Dr. Yates listened to previous presentations I have made in the past years at local work-in-progress meetings. In addition, I would like to especially thank Dr. Weber for agreeing to be my Co-advisor and allowing me to use lab and office space in the Weber laboratory after my group relocated to Nashville, TN.

Within the RASR laboratory, I would like to thank my previous co-workers Dr. Adam Evans and Dr. Zhiyun (Judy) for training me and teaching me the basics in the lab. Along with training me, Judy was very friendly and helped me understand how to analyze the results from my first experiment. Adam was very tough, but he taught me to have grit and push forward through adverse situations. Dr. Liqing Gu helped me maintain the lab when the group was very small and was a funny guy, who brought laughter to the lab. In the current group, I would like to thank Dr. Bushra Amin and Mostafa Khan for helping me think through potential experiments and results obtained from my projects. I would also like to thank my other co-workers for listening to my presentations and giving feedback to improve my work.

In the Department, I would like to thank Dr. Adrian Michael for being my proposal advisor. He made this process very positive and even encouraged me to consider a career in academia. I would also like to thank Dr. Bhaskar Godugu for training me to work in the MS facility. During this time, I learned how to operate and troubleshoot several different types of mass spectrometers and run samples from other students and staff in the Department and the University. Among the staff, I would like to thank both Evon Nigro and Christie Hay for helping me navigate my funding options for Summer and Fall 2018 semesters. I would also like to thank

Mary Beth Conroy for quickly providing the resources necessary to fix building issues related to our lab space and encouraging me to continue with graduate school when times were tough.

Lastly, I would like to thank my family and friends who have supported me throughout these years.

1.0 INTRODUCTION

(*please note, portions of this Chapter are based-off-of the following publications[1-2]: 1) "King, C.D; Singh, D.; Holden, K.; Govan, A.B.; Keith, S.A.; Ghazi, A., Robinson, R.A.S. *Journal of Proteomics*, **2018**, 181: 92 – 103" and 2) "King, C.D.; Dudenhoeffer, J.D.; Gu, L.; Evans, A.R.; Robinson, R.A.S. *J Vis Exp,* **2017,** 123. Doi: 10.3791/55406")

1.1 AGING AND IMMUNITY

Immunonescence, the gradual decline of aging, is an inevitable process that results in several physiological changes, including alterations in the response from both the immediate (innate) and specialized (adaptive) immune responses. Within the body, changes related to decreases in neutrophil function,[3] T cell receptor diversity,[4] inflammatory cytokine production,[5] and other deficits accompany and actuate age-related immune failure. Middle-aged individuals exhibit defects in nearly every cell type and process required for both the innate and adaptive immune responses. These molecular defects also appear to be common to invertebrates.[6] There is an increasing population of aging individuals, therefore studying the mechanisms that are involved in aging and infection is quite important.

One result of a declined immune response includes a higher susceptibility of infection and infectious diseases from opportunistic pathogens. Some well-studied species include Gram-positive (*Streptococcus aureus, S. aureus)* and Gram-negative (*Pseudomonas aeruginosa, P.*

aeruginosa) bacteria; *S. aureus* and *P. aeruginosa* are responsible for a significant number of hospital-acquired infections in immunocompromised patients.[7] Specifically, infections from *P. aeruginosa* can also result in sepsis, a systemic inflammatory response induced by an infection, which occurs more frequently in individuals with immunocompromised systems.[7] The rapid evolution of *P. aeruginosa* and its growing antibiotic resistance makes investigations of the versatile strains important, especially with respect to immunosenescence.[7] Better understanding the dynamics of host-pathogen interactions in this context could facilitate the development of either more effective antibiotics, or pharmaceutical enhancers of intrinsic immune function in high-risk patient groups.

1.1.1 Studying Aging and Host-Response to Infection in Model Organisms

In order to study aging, model organisms have been employed. Animal models provide a wealth of information in understanding the mechanisms involved in responding to infection. They are optimal systems for elucidating the molecular details of microbial pathogenesis and host immunity, and for accelerating the translation of discoveries into clinical outcomes. Models used to study host-response to infection include *D. melanogaster* (fruit fly)*, M. mulatta* (Rhesus monkey)*, Rattus norevegicus* (rat)*, M. musculus* (mouse)*,* and *C. elegans* (roundworm). In particular, the roundworm is an ideal model to use to study both aging and host-response to infection because it develops to adulthood within a few days, has large progeny (~100s), has a short lifespan of ~28 days, is transparent, and most importantly, its innate immune system is evolutionarily conserved.

C. elegans is subject to infection by various human bacterial pathogens[8], many of which enact infectious processes that are quite comparable, at the cellular level, to their modes of pathogenesis in humans.[9] The capacity of multiple *P. aeruginosa* strains to rapidly kill *C. elegans* populations through both biofilm-like-colonization mediated infections and via secreted exotoxins has been thoroughly characterized.[10-12] Additionally, while lacking an adaptive immune system, the critical regulatory elements currently known to coordinate innate immunity in *C. elegans* are highly conserved in vertebrates, such as the p38 mitogen-activated protein kinase (MAPK), transforming growth factor (TGF)-β, and DAF-2 insulin/IGF1 signaling pathways.[13-15] Furthermore, *C. elegans*' infection-resistance mechanisms undergo immunosenescent decline with age in a manner dependent on deteriorating p38 MAPK function.[16]

Currently, *C. elegans'* response to infection has been characterized at genomic-, transcriptomic- and proteomic- levels by full-genome microarrays, RNA-sequencing, and proteomics analyses. These studies have shown that specific genes are either up- or down-regulated at the transcriptional level in response to several pathogens, including *P. aeruginosa,*[17-18] *D. coniospora,*[19-20] *S. aureus, S. marcescens,*[19] *and Y. pestis.*[21] Proteomics analyses have also identified both general and pathogen – specific responses from *S. aureus,*[22] pathogenic *E. coli,*[23] *P. aeruginosa,*[24-25] and others[26]; however, long term proteome changes following infection are unknown and no studies comparing proteomic alterations in young versus old animals facing pathogenic challenges have been reported.

1.1.2 Aging and Alzheimer's Disease

Alzheimer's disease (AD) is a devastating neurodegenerative disorder that causes cognitive decline over 7-10 years.[27] Symptoms include short-term memory loss and the inability to perform every-day tasks. As AD becomes more severe, an individual's ability to take care of themself is impaired, therefore, requiring assistance from caregivers. AD is a top-ten cause of death in the United States that neither can be prevented nor has a cure. This condition affects women more frequently and cost the United States >~$200 billion to treat in 2017.[27] Comorbidities, including cardiovascular disease,[28] hypertension,[29] diabetes,[30-32] and Down syndrome,[33] increase the risk of developing AD, however, the largest risk factor is increasing age.[27]

There are two types of AD that occur either early (early – onset AD) or later (late – onset AD) in life that result in cognitive decline. Early – onset AD is caused by mutations in amyloid precursor protein (APP-1), presenilin-1 (PS-1), and presenilin-2 (PS-2).[34-36] The etiology of late – onset AD, however, is based on the formation and aggregation of amyloid-beta (Aβ) plaques.[37] AD begins to present as preclinical AD[38] and develops into mild cognitive impairment (MCI)[39-40]; the disorder then develops into prodromal AD[41-42] and clinical AD. Late – onset AD[43] is prominent after 65 years of age whereas early – onset AD occurs between 30 – 50 years of age. Cognitive[27] and neuroimaging[44-48] tests, and sampling of cerebrospinal fluid (CSF) are most commonly performed to diagnose AD ante-mortem while classical hallmarks of AD, including the presence of senile Aβ plaques and neurofibrillary tangles (NFT), are identified post-mortem. To diagnose, treat, and potentially prevent AD, studies have been performed to identify biomarkers associated with AD pathology ante- and post-mortem. These analyses focus on

changes occurring during the course of AD in both animal models and in individuals with AD (e.g. plasma, CSF, and post-mortem brain tissues). The most well-known genetic marker, apolipoprotein E, is used to determine if there is an increased susceptibility to developing AD; individuals with the allele type 4 are more likely to have AD than people with alleles 2 or 3.[49-51] To understand the pathogenesis of AD, a host of studies related to the genome, transcriptome, and proteome of AD samples have been performed. However, most of these studies have focused on brain tissues and CSF and they have neglected to consider the contribution of peripheral tissues. Such studies are warranted in order to understand the relationships with abnormalities and to increase the opportunities for biomarker development and therapeutic target. Below is a general scope of proteomics as it is used one of the major tools that can be used to better understand disease.

1.2 PROTEOMICS

Proteomics is the large-scale study of proteins. Protein extracted from tissues, plasma, cells, or other bodily fluids are studied by using a combination of biological and analytical techniques, thus yielding information about the identity and quantity of proteins present. Statistical tests and bio-informatics analyses identify statistically – significant proteins, pathways, molecular functions, and cell compartments related to disease-state and progression, kinetics, post-translational modifications, and other types of changes related to the organism. Over the past twenty five years, proteomics has grown to being able to analyze proteins in a range of states, from their intact, native form, to proteolytically digested peptides. Advancements

in proteomics have been made possible by several contributing factors, including the development of soft ionization methods such as electrospray ionization (ESI)[52] and matrix assisted laser desorption ionization (MALDI),[53-54] improvements in sample preparation, and novel MS instrumentation.

Currently, there are three broad sets of techniques (e.g. top-down, middle-down, or bottom-up) applied in proteomics. Top-down techniques analyze intact proteins to gain information about protein structure and protein-protein interactions. Bottom-up techniques, however, analyze peptide samples with MS and MS/MS and use protein-based software to obtain protein identifications. Specifically, the proteome database of the organism being studied is used to generate an *in silico* digest and theoretical MS/MS spectra are compared to experimentally obtained MS/MS spectra. Experimental spectra that are highly scored are assigned with the proper protein. Lastly, middle-down techniques use a combination of both top-down and bottom-up methods to analyze proteins. In the work presented below, bottom-up proteomics has been especially helpful in answering biological inquiries.

1.2.1 Bottom-up Proteomics

Bottom-up proteomics takes information obtained about peptides and uses search algorithms to reference them to their respective proteins (Figure 1.1). First, protein is extracted from the source (e.g. cells, serum, plasma, blood, tissue, urine) and the protein concentration is determined by using a UV-Vis-based assay. To prevent protein modifications due to sample handling, protease inhibitors can be added to samples. After protein concentration is determined, proteins are digested using proteolytic enzymes (e.g. trypsin, lys-C, glu-C, glu-N) to generate

peptides. Typically, trypsin is used for proteolytic digestion; this enzyme cleaves at the C-terminus of lysine and arginine residues. Depending on the type of analysis, different enzymes may be used to cleave at different amino acids. For instance, Lys-C only cleaves at lysine residues at the C-terminus, Glu-C cleaves at the C-terminus of glutamic acid and Glu-N cleaves at the N-terminus of glutamic acid. Peptides are then separated using reversed-phase high performance liquid chromatography (RP-HPLC). To reduce sample complexity, an orthogonal separation technique, which allows for greater depth in analyzing the proteome(s) of interest, can be performed prior to RP-HPLC analysis. Methods such as ion exchange (e.g. strong cation, strong anion, weak cation, and weak anion) and more recently, high pH reversed phase fractionation (h-pH) can be performed either on- or off-line to separate peptides by charge or hydrophobicity. Fractions generated are then separated by RP – HPLC and analyzed by mass spectrometry.

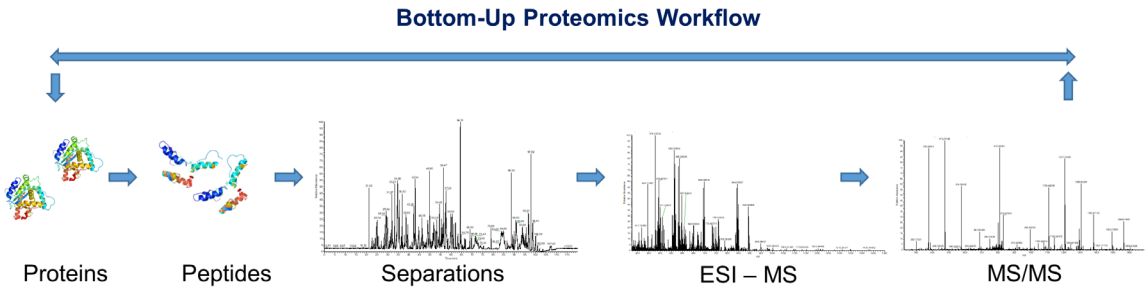

Figure 1.1 Bottom-up Proteomics Workflow.

As peptides are introduced into the mass spectrometer, they are ionized, selected, sorted by the mass analyzer, and detected. Peptides can be fragmented by several types of dissociation techniques, including collision – induced dissociation (CID), higher energy collision-induced dissociation (HCD), electronic capture dissociation,[55] electronic – transfer dissociation,[56] surface induced dissociation,[57] photo dissociation, and electronic – transfer higher energy collision – induced dissociation.[58] These dissociation techniques cause fragmentation at different bonds (Figure 1.2) along the peptide backbone using a range of energies. To fragment at the peptide bond (generating b and y ions), CID is applied with a range of normalized collision energies of 20 – 35%. Inside the ion-trap, precursor ions of interest are excited by a resonance excitation RF voltage to gain kinetic energy. Ions collide with a neutral, buffering gas (e.g. helium), and convert kinetic energy into internal energy.[59-60] Once ions gain enough internal energy, they dissociate into product ions and are detected. Another commonly used dissociation technique is HCD. This method is performed in a multipole collision cell in which a higher normalized collision energy of 50 – 60% is applied. Similar to CID, kinetic energy will be converted into internal energy, resulting in product ions. The advantage of this dissociation technique, however, is the ability to detect ions in the low-mass region, which may include ions that provide quantitative information.

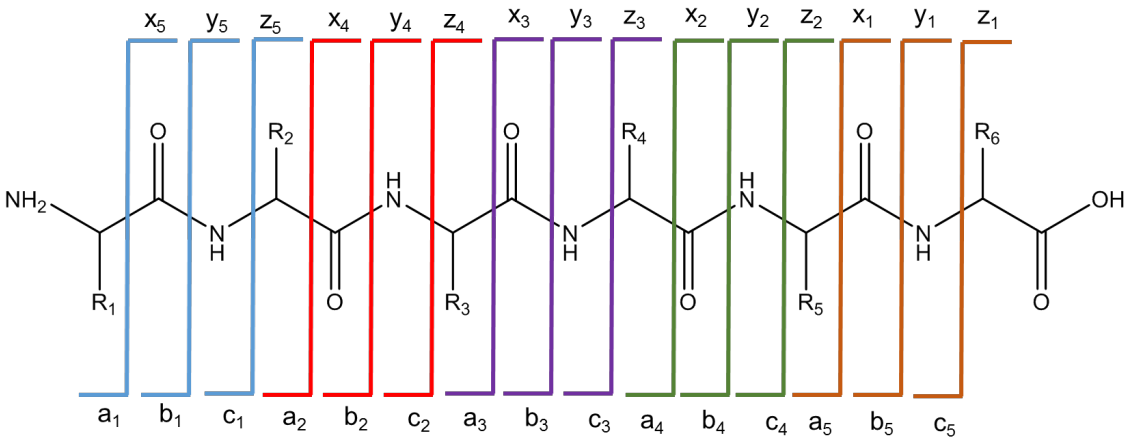

Figure 1.2 Potential Fragmentation Positions of Peptides.

The data obtained from fragmentation spectra are analyzed using protein software, such as Proteome Discoverer (PD, ThermoFisher Scientific), Maxquant,[61] or Skyline,[62] to gain qualitative and quantitative information. Exported results from protein software are further analyzed by applying statistical tests (e.g. student t-test or one-way ANOVA) to identify statistically – significant proteins and bioinformatics tools are used to gain biological insight and/or implications of a given condition or disease. Bioinformatics tools compare the proteome of the organism being studied to a list of statistically – significant proteins added to the platform. If a significant difference of proteins related to specific gene ontology (GO) parameters (e.g. biological processes, molecular functions, or cell compartments) are present, then that specific GO term will be labeled as statistically – significant. Bioinformatics analyses typically provide qualitative information about pathways that are dysregulated in disease. Quantitative proteomics techniques can be employed to learn more about proteins that change in a sample.

1.2.2 Quantitative Proteomics

Label – free quantitative (LFQ) proteomics methods use chromatographic peak areas,[63] peptide spectral counts,[64] peptide signal intensities,[65-66] or a combination of peptide and spectral counts, and MS/MS spectra (i.e. normalized spectral index),[67] gain quantitative information. Some benefits of using label – free methods includes increased flexibility of MS platforms for sample analysis, increased dynamic range, and higher proteome coverage.[68] Challenges associated with LFQ are related to obtaining accurate quantification and sample-to-sample variability. Since each sample is being prepared individually, experimental error may vary differently across samples, thus contributing to inaccurate quantification.[69]

To reduce these limitations, techniques using stable isotopes from small molecular weight chemical groups can be applied to protein samples. Labeling can be performed with cells, entire organisms, proteins, and peptides. Protein amounts are determined by either absolute or relative quantification, and are based on the intensity of either the tagged intact peptide or peptide fragment.

At the organism or cell level, heavy isotopes are incorporated into food and fed to cells, worms, mice, rats, etc.[70-71] After several generations of the label being incorporated, the tagging efficiency should be ~99%. Once this efficiency is reached, samples can be prepared using bottom-up proteomics techniques and analyzed. Heavy nitrogen has been demonstrated to label samples prior to protein homogenization.[70] These heavy nitrogen atoms result in all amino acids being labeled at the amide bond. This method is simple and straightforward, but as all nitrogen atoms are labeled, quickly determining the masses of labeled peptides can be challenging. Since the number of nitrogen atoms present in each peptide may differ, the corresponding mass shift between unlabeled and heavy-labeled peptides will not be consistent, thus complicating the process of searching for peak pairs. In addition, this method only allows two samples to be multiplexed at once. To address both of these issues, stable – isotope labeling by amino acids in cell culture/mammals (SILAC/SILAM) can be used.[71-72] SILAC/SILAM starts with using cells or organisms, however heavy isotopes (e.g. ^{13}C or ^{15}N) only label specific residues (i.e. lysine, arginine, leucine, and proline) with ^{2}H, ^{13}C, or a combination of ^{15}N and ^{13}C. Because labeling occurs at specific residues, mass shifts are more predictable. To multiplex more samples (e.g. 18 samples), NeuCode SILAC mass tags can be incorporated.[73-74] In these tags, mass differences resulting from neutron-binding energy variation in stable isotopes are encoded into amino acids.[73] The major limitation of using metabolic labeling methods would be the condition of the

sample. If the sample(s) are not cells or rodents, then this method cannot be used. To chemically-label protein or peptide samples already extracted, other labeling methods can be applied.

Protein samples arising from any origin can be labeled at either the protein or peptide level by using either isotopic or isobaric tagging strategies. Similar to SILAC, isotopic labeling methods use chemical groups that include heavy isotopes. These methods typically label the N-terminus of peptides and lysine residues. Common labeling methods include acetylation[75] and dimethylation.[76] These methods allow between three and five samples to be analyzed at once, with mass shifts of at least two Da. The major challenge with isotopic labeling includes the potential issue with isotopic clusters between light and heavy pairs overlapping in the precursor scan. To circumvent this issue, heavy isotope tags with a larger mass difference (e.g. >6 Da) than the light tags can be used.

Another chemical labeling strategy that can be applied is isobaric tagging. This method uses a chemical reagent tag that consists of a mass reporter group, a normalizing group, and a reactive group. Common isobaric tagging reagents include Tandem Mass Tags (TMT)[77], Isobaric Tag for Relative and Absolute Quantification (iTRAQ)[78], and N,N-Dimethyl Leucine (DiLeu)[79], and are available commercially (TMT and iTRAQ) or may be synthesized in the laboratory (DiLeu). In an isobaric tagging experiment, the N-terminus of peptides and lysine residues react with the reactive group (e.g. N-hydroxysuccinimide) via a carbonyl attack, leaving the mass reporter and normalizing group attached to peptides (Figure 1.3).

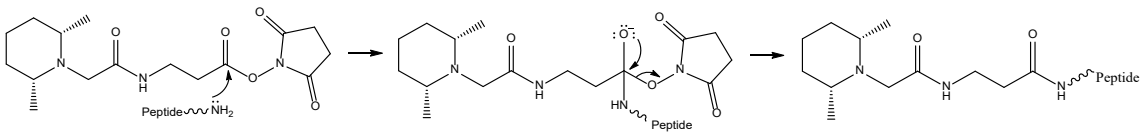

Figure 1.3 TMT Chemical Reaction.

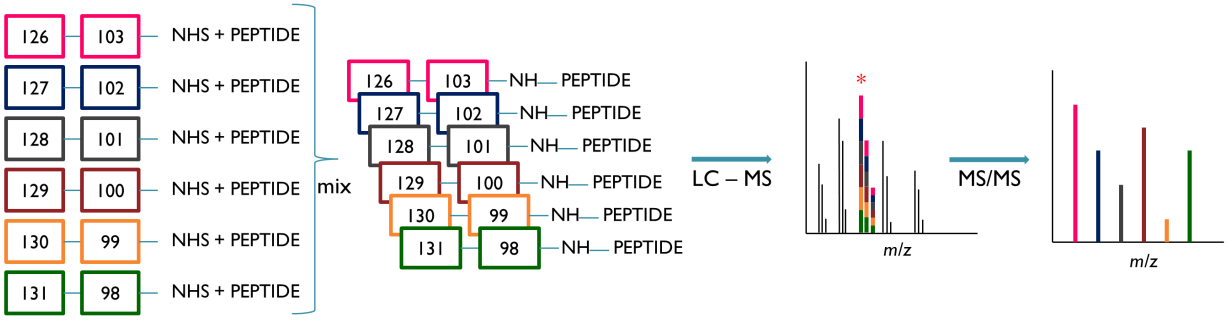

Figure 1.4 TMT^{6}-plex Labeling Strategy.

Several samples are multiplexed by performing this reaction with different variants of the isobaric tag (Figure 1.4). In Figure 1.4, six samples are chemically-tagged (individually) by using six versions of the isobaric tagging reagent. After the reactions are completed and quenched, tagged peptides are combined into one sample and subjected to LC – MS/MS analysis.

A peptide present in several samples (e.g. 6 – 11) will have the same mass, therefore they will elute at the same time. Once a peptide is fragmented by HCD, reporter ion intensities corresponding to that peptide will be detected, thus providing relative quantitative information for that peptide. Current isobaric tagging reagents allow for 1 – 12 samples to be analyzed at once. If more than 12 samples need to be analyzed at once, enhanced-multiplexing methods can be applied.

Both isotopic labeling and isobaric tagging strategies have several advantages. For example, sample throughput increases directly in proportion to the number of samples that can be multiplexed. Less experimental error is achieved as after the tags are introduced, therefore, all samples are subject to the same experimental errors in sample preparation. There are also practical advantages of reducing MS analysis time, labor, and costs. While there are many benefits to multiplexing, there are a few challenges as well. For example, inefficient labeling of proteins or peptides can complicate MS spectra and data analysis and lead to inaccurate relative protein quantitation. Some labeling reactions are pH and buffer specific[76-77, 80] and if the reaction conditions are incorrect, undesirable side products may be produced[77] and reduce the labeling efficiency. Other labeling methods require several iterations to achieve high labeling efficiencies[71-72] which lengthens sample preparation time. To ensure that both peptides within a pair (or multiplets) are selected for MS analysis, peptide co-elution is necessary. Depending on the types of heavy isotope atoms used, isotopically – labeled pairs (or triplets) can be resolved in

the LC separation.[81] This issue has been addressed by incorporating tags with fewer atoms of ^{2}H and more atoms of ^{18}O, ^{13}C, and/or ^{15}N. [29, 75, 81-82] Due to the fact that every peptide will appear as a doublet or triplet in the precursor *m/z* spectra, spectral complexity is increased. This may be problematic if one peak in the multiplet is selected more frequently for fragmentation as only information for that sample is obtained. Lastly, reagent costs for multiplexing can vary from a few dollars to >$500 per experiment. Furthermore, isobaric tagging reagents mostly require the use of high-resolution instruments to distinguish between reporter ions.

1.3 ENHANCED MULTIPLEXING TECHNIQUES

Multiplexing with isotopic and/or isobaric tagging strategies allow for many samples to be analyzed at once, however limitations are present. If more than 12 samples need to be analyzed, enhanced-multiplexing tagging methods can be employed.[73-74, 80, 83-88] One strategy used in our laboratory is combined precursor isotopic labeling and isobaric tagging (cPILOT).

1.3.1 Combined Precursor Isotopic Labeling and Isobaric Tagging (cPILOT)

Our laboratory developed cPILOT, which labels the N-terminus of peptides with heavy isotopes and lysine residues with isobaric tags.[83] Initially, this method was applied to study the post-translational modification (PTM) 3-nitrotyrosine (3NT) in which N-termini and lysine residues were blocked with light and heavy acetyl groups. 3NT modified peptides were then reduced to 3-aminotyrosine (3AT) and tagged with either TMT or iTRAQ to be isobarically

tagged. cPILOT was shown to selectively label the N-terminus and lysine residues and was able to identify and quantify peptides; however, issues with co-isolation and quantitation were evident due to the use of a $^{2}H_{3}$ acetylation heavy tag and missing reporter ion information. In order to maximize the number of peptides that are quantified and have signal in reporter ion channels and broaden the types of analyses that can be studied, different sample preparation strategies and data acquisition methods were developed.

The first change made was related to the isotopic labeling strategy used. This labeling method was changed to dimethylation (Figure 1.5). This reaction was performed at low pH (pH ~2.5-3), to selectively label the N-terminus of peptides. In addition, using dimethylation reduced co-isolation between peptide pairs. To improve quantification, MS^3 acquisition with a top-ion or selective-y_1-ion method was employed. This helped reduce reporter ion interference and improve quantitative accuracy of cPILOT.[80] Changes made in cPILOT reactions and data acquisition were applied to study the brain proteome of an Alzheimer's disease mouse model (APP/PS-1) and showed that cPILOT successfully labeled peptides with high efficiencies (i.e. 98%) and quantified reporter ions better by MS^3.

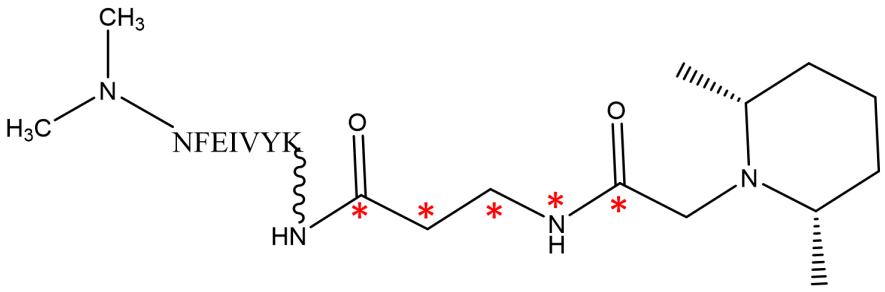

Figure 1.5 Example Peptide after cPILOT Labeling.

To study cysteine, the amino acid selective approach cysteine cPILOT (cyscPILOT) was developed.[85] As cysteine containing peptides are low (~14%) in abundance, sample preparation included cysteine enrichment. Labeling by cPILOT was adjusted by performing on-resin dimethylation and using iodo-TMT tagging reagents. Results showed that labeling with cyscPILOT was successful and that changes in the liver proteomes of APP/PS-1 mice were able to be detected. With the techniques learned from cyscPILOT, OxcyscPILOT[89-90] was developed. This method uses similar methodology as cyscPILOT, but was altered to select specific oxidative cysteine modifications. To prepare S-nitrosylated samples, free thiols were blocked, SNO-containing peptides were enriched, and on-resin labeling by cPILOT was performed. This method was used to study SNO modifications in APP/PS-1 brain samples and showed that 1) OxcyscPILOT successfully enriched SNO containing peptides and 2) endogenous SNO levels in AD were able to be quantified.

cPILOT has also been employed to study liver tissues[84] and more recently, brain, heart, and liver tissues (**Chapter 4**) from 14-month-old APP/PS-1 mice. In the study of the liver proteome, samples from AD and WT mice were labeled by cPILOT and analyzed by using a two-tiered data-dependent acquisition (DDA) method. This method was employed to increase overall peptide identifications and to identify and quantify a wider dynamic range of peptides.

The development and improvements of cPILOT labeling and analysis methods show the versatility and flexibility of using this method. Recently, cPILOT multiplexing capabilities have been increased to 24 samples by using DiLeu 12-plex.[91] DiLeu tags can be synthesized in the laboratory, therefore using these tags can dramatically decrease sample preparation costs. This and further innovations of this enhanced strategy will enable larger sample multiplexing (i.e. >24 samples).

1.4 OVERVIEW OF DISSERTATION

This body of work is a compilation of projects that employ quantitative proteomics techniques to study aging, infection, and Alzheimer's disease in both worm and mouse models, along with post-mortem human tissues. Host – response of young- and aging-adult *Caenorhabditis elegans (C. elegans)* exposed to the opportunistic pathogen *Pseudomonas aeruginosa* strain PA01 are studied (**Chapter 2**), providing novel insights into the relationship between age and immunosenescence in metazoans. Improvements in Orbitrap instrumentation are applied to same *C. elegans* samples (**Chapter 3**) to better understand the Elite MS and gain additional information about the effects of aging on the molecular mechanisms involved in response to pathogen exposure. To study larger sample-cohorts (e.g. 36 samples), the enhanced multiplexing strategy combined precursor labeling and isobaric tagging (cPILOT) is applied. This technique is especially helpful when studying multiple tissues and biological replicates in models of disease, such as Alzheimer's disease. Specifically, cPILOT optimization on an Orbitrap Lumos platform and its application to brain, heart, and liver proteomes of an Alzheimer's disease mouse model (**Chapter 4**) and human post-mortem (**Chapter 5**) tissues are studied. Lastly, future directions are discussed (**Chapter 6**).

2.0 PROTEOMICS ANALYSIS OF VIRULENCE-RELATED FACTORS IN YOUNG AND AGING C. *ELEGANS* EXPOSED TO *PSEUDOMONAS AERUGINOSA* PA01- PART 1*

(*please note, contents of this Chapter are based off of the following publication: "King, C.D; Singh, D.; Holden, K.; Govan, A.B.; Keith, S.A.; Ghazi, A., Robinson, R.A.S. *Journal of Proteomics*, **2018**, https://doi.org/10.1016/j.jprot.2018.04.006") [1]

2.1 INTRODUCTION

Aging is characterized by the progressive accumulation of a variety of physiological impairments. One of the more challenging and early age-associated declines is immunosenescence- the gradual deterioration of the immune system with increasing age. Conserved across a wide evolutionary scale, immunosenescence contributes substantially to the increased morbidity and mortality of elderly populations.[92-93] Starting in middle age, both vertebrates and invertebrates exhibit defects in nearly every cell type and process required for immune capability. Given the rapidly aging global population,[94] there is an urgency to understand the cellular and molecular mechanisms underlying immunosenescence.

The major consequence of immunosenescence is an increased susceptibility to infectious diseases, including those caused by opportunistic pathogens.[95] The Gram-negative bacterium

Pseudomonas aeruginosa is a well-known pathogen responsible for a significant number of hospital-acquired infections[96] especially in individuals suffering from cystic fibrosis,[97] cancer,[98] AIDS,[99-100] or other immune-suppressing illnesses. This is partly due to the microbe's propensity for colonizing inserted medical care devices.[101] *P. aeruginosa* infection is accompanied by biofilm formation and exotoxin secretion, and can result in sepsis- a potentially fatal systemic inflammatory response. The rapid evolution of *P. aeruginosa* and its growing antibiotic resistance makes investigations of the versatile strains important, especially with respect to immunosenescence. Better understanding the molecular dynamics of host-pathogen interactions in this context could facilitate the development of more effective antibiotics, or pharmaceutical enhancers of intrinsic immune function in high-risk patient groups.

The nematode *Caenorhabditis elegans*[102] is subject to infection by various human bacterial pathogens, many of which enact infectious processes that are quite comparable, at the cellular level, to their modes of pathogenesis in humans.[8] Indeed, the capacity of multiple *P. aeruginosa* strains to rapidly kill *C. elegans* populations through both biofilm-like-colonization mediated infections and via secreted exotoxins has been described extensively.[9-11] Additionally, while lacking an adaptive immune system, the critical regulatory elements known to coordinate innate immunity in *C. elegans* are highly conserved in vertebrates, such as the p38 mitogen-activated protein kinase (MAPK), transforming growth factor (TGF)-β, and DAF-2 insulin/IGF1 signaling pathways.[12-14] Further, *C. elegans*' infection-resistance mechanisms undergo immunosenescent decline with age in a manner dependent on deteriorating p38 MAPK function.[15] Collectively, the ability to recapitulate infection phenotypes for numerous microorganisms, efficient and inexpensive culture methods, and relative ease of performing

genetic manipulations have made the worm an ideal model for examination of innate immune responses to pathogen.

Given the fully sequenced and curated *C. elegans* genome,[102] the worm offers a unique capacity for large-scale explorations of molecular factors either induced or repressed by infection. Full-genome microarrays and RNA-sequencing have been implemented to survey genes that are either up- or down-regulated at the transcriptional level in response to *P. aeruginosa, Drechmeria coniospora, Staphylococcus aureus, Serratia marcescens,* and *Yersinia pestis* and others.[9, 14, 18-21, 103] These efforts have provided considerable insight into common pathogen-specific immune events. However, despite recent technical advances in performing proteomics analysis with *C. elegans,*[104-107] to-date studies profiling protein-level expression changes in pathogen-challenged worms have been limited[22-26, 107-109] and studies comparing the proteomic alterations observed in Day 1 vs. Day 5 animals facing pathogenic challenges have been not been reported.

In the present study, we employed two independent quantitative proteomics approaches, Tandem Mass Tag (TMT^6) isobaric tagging and reductive dimethylation chemical labeling to profile the protein-level changes experienced by Day 1 and Day 5 *C. elegans* exposed to pathogenic *P. aeruginosa* strain PA01 *(*henceforth labeled '*P. aeruginosa* PA01'*)* relative to *C. elegans* fed on the laboratory diet of *Escherichia coli* strain OP50 (henceforth labeled '*E. coli* OP50'). Overall, we identified 55 unique proteins that exhibited significantly altered levels in Day 1 or Day 5 worms upon pathogen exposure of which ten were identified at both ages. The proteins common between Day 1 and Day 5 worms' response to pathogen included cytoskeletal proteins involved in locomotion as well as enrichment of reproductive functions. In Day 5 worms in particular, proteins representing multiple stress-response pathways were elevated. In

accordance with our proteomic predictions, we observed that PA01 exposure increased protein carbonylation suggesting sustained oxidative stress after pathogen exposure. Additionally, we evaluated the lifespan of mutants for the protein, UNC-60, whose levels were altered by both age and pathogen exposure and found that mutants of *unc-60* have reduced lifespan. Overall, our data provide novel insights into the cellular responses mounted by metazoans when exposed to the clinically relevant pathogen *P. aeruginosa*, and into the molecular changes that occur at the intersection of aging and immunity.

2.2 EXPERIMENTAL PROCEDURES

2.2.1 Nematode and Bacterial Culture

C. elegans N2 Bristol wild type worms were maintained via standard laboratory techniques on nematode growth medium (NGM) plates seeded with *Escherichia coli* OP50, the normal laboratory diet.[110] *P. aeruginosa* PA01–seeded pathogenicity–assay plates were generated as described previously for *P. aeruginosa* PA14 ″slow killing″ (SK) assays.[111] Briefly, ~5 mL liquid LB was inoculated from an individual PA01 colony and grown 8 – 16 h at 37 ºC with shaking. Approximately 75 µL liquid culture was then seeded to SK plates,[111-112] which were kept at room temperature for at least two days until the bacteria had formed a thick, contiguous lawn.

2.2.2 Pathogenicity Assays

Synchronized *C. elegans* populations of wild-type strain, N2, were obtained by isolating eggs via sodium hypochlorite treatment and allowing hatching overnight in M9 buffer (0.09 M NaCl, 0.04 M Na_2HPO_4, 0.02 M KH_2PO_4) at 20 ºC.[113] The resultant L1 larvae were then transferred to standard *E. coli* OP50–seeded NGM plates and incubated at 20 ºC until Day 1 adulthood. In order to evaluate pathogen resistance in Day 1 animals, one subset of worms were transferred to *P. aeruginosa* PA01–seeded SK plates on Day 1 of adulthood (~48 h post-L1 incubation), while the control group remained on *E. coli* OP50–seeded NGM plates for the duration of the assay. Experimental and control subpopulations consisted of 60-100 individuals evenly distributed over five plates (15 – 20 worms/plate). To examine the pathogen resistance of Day 5 worms, synchronized populations were maintained on *E. coli* OP50–seeded NGM plates until Day 5 of adulthood before being distributed to *P. aeruginosa* PA01 plates or control *E. coli* OP50 plates, as was done for Day 1 animals. All worms were transferred to fresh plates every other day through the reproductive span to avoid both overcrowding and confusion between the study population and its progeny. Assay plates were incubated at 20 ºC and scored for survival daily. Worms were considered dead upon failure to respond to repeated prodding with a platinum wire pick. Data reflecting worms that crawled off the media, exploded, bagged, or became contaminated were censored. The resulting survival data were used to generate Kaplan Meier curves with OASIS (Online Application of Survival Analysis),[114] and P values were calculated via log rank (Mantel Cox method) test with the same software.[114] Lifespan assays of the *unc-60* mutant strains, CB77 {*unc-60(e677)*}, ON19 {*unc-60(su158)*} and N2 controls were conducted similarly at 20 ºC.

2.2.3 Sample Preparation for Proteomics Analysis

Sodium hypochlorite-mediated, L1–synchronized N2 worm populations were obtained in large numbers and reared to early adulthood on *E. coli* OP50–seeded NGM at 20 ºC, (~80,000 – 100,000 total worms). To examine the proteome of Day 1 adults challenged with *P. aeruginosa*, one group of ~20,000 worms was transferred to *P. aeruginosa* PA01–seeded SK plates (or control *E. coli* OP50–seeded NGM plates) on Day 1 of adulthood and maintained at 20 ºC for 18 h before harvesting. For Day 5 pathogen-exposure studies, worms were transferred to *E. coli* OP50–seeded NGM plates as described above, and maintained on the same food until Day 5 of adulthood (transferring to fresh plates every other day to avoid progeny contamination). On Day 5, half the worms were transferred to *P. aeruginosa* PA01–seeded SK plates (the other control half to *E. coli* OP50–seeded NGM plates) and maintained at 20 ºC for 18 h before harvesting both groups. Parents were separated from eggs and progeny during transfers by serially washing adults off the plates with M9 and then allowing the adults to settle by gravity. At their respective time points, worms were floated off plates with M9 buffer[110] and washed two times to remove extraneous bacteria and obtain sample pellets. Two independent biological replicates were collected for the proteomic studies from each age group and bacterial exposure.

2.2.4 Protein Extraction

Worms were harvested, washed with M9 buffer to remove bacteria, and centrifuged to obtain a pellet. Pellets were re-suspended in Reassembly (RAB) buffer (0.1 M MES, 1 mM EGTA, 0.1 mM EDTA, 0.5 mM $MgSO_4$, 0.75 M NaCl, 0.02 M NaF) with Roche Complete

Protease Inhibitor (Roche Applied Science). Protein homogenate was sonicated for 10 s, followed by 50 s on ice, incubated for 10 min on ice and centrifuged at 14000 g. The amount of protein was determined by BCA assay (Thermo Scientific). A pooled sample (Sample #5) containing equimolar ratios of Day 1 *E. coli* OP50 (Sample #1) and *P. aeruginosa* PA01 (Sample #2) and Day 5 *E. coli* OP50 (Sample #3) and *P. aeruginosa* PA01 (Sample #4) samples, was also prepared.

2.2.5 Protein Digestion

Protein was purified using acetone precipitation and quantified by BCA assay. Protein (~80 – 100 µg) was denatured with an extraction buffer (0.2 M Tris, 8 M urea, 10 mM $CaCl_2$, pH 8.0), reduced with 1:40 molar excess of dithiothreitol (DTT) for 2 h at 37 ºC, and then alkylated with 1:80 molar excess of iodoacetamide (IAM) for 2 h on ice. The alkylation reaction was quenched by adding 1:40 molar excess of cysteine and the mixture was incubated at room temperature for 30 min. Tris buffer (0.2 M Tris, 10 mM $CaCl_2$, pH 8.0) was added to dilute the urea concentration to 2 M. Each sample was incubated with bovine TPCK-treated trypsin (Sigma–Aldrich) at 50:1 substrate/enzyme ratio for 24 h at 37 ºC.

2.2.6 TMT Labeling

Digested samples were desalted with an HLB cartridge and dried by centrifugal evaporation. Each sample was labeled with a TMT^6-plex reagent following the manufacturer's protocol (Thermo Scientific). TMT^6 reagents were equilibrated to room temperature, solubilized

with 41 µL of acetonitrile, and transferred to peptide samples reconstituted in triethylammonium bicarbonate (TEAB) buffer. After 1 h of incubation (~25 ºC), the reaction was quenched using 5% hydroxylamine. Equimolar amounts of samples were combined such that reagents that generate reporter ions at *m/z* 126:127:128:129:130 correspond to D1 OP50, D1 PA01, D5 OP50, D5 PA01, and the pooled sample, respectively.

2.2.7 Dimethylation Labeling

Peptides (~50 µg) were reconstituted in 100 mM TEAB buffer (pH 8.5). The following solutions were added to *E. coli* OP50 samples for light $(\text{-CH}_3)_2$ labeling and to *P. aeruginosa* PA01 samples for heavy $(\text{-}^{13}\text{C}^2\text{H}_3)_2$ labeling: 4% formaldehyde (16 µL) and 0.6 M sodium cyanoborohydride (16 µL) (Sigma–Aldrich) or 4% ^{13}C, D_2 – formaldehyde (16 µL) and 0.6 M sodium cyanoborodeuteride (16 µL) (Sigma–Aldrich), respectively. Samples were vortexed for 10 min, quenched with 1% ammonia, and acidified with 5% formic acid. Samples were then desalted with an HLB cartridge, dried by centrifugal evaporation, and stored in the – 80 ºC freezer until further analysis.

2.2.8 Strong Cation Exchange (SCX) Fractionation

SCX fractionation was performed on a PolySulfoethyl A 100 mm x 2.1 mm, 5µm, 200 Å column (The Nest Group, Inc.) with buffers as follows: mobile phase A was 5 mM monopotassium phosphate (25% v/v acetonitrile, pH 3.0), and mobile phase B was 5 mM monopotassium phosphate, 350 mM potassium chloride (25% v/v acetonitrile, pH 3.0). Dried

TMT^6– labeled samples were re-suspended in 200 µL of mobile phase A and injected onto the column. The gradient was as follows: 0 – 5 min, 0% B; 5 – 45 min, 0 – 40% B; 45 – 90 min, 40 – 80% B; 90 – 100 min, 80 – 100% B; 100 – 110 min, 100% B; 110 – 121 min, 0% B. Eluent was collected every minute and combined into 20 fractions. Each fraction was desalted using Supel-Tips C18 micropipette tips (Sigma – Aldrich). Fractions were solubilized in 50 µL and filtered with a 0.45 µm filter (Thermo Fisher Scientific).

2.2.9 LC – MS Analyses

Online desalting and reversed-phase chromatography was performed with a Nano liquid chromatography (LC) system equipped with an autosampler (Eksigent). Mobile phases A and B used for reversed phase (RP)-LC separation of peptides were 3% (v/v) acetonitrile with 0.1% formic acid and 100% acetonitrile with 0.1% formic acid, respectively. SCX fractions (10 µL) were loaded onto a trapping column (100 µm i.d. x 2 cm), which was packed in house with C_{18} (3 µm, 200 Å) stationary phase material (Michrom Bioresource Inc,) at 3 µL/min in 3% mobile phase B for 3 min. After desalting, the sample was loaded onto an analytical column (75 µm i.d. x 13.2 cm) which was packed in-house with C_{18} (3 µm, 100 Å) stationary phase material (Michrom Bioresource Inc). The gradient was as follows: 0 – 7 min, 10% mobile phase B; 7 – 67 min, 10 – 30% B; 67 – 75 min, 30 – 60% B; 75 – 77 min, 60 – 90% B; 77 – 82 min, 90% B; 82 – 83 min, 90 – 10% B; 83 – 95 min, 10% B. The LC eluent was analyzed with positive mode nanoflow electrospray using a LTQ Orbitrap Velos mass spectrometer (Thermo Fisher Scientific). Data-dependent acquisition parameters were as follows: the MS survey scan in the Orbitrap (300 – 1800 *m/z*) was 60000 resolution; the top seven most intense peaks were isolated

and fragmented with collision-induced dissociation (CID) in the LTQ (normalized collision energy of 35%). Directly after each MS/MS scan, the most intense fragment ion over the m/z range 200 – 1545 was selected for higher-energy collisional dissociation (HCD) triple staged mass spectrometry (MS^3). The fragment isolation width was set to 4 *m/z*, the MS^3 AGC was 3 x 10^5, the normalized collision energy was 60%, the resolution was 7500 and the maximum ion time was 250 ms. HCD spectra were recorded in the Orbitrap. Each fraction was subject to duplicate injections.

Dimethylated samples were analyzed by LC – MS/MS. Similar mobile phases, trapping and analytical column settings, and instrument settings were used to perform the analysis, except the analytical gradient was: 0 – 5 min, 10% mobile phase B; 5 – 40 min, 5 – 40% B; 40 – 90 min, 15 – 25% B; 90 – 115 min, 25 – 30% B; 115 – 130 min, 30 – 60% B; 130 – 135 min, 60 – 80% B; 135 – 145 min, 80% B; 145 – 150 min, 80 – 10% B; 150 – 180 min, 10% B. Data-dependent acquisition parameters: MS survey scan in the Orbitrap (300 – 1800 *m/z*) with 60000 resolution; the top fifteen most intense peaks were isolated and fragmented with CID in the LTQ (normalized collision energy of 35%). Each fraction was also subjected to duplicate injections (technical replicates).

2.2.10 Data Analyses

RAW files were analyzed with PD 1.4 software (Thermo Scientific). Spectra were used to obtain sequence information against the Uniprot *C. elegans* database (11/26/2013, 25673 sequences). SEQUEST search parameters were as follows: two maximum trypsin miscleavages, precursor mass tolerance of 10 ppm, fragment mass tolerance of 0.8 Da; static modifications

were TMT six-plex/+229.163 Da (N-terminus, Lys) and carbamidomethyl modification/+57.021 Da (Cys); dynamic modification was oxidation modification/+15.995 Da (Met). Decoy database searching was employed to generate medium ($p<0.05$) and high ($p<0.01$) confidence peptide lists. All the peptides with medium and high confidence were used to identify and quantify proteins. To filter peptides, the following parameters were applied: peptide confidence level of medium or high, peptide rank of 1, and peptide deviation of 10 ppm. Peptides with a PSM (peptide to spectral match) count of 1 (per technical replicate) were not considered for analysis. The reporter ions (i.e. *m/z* 126 – 130) were identified with the following parameters: most confident centroid and 20 ppm for reporter ion mass tolerance. Furthermore, reporter ion values were normalized 126/130, 127/130, 128/130, and 129/130 and final ratio reporting given as 127/126 and 129/128. Proteins belonging to multiple isoforms were grouped into a single accession number and final ratios were reported.

A power analysis was performed using protein ratios from TMT^6-plex data to generate an appropriate fold-change cutoff. Coefficient of variation (CV) values were calculated as previously explained for reporter ion ratios of proteins quantified in both biological replicates.[115] The mean CV value from both biological replicates was calculated and used as the total biological variation, S_b, (i.e. 0.36). The technical variation, S_t, was calculated for proteins quantified in at least one technical replicate of each biological replicate, and was 0.22. The power of the test and the significance level was set to 0.8 and 0.05, respectively. Filter criteria were applied to generate a list of proteins showing differential levels as follows: 1) proteins identified and quantified in at least one technical replicate and both biological replicates, 2) CV values ≤ 0.36, and 3) fold-change cutoff ≥ 1.4 or ≤ 0.72.

Data from the dimethylation experiment was treated by applying the following criteria: 1) proteins identified and quantified in both technical replicates and 2) fold-change cutoff dependent on $p < 0.05$ such that ≥ 1.4 or ≤ 0.70.

2.2.11 Measurement of Protein Carbonylation Levels

Immunoblot assays were performed using one biological cohort of Day 1 and Day 5 *C. elegans* to measure oxidative stress in *C. elegans* exposed to *P. aeruginosa* PA01. Protein carbonylation (PCO) measurement was performed using Dot/Slot blot. Protein from samples 1 – 4 (5 µL) were dissolved in 1× PBS, 12% SDS and derivatized with 20 mM 2,4-dinitrophenylhydrazine (DNPH) for 20 min. The reactions were quenched using neutralization buffer and the samples were diluted using 1× PBS buffer to have a concentration of 1 ng/µL. Nitrocellulose membrane and filter paper (2) were briefly soaked in PBS buffer and the Dot/Slot blot apparatus was assembled. The membrane was rinsed with 200 µL of PBS, protein samples (250 ng) were loaded onto the Dot/Slot blot apparatus, and then the membrane was rinsed an additional time. The membrane was removed and samples were incubated in blocking buffer (3% *w/v* BSA in wash blot) for 90 min (room temperature). Primary antibody (anti – 2,4-dinitrophenyl) was added with a dilution of 1:2000 and left to incubate overnight (4 ºC). The following day, the membrane was brought up to room temperature for 30 min, then washed 4 times with wash blot (5 min intervals). Secondary antibody (anti-rabbit IgG alkaline phosphatase) was added with the dilution factor 1:5000 with 20 mL wash blot and the membrane was incubated for 60 min (room temperature). The membrane was rinsed in wash blot (3 times, 5 min intervals) and developed using 5-bromo-4-chloro-3-indolyl phosphate (BCIP)/nitro blue

tetrazolium (NBT). The solution was allowed to incubate till blue spots appeared. Results were analyzed using Scion Image software. Six technical replicates were performed.

2.3 RESULTS

2.3.1 C. elegans Resilience to P. aeruginosa PA01 Declines with Increasing Age

The reliability of our proteomics data first depended on a *bona fide* bacterial infectivity and pathogenicity *C. elegans* model. This confirmatory step was particularly critical given the non-traditional solid – SK – media platform required to generate large cohorts of *C. elegans*. Hence, we performed standard pathogenicity assays to assess the lethality of *P. aeruginosa* PA01 on wild-type *C. elegans* and to directly compare the survivals of Day 1- and Day 5 animals challenged with this pathogen. Similar to *P. aeruginosa* PA14[15], *P. aeruginosa* PA01 exposure resulted in a dramatic decrease in the lifespan of both age groups in comparison with *E. coli* OP50 controls (Figure 2.1).

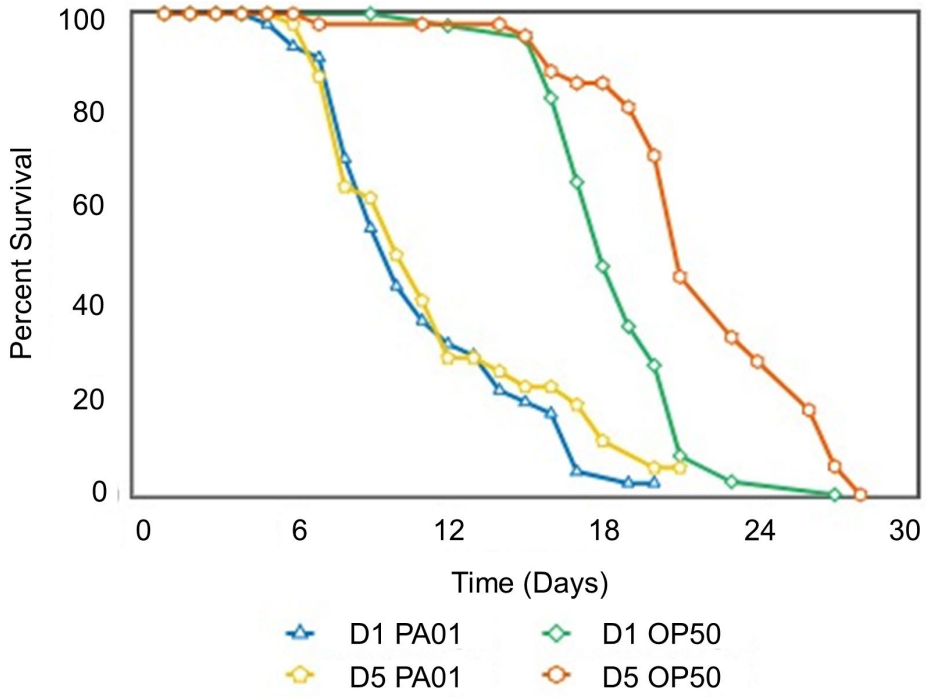

Figure 2.1 Survival Curves of Exposed and Control *C. elegans.* The lifespans of Day 1 (D1) and Day 5 (D5) adult control and exposed D1 and D5 C. elegans were compared to survival on the standard laboratory diet of E. coli OP50. N2 (E. coli OP50) D1 OP50 (green; m= 18.7 ± 0.4, n= 39/44), D1 PA01 (blue; m= 11.2 ± 0.6, n= 41/49, P vs. N2 <0.001), N2, D5 OP50 orange; m= 21.9 ± 0.7, n= 36/46) D5 PA01 (yellow; m= 11.7 ± 0.7, n= 37/46, P vs. N2 <0.0001).

C. elegans reared on *E. coli* OP50 and transferred to *P. aeruginosa* PA01 – seeded SK plates on Day 1 of adulthood had a mean lifespan of 11.2 ± 0.6 days vs. mean lifespan of 18.7 ± 0.4 on E. coli OP50 while those transferred as Day 5 adults perished after 11.7 ± 0.7 days, vs. mean lifespan of 21.9 ± 0.7 on E. coli OP50. Upon pathogen exposure, Day 5 adults began to perish within 24 h while Day 1 adults maintained 100% survival for several days. Both Day 1 and Day 5 adults' survival were reduced in the presence of pathogen. In an independent trial, a 29% reduction in the survival of Day 5 adults exposed to pathogen was observed (Appendix A Table A2.1). These data confirmed that *P. aeruginosa* PA01, similar to the PA14 strain of the same pathogen[15], reduces *C. elegans*' survival and the detrimental effects are stronger in Day 5 adults than Day 1. It also shows that both Day 1 and Day 5 had initial differences in survivability upon exposure to pathogen. Therefore, proteome changes identified in this work are likely reflective of genuine *C. elegans* infection responses.

2.3.2 Mapping the C. elegans Proteome upon P. aeruginosa PA01 Exposure

In a recent report, Vigneshkumar et al. used two-dimensional difference in gel electrophoresis (2D-DIGE) to identify 19 proteins whose levels are altered upon PA01 infection in Day 1 worms.[25] However, little is known about genome-level proteome changes that occur in worms following infection with bacterial pathogens, especially with respect to the influence of aging. To systematically address this, we applied a proteomics workflow that takes advantage of isobaric tagging to simultaneously assess changes in the *C. elegans* proteome upon exposure to *P. aeruginosa* PA01 in Day 1 of adulthood vs. Day 5 of adulthood worms (Figure 2.2, Full Mass Spectrum). Four cohorts of *C. elegans* (~20,000 worms/sample) were bred, exposed to *P.*

aeruginosa PA01 at Day 1 or Day 5 and harvested 18 hours after *P. aeruginosa* PA01 exposure. This time-point was selected because it allowed a suitable exposure time to the pathogen to establish an infection-related proteome and, as is evident from the lifespan curves in Fig. 1, was a stage before large-scale death commenced. This ensured that the proteome responses measured were likely to be primarily related to immune responses and not mortality processes (e.g., apoptosis, degradation, etc.), and to give insight into immediate host responses to pathogen. As shown in Figure 2.2, proteins from each of the groups including a pooled sample were tryptically digested. Peptides were tagged with TMT^6 reagents and analyzed by LC – MS/MS and MS^3 as follows: Day 1 *C. elegans* fed on *E. coli* OP50 (*m/z* 126), Day 1 *C. elegans* exposed to *P. aeruginosa* PA01 (*m/z* 127), Day 5 *C. elegans* fed on *E. coli* OP50 (*m/z* 128), Day 5 *C. elegans* exposed to *P. aeruginosa* PA01 (*m/z* 129), and the pooled sample (*m/z* 130). MS^3 was employed to help minimize ratio compression associated with reporter ion signals.[80, 116-117] Biological and technical replication helped ensure we were observing reproducible changes.

Example data from the proteomics workflow is shown in Figure 2.2. The peptide, N(TMT^6)ANADIQQWK(TMT^6) belongs to the myosin-4 protein and the MS and MS/MS spectra contain signal from samples for each of the four groups. After MS^3 of the b_4 fragment ion at *m/z* 601.49 is performed, reporter ions that track the sample origin for each group are detected. For this particular peptide, its relative abundance is higher in *C. elegans* exposed to *P. aeruginosa* PA01 relative to controls at both ages (i.e., D1 PA01/D1 OP50 = 3.12 and D5 PA01/D5 OP50 = 1.34). In addition, it's clear that myosin-4 has higher levels overall in Day 5 *C. elegans* in comparison to Day 1 *C. elegans*.

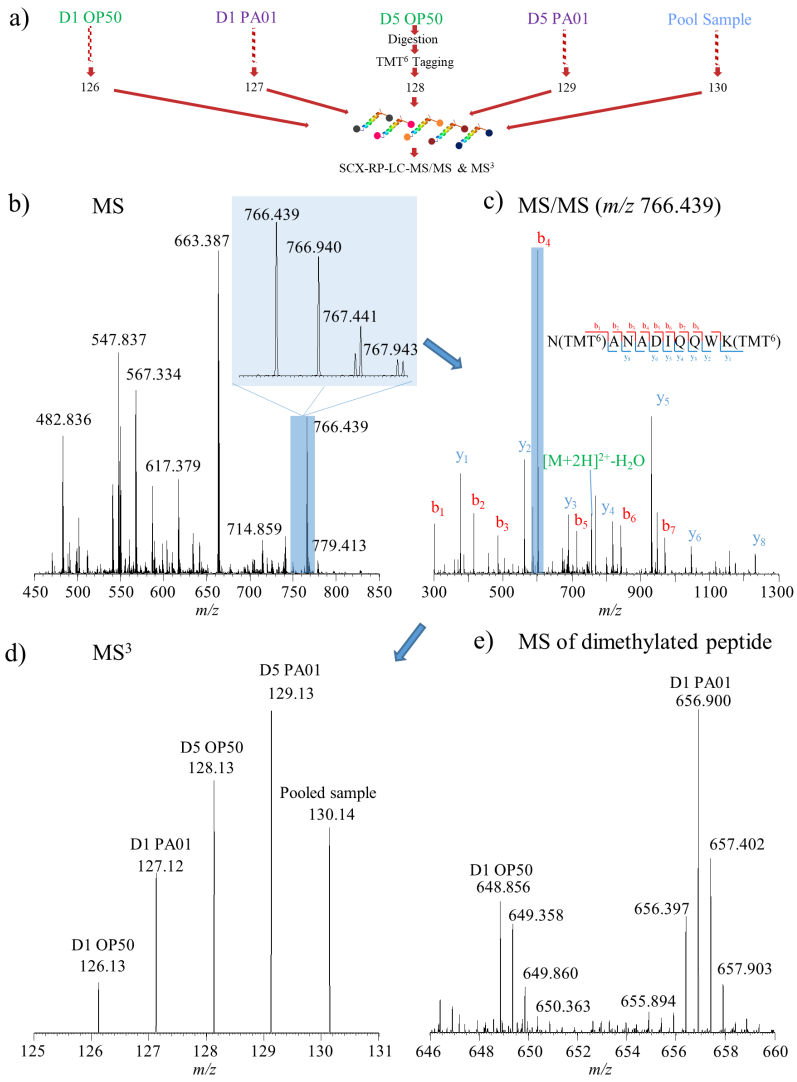

Figure 2.2 Proteomics Experiments and Mass Spectra of *C. elegans* Exposed to *P. aeruginosa* PA01.a) Proteomics workflow used to analyze *C. elegans* exposed to *P. aeruginosa* PA01. Representative b) MS, c) MS/MS and, d) MS^3 spectra from TMT^6 labeled peptides is shown. The peptide sequence N(TMT^6)ANADIQQWK(TMT^6) belongs to myosin-4 and was selected at *m/z* 766.439 (SCX fraction 8, t_r = 29.46 min), isolated, and fragmented. The fragments produced CID-MS/MS spectra. Next, the b_4 ion at *m/z* 601.490 was isolated, selected, and fragmented, generating HCD-MS^3 spectra. A zoom – in at low *m/z* of this spectra is shown, displaying reporter ions for this fragment. An example mass spectrum from a pooled sample of light (*m/z* 648.856) and heavy (*m/z* 656.900) e) dimethylated labeled D1 OP50 and D1 PA01 samples, respectively, at t_r=62.48 is also shown. The peptide pair corresponds to N(dimethyl)TSLFTNLESTK(dimethyl) of myosin-4.

The spectra in Figure 2.2 are representative of the entire dataset, whereby ~1.6 x 10^6 MS/MS spectra were acquired. These spectra led to the identification of 897 unique proteins (4248 peptides) using the conservative criteria of Peptide to Spectral Match (PSM) ≥2 combined from any two technical replicates (Appendix A Table A2.2). With less conservative filters (PSM>1 across the 4 technical replicates), 1015 unique proteins were identified (Appendix A Tables A2.2 and A2.3).

2.3.3 Dimethylation Labeling Verifies TMT^6-based Identification of Proteins Whose Levels are Altered in PA01 Infection

We employed reductive dimethylation as a complementary means to measure protein expression *(*Figure 2.3)[118] such that in a single analysis (see Experimental) Samples 1 vs. 2 (D1 OP50 vs. D1 PA01) or Samples 3 vs. 4 (D5 OP50 vs. D5 PA01) were compared. Protein samples from one of the biological cohorts were analyzed according to the workflow shown in Figure 2.3.

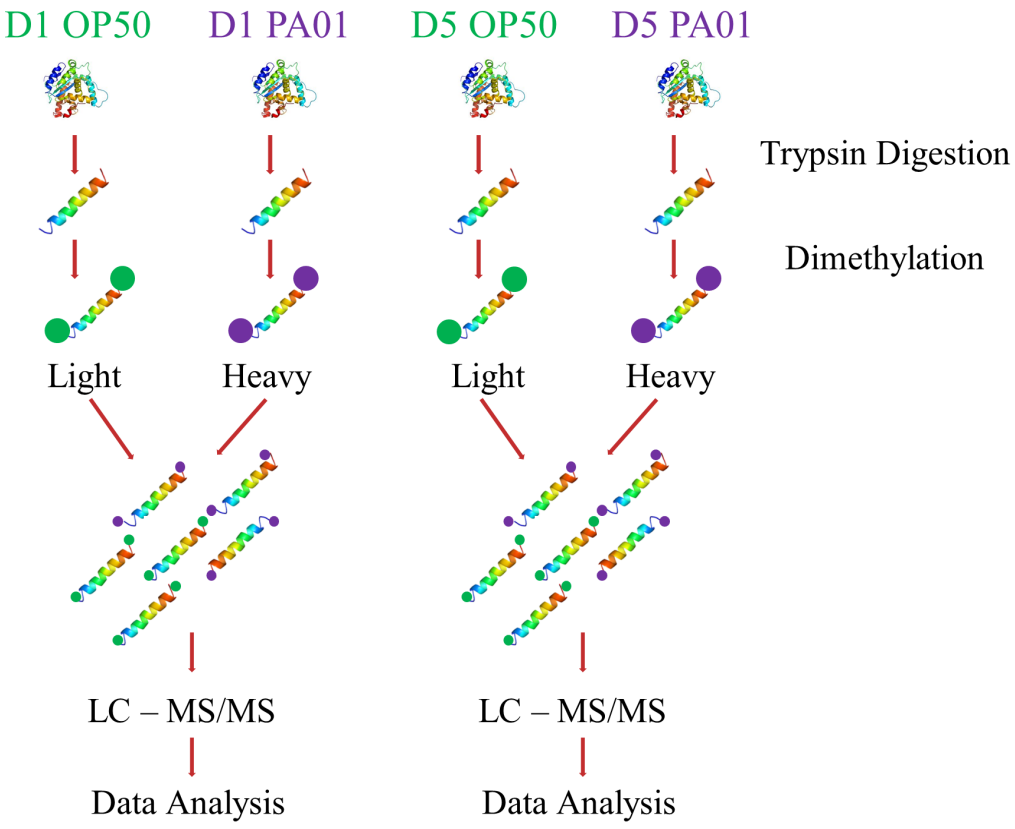

Figure 2.3 Proteomics Workflow using Dimethylation Labeling.

Figure 2.2 provides a sample MS spectrum of a dimethylated peptide pair with the light peak at *m/z* 648.856 and the heavy peak at *m/z* 656.900. These peaks have the sequence N(dimethyl)TSLFTNLESTK(dimethyl) and belong to myosin-4. Similar to the TMT^6 data, this protein was expressed at higher levels (D1 PA01/D1 OP50 = 1.86 ± 0.00) after *P. aeruginosa* PA01 exposure compared to *E. coli* OP50 controls in Day 1 *C. elegans*. The combined dimethylation experiments resulted in the identification of 3125 peptides and 662 proteins (Appendix A Tables A2.4 and A2.5). Overall, from both TMT^6 and dimethylation datasets, 1206 unique *C. elegans* proteins were identified and 462 proteins were common (Figure 2.4a).

We compared the list of proteins with differential levels identified through TMT^6 labeling (Table 2.1) with those found to exhibit differential levels through the dimethylation approach. Eighteen proteins were common between these groups and their PA01/OP50 ratios are shown in Figure 3b. Overall, 13 of the 18 proteins (Figure 2.4b) shared similar changes between the two techniques (i.e., <25% coefficient of variation), enhancing our confidence in the list of proteins that showed differential levels (Table 2.1).

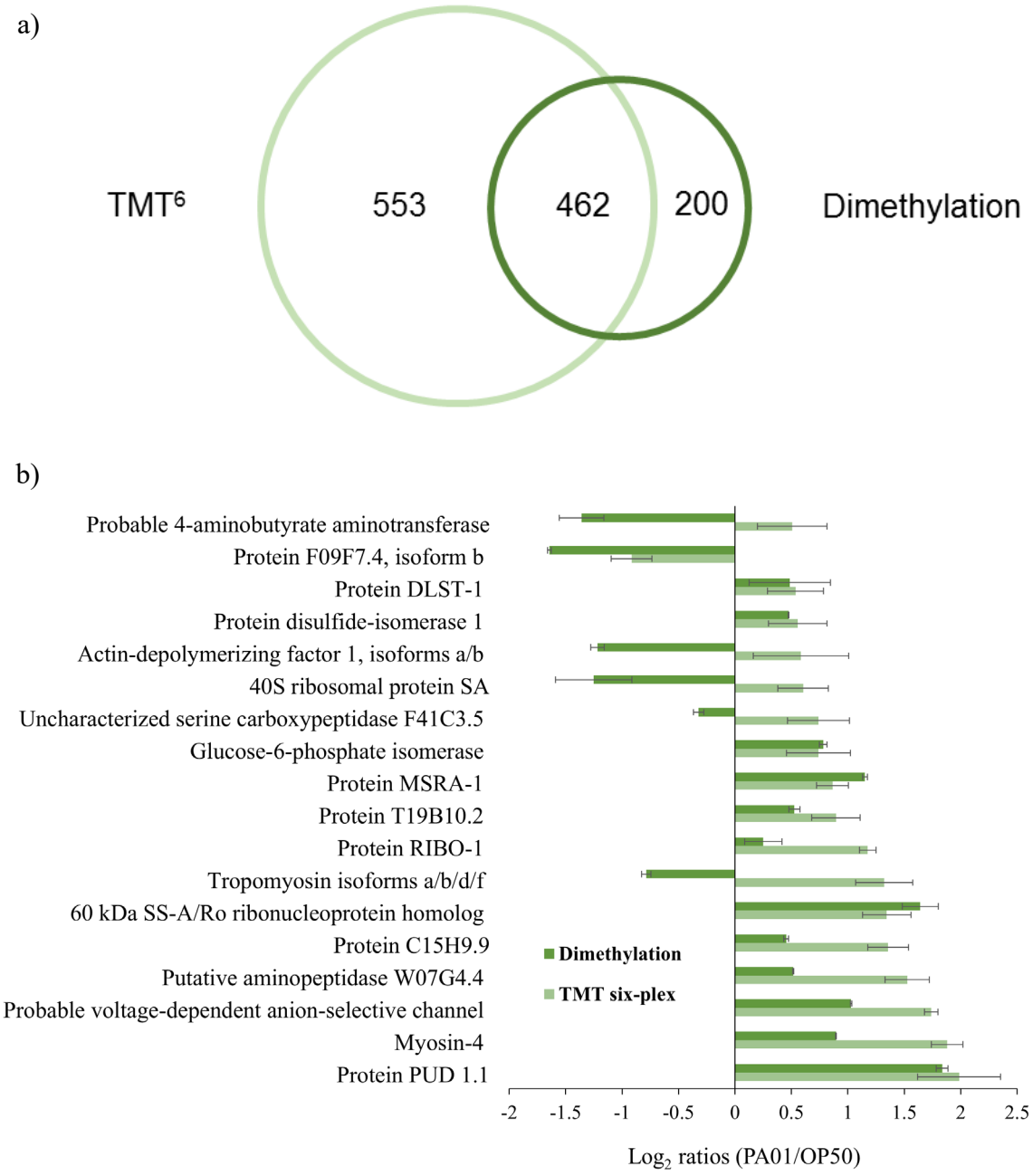

Figure 2.4 Comparisons of Proteins from TMT^6 and Dimethylated-Labeled Peptides. a) Venn diagram of proteins identified in TMT^6 and dimethylation experiments and b) histogram plot of proteins exhibiting differential levels in both TMT^6 and dimethylation experiments. Error bars represent standard error from the mean of the fold change.

2.3.4 Major Biological Pathways Influenced in C. elegans Proteome after Exposure to P. aeruginosa PA01

We performed two gene ontology searches on the list of proteins with differential levels in Day 1 and Day 5 adult *C. elegans* using the STRING database platform (Figures 2.5 and 2.6).[119] Overall, the proteins whose levels changed in response to pathogen (independent of age) included many cytoskeletal and structural proteins mediating myofibril assembly as well as those involved in biological processes such as reproduction, locomotion, stress response, metabolism, protein translation, and development (Table 2.1, Appendix A Table A2.6).

In Day 1 *C. elegans* in particular, significant association was observed with the biological process (Appendix A Table A2.7) generation of precursor metabolites and energy ($P < 0.05$) whereas, in Day 5 *C. elegans* the most significant associations (Appendix A Table A2.8) were with protein folding and stress response, including the unfolded protein response (UPR) and endoplasmic reticulum stress response (UPR^{ER}). As *C. elegans* age, increased protein aggregation occurs and their ability to maintain protein homeostasis declines,[107] and these observations correspond with our findings.

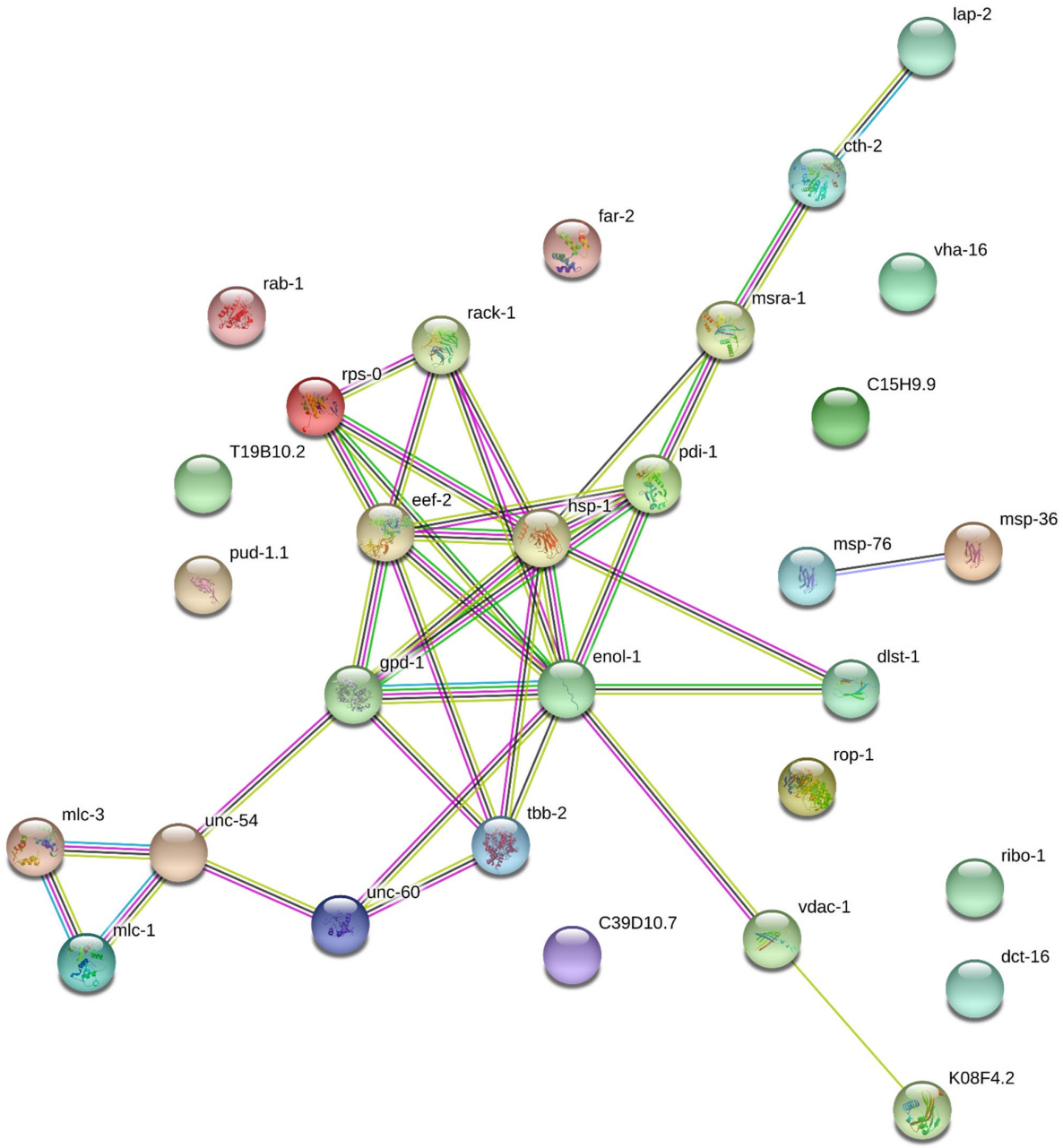

Figure 2.5 Interactions of Statistically – Significant proteins in D1 *C. elegans* Exposed to *P. aeruginosa* PA01.

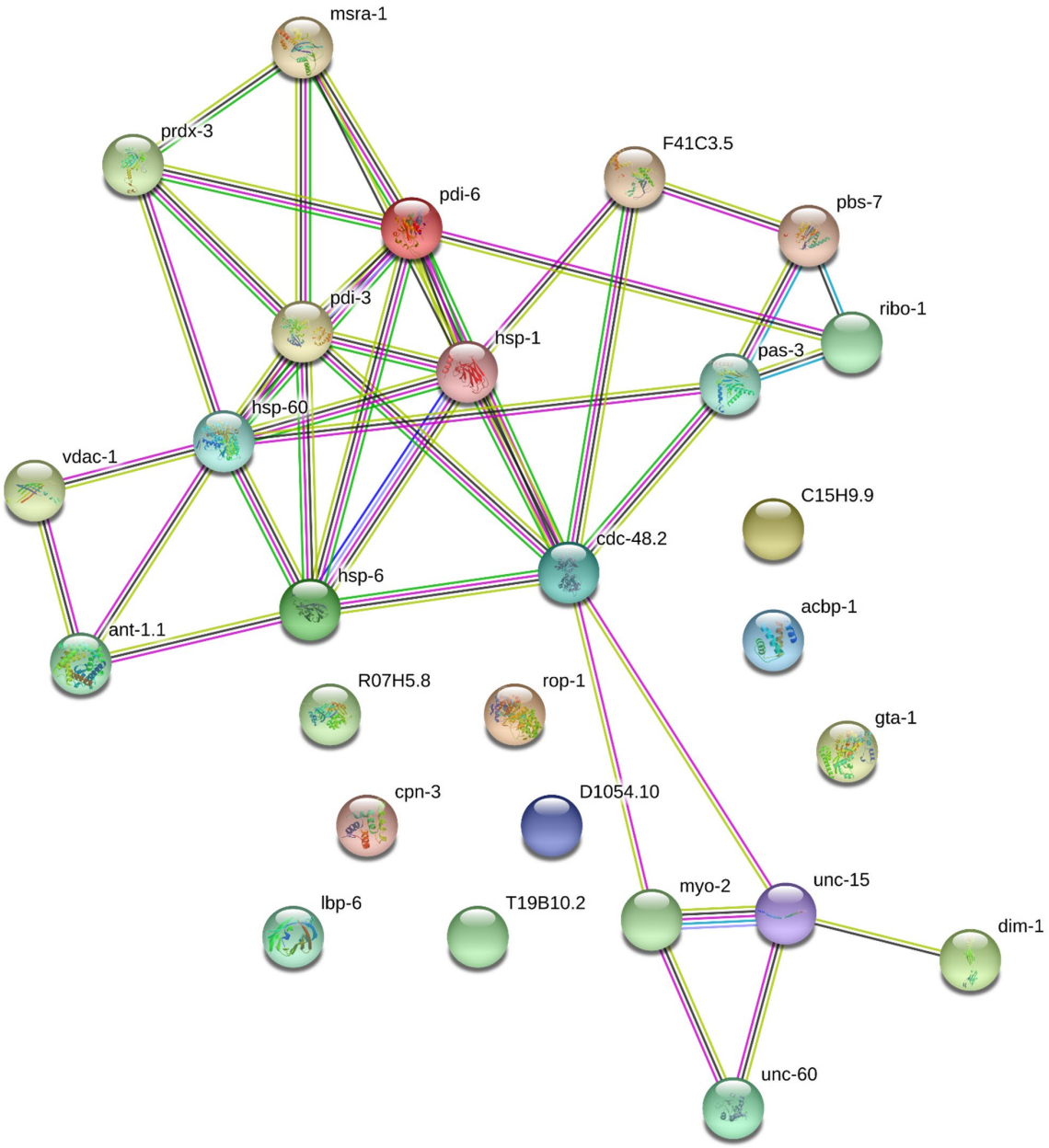

Figure 2.6 Interactions of Statistically – Significant proteins in D5 *C. elegans* Exposed to *P. aeruginosa* PA01.

Table 2.1 Proteins Whose Levels are Altered in *C. elegans* upon *P. aeruginosa* PA01 Exposure

Acc. no.[a]	Gene name[b]	Protein name	Day 1 (PA01/OP50)[c]	Day 5 (PA01/OP50)[c]
G5EET8	*pud-1.2*	Protein PUD - 1.1	**3.96 ± 1.40**	**3.34 ± 1.78**
P02566	*unc-54*	Myosin-4	**3.68 ± 0.49**	**1.24 ± 0.10**
Q27245	*lap-2*	Putative aminopeptidase W07G4.4	**2.88 ± 0.63**	**1.40 ± 0.54**
Q22866	*lev-11*	Tropomyosin isoforms a/b/d/f	**2.50 ± 0.68**	**1.30 ± 0.39**
Q86NC1	*n/a*	Phosphorylase	**2.37 ± 0.39**	**1.15 ± 0.5**
Q21215	*rack-1*	Guanine nucleotide-binding protein subunit beta-2-like 1	**2.34 ± 0.78**	**1.20 ± 0.35**
Q27527	*enol-1*	Enolase	**2.20 ± 0.77**	**1.04 ± 0.31**
Q21351	*gtbp-1*	Protein GTBP - 1	**2.19 ± 0.43**	**2.52 ± 0.73**
P19625	*mlc-1*	Myosin regulatory light chain 1	**2.19 ± 0.14**	**1.11 ± 0.19**
P55216	*cth-2*	Putative cystathionine gamma-lyase 2	**2.05 ± 0.28**	**2.76 ± 1.1**
Q9XX57	*dct-16*	Protein DCT - 16, isoform a	**2.00 ± 0.70**	**2.71 ± 1.5**
G3MU53	*eef-2*	Elongation factor 2	**1.93 ± 0.32**	**0.92 ± 0.64**
P04970	*gpd-1*	Glyceraldehyde-3-phosphate dehydrogenase 1	**1.86 ± 0.61**	**1.18 ± 0.72**
Q95YD5	*vha-16*	Protein VHA - 16	**1.84 ± 0.37**	**n/a**
P53014	*mlc-3*	Myosin, essential light chain	**1.80 ± 0.22**	**0.97 ± 0.44**
Q9UAQ6	*rab-1*	Protein RAB-1	**1.74 ± 0.48**	**1.71 ± 0.85**
P52275	*tbb-2*	Tubulin beta-2 chain	**1.71 ± 0.39**	**0.97 ± 0.32**
Q18529	*n/a*	Protein C39D10.7	**1.56 ± 0.56**	**1.87 ± 0.84**
P46769	*rps-0*	40S ribosomal protein SA	**1.52 ± 0.43**	**1.29 ± 0.81**
Q17967	*pdi-1*	Protein disulfide-isomerase 1	**1.47 ± 0.49**	**2.15 ± 1.31**
O45148	*dlst-1*	Protein DLST - 1	**1.45 ± 0.40**	**0.96 ± 0.84**
P34383	*far-2*	Fatty-acid and retinol-binding protein 2	**1.45 ± 0.31**	**1.58 ± 0.70**
P05634	*msp-10/36/57/76*	Major sperm protein isoforms 10/36/56/76	**0.61 ± 0.04**	**n/a**
Q8MNT7	*n/a*	Protein F09F7.4, isoform b	**0.53 ± 0.11**	**1.27 ± 0.076**
Q21752	*vdac-1*	Probable voltage-dependent anion-selective channel	**3.34 ± 0.24**	**1.78 ± 0.22**
Q18032	*n/a*	Protein C15H9.9	**2.56 ± 0.45**	**2.24 ± 0.63**
Q27274	*rop-1*	60 kDa SS-A/Ro ribonucleoprotein homolog	**2.54 ± 0.61**	**1.90 ± 0.52**
Q9GZH4	*ribo-1*	Protein RIBO-1	**2.26 ± 0.16**	**1.60 ± 0.07**
O02089	*msra-1*	Protein MSRA-1	**1.82 ± 0.23**	**1.48 ± 0.54**
Q9U1Q2	*gpi-1*	Glucose-6-phosphate isomerase	**1.67 ± 0.51**	**2.55 ± 0.84**
H2FLH3	*unc-22*	Protein UNC-22, isoform g	**1.65 ± 0.25**	**2.27 ± 0.36**
Q22562	*n/a*	Protein T19B10.2	**1.48 ± 0.30**	**1.86 ± 0.39**
P09446	*hsp-1*	Heat shock 70 kDa protein A	**1.42 ± 0.33**	**1.81 ± 0.34**
Q07750	*unc-60*	Actin-depolymerizing factor 1, isoforms a/b	**0.54 ± 0.02**	**1.50 ± 0.53**
Q21824	*prdx-3*	Probable peroxiredoxin prdx-3	**0.83 ± 0.23**	**2.97 ± 0.39**
P10567	*unc-15*	Paramyosin	**n/a**	**2.52 ± 0.71**
Q9N599	*pas-3*	Proteasome subunit alpha type-4	**1.22 ± 0.19**	**2.46 ± 0.52**
G5ED07	*pdi-3*	CeERp57	**1.21 ± 0.43**	**2.31 ± 0.45**
Q93934	*n/a*	Protein R07H5.8	**1.08 ± 0.31**	**2.10 ± 0.55**
P90868	*pbs-7*	Protein PBS-7	**1.16 ± 0.26**	**2.08 ± 0.55**
Q18066	*dim-1*	Disorganized muscle protein 1	**1.02 ± 0.13**	**2.04 ± 0.59**
O45865	*ant-1.1*	Protein ANT-1.1, isoform a	**1.43 ± 1.00**	**2.02 ± 0.73**
Q18943	*n/a*	Protein D1054.10	**n/a**	**2.01 ± 0.67**
O01812	*lbp-6*	Fatty acid-binding protein homolog 6	**1.24 ± 0.54**	**1.78 ± 0.44**
P11141	*hsp-6*	Heat shock 70 kDa protein F, mitochondrial	**1.09 ± 0.06**	**1.74 ± 0.62**
O01542	*cpn-3*	Protein CPN-3	**1.13 ± 0.05**	**1.74 ± 0.48**
P12845	*myo-2*	Myosin-2	**n/a**	**1.72 ± 0.17**
P52717	*n/a*	Uncharacterized serine carboxypeptidase F41C3.5	**1.42 ± 0.73**	**1.67 ± 0.51**
O01805	*acbp-1*	Acyl-CoA-binding protein homolog 1	**2.26 ± 1.20**	**1.62 ± 0.52**
Q11067	*tag-320*	Probable protein disulfide-isomerase A6	**1.73 ± 0.79**	**1.61 ± 0.39**
P50140	*hsp-60*	Chaperonin homolog Hsp-60, mitochondrial	**1.02 ± 0.15**	**1.60 ± 0.49**
H9G2R5	*n/a*	Protein F08B12.4, isoform c	**2.46 ± 2.02**	**1.45 ± 0.48**
Q21217	*gta-1*	Probable 4-aminobutyrate aminotransferase, mitochondrial	**2.18 ± 1.15**	**1.42 ± 0.45**
G8JY74	*eef-1.a2*	Protein EEF-1A.2, isoform d	**n/a**	**0.71 ± 0.06**
P54812	*cdc-48.2*	Transitional endoplasmic reticulum ATPase homolog 2	**n/a**	**0.16 ± 0.03**

Proteins were quantified in both biological replicates. N/A indicates missing reporter ions. Bold values indicate changes at differential levels ($P < .05$), with the ratio > 1.4 or < 0.72.

[a] The accession number from the Uniprot *C. elegans* database (11/26/2013, 25,673 sequences).

[b] Gene name from Uniprot.

[c] Mean ± standard deviation values calculated based on reporter ion ratios (PA01/OP50) at Day 1 and Day 5.

2.3.5 PA01 Exposure Elevated Protein Carbonylation in C. elegans

Protein carbonyls are products of metal-catalyzed oxidation of amino acids that are irreversible, unlike reversible oxidative changes that can be transient. Hence, levels of protein carbonylation (PCO) are an indirect but reliable and permanent marker of oxidative stress. Additionally, PCO increases with age in worms as in many other species.[120] Many pathogens, including *P. aeruginosa*, causes increased oxidative stress upon infection. But, whether these stress-responses are similarly affected in animals of different ages is not clear. To examine the permanent, oxidative consequences of PA01 infection in Day 1 and Day 5 *C. elegans*, we measured PCO levels in our samples using immunoblot assays (Figure 2.7). Relative to Day 1 *C. elegans* fed OP50, oxidized PCO levels in Day 1 *C. elegans* after pathogen exposure increases by 16% ($P < 0.05$). We observed, as previously noted, that aging caused higher PCO levels. In Day 5 *C. elegans* fed OP50 compared to Day 1 *C. elegans,* PCO levels were higher by 15% ($P < 0.05$). However, pathogen exposure in Day 5 *C. elegans* did not result in any further increase in PCO levels. Thus, pathogen infection appears to enhance oxidative damage to the animals' proteome that is also exhibited by age, and is not further exacerbated upon infection of older worms.

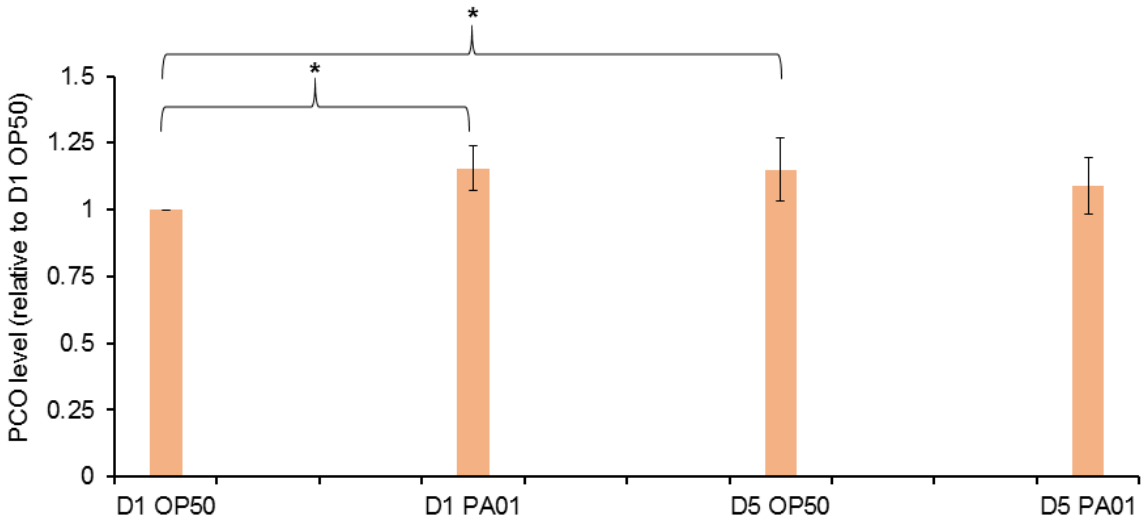

Figure 2.7 Comparisons of Protein Carbonylation (PCO) Levels in Day 1 and Day 5 Adult *C. elegans* Exposed to *P. aeruginosa* PA01 and Aged – Matched Controls.

2.3.6 unc-60 Mutants Have Reduced Lifespan

In our analyses, one protein, UNC-60, exhibited differential levels both as a result of pathogen exposure as well as a function of age (Table 2.1, Appendix Table A2.9). UNC-60 expression decreased with pathogen exposure in Day 1 *C. elegans* (0.54 ± 0.02 on comparing Day 1 OP50 vs. Day 1 PA01) whereas, in Day 5 adults its level was elevated upon pathogen exposure (1.50 ± 0.53). With age, UNC-60 expression increased substantially on *E. coli* OP50 (2.85 ± 0.98 in Day 5 vs. Day 1 adults) and even more dramatically upon PA01 exposure (7.33 ± 2.02 in Day 5 adults on PA01 vs. Day 1 adults on PA01).

UNC-60 is an actin-polymerizing factor, cofilin, that is critical for numerous developmental steps as well as for normal locomotion in adults.[121] Importantly, UNC-60 is required for C. elegans to avoid pathogenic bacteria. UNC-60 knockdown hastens mobility decline in aging animals and limits pathogen avoidance.[122-123] Our data suggested that UNC-60 confers locomotory ability under normal aging conditions, whereas, upon pathogen exposure, its levels may be elevated to facilitate avoidance behavior. We tested this by measuring the lifespan of two *unc-60* mutant strains, CB677 {*unc-60(e677)*} and ON19 {*unc-60(su158)*}. Both mutants exhibited severe whole-body paralysis and sickness[121] and were significantly shorter-lived compared to wild-type controls. CB677 exhibited a mean lifespan of 7.0 ± 0.1 days, whereas, for ON19 lived for 7.3 ± 0.2, as compared to the 18.6 ± 0.2 days mean lifespan of the control population (Figure 2.8, Appendix Table A2.9).

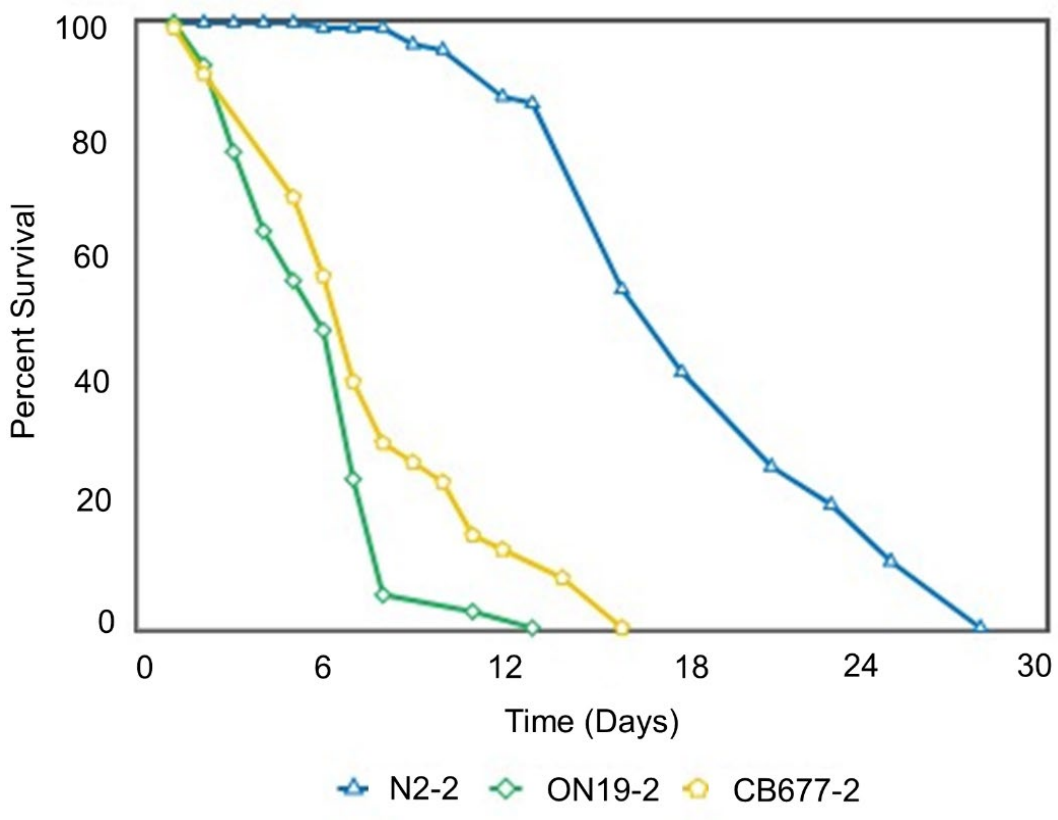

Figure 2.8 Survival Curves of Day 1 Adult *unc-60* Mutants and Control *C. elegans.* Mean lifespans of two loss-of-function *unc-60* mutants compared to wild-type, N2, *C. elegans* grown on standard laboratory diet of *E. coli* OP50 throughout their lives were measured at 20ºC. (blue; m= 18.9 ± 0.1, n= 80/116), ON19 {*unc-60(su158)*} (green; m= 5.9 ± 0.1, n= 38/43, P vs. N2 <0.0001), CB677 {*unc-60(e677)*} (yellow; m= 7.8 ± 0.1, n= 104/119, P vs. N2 <0.0001). Data from additional trials are in Appendix Table A2.9.

The dramatic 60% lifespan reduction seen on normal food itself precluded survival analysis upon pathogen exposure. These observations are in keeping with our proteomics data and other reports that indicate that mutations in *unc-60* reduce the lifespan of WT adult *C. elegans*.

2.3.7 Comparing C. elegans Host Response when Exposed to P. aeruginosa PA01 and Other Pathogens

Several reports have examined the gene- and –protein-expression changes in *C. elegans* as a result of infection by a variety of pathogens.[9, 14, 18, 20-23, 109] These efforts have primarily focused on such changes at the transcriptional level. Proteomics has been used to investigate host-pathogen response for the Gram-positive human pathogen *Staphylococcus aureus (S. aureus),* a pathogenic *Escherichia* strain, *E. coli* LF82[22-23] and recently, *P. aeruginosa* PA01.[25, 103] Transcriptomic studies have also been performed on the canonical pathogenic *P. aeruginosa* strain PA14, a human clinical isolate.[14, 18] We anticipated that there would have been higher overlap of our changes with those from the other *P. aeruginosa* PA01 study which examined exposure at time intervals such as 12, 24, and 48 hours in Day 1 adult *C. elegans*.[24]

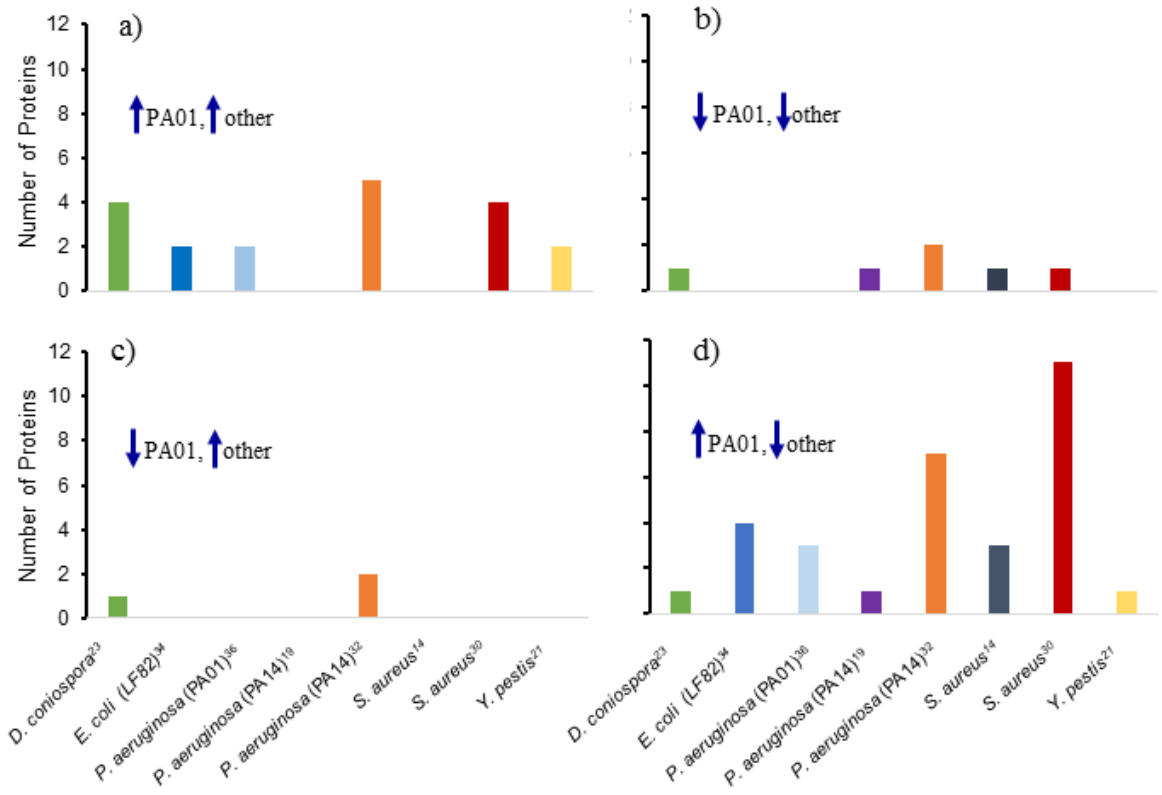

Figure 2.9 Comparison of Differentially – Expressed genes/proteins from this Study to other Pathogenicity Studies. The bar graph shows the number of shared proteins/transcripts present at differential levels from *P. aeruginosa* PA01 and other pathogens. The quadrants represent categories of proteins with, a) higher levels in *P. aeruginosa* PA01 exposed *C. elegans* as well as the other pathogen(s), b) lower levels in *P. aeruginosa* PA01 and in the other pathogen(s), c) lower levels in *P. aeruginosa* PA01 in our study and higher levels in the other pathogen(s), d) and higher levels in *P. aeruginosa* PA01 while lower in the other pathogen(s).

Two proteins (i.e. disorganized muscle protein and receptor of activated protein c kinase 1) had consistent direction of change between both studies and showed higher differential levels (Figure 2.9a), whereas three proteins (i.e. elongation factor 2, fatty-acid binding protein homolog 6, and pud 1.1) had an opposite direction of change (Figure 2.9d). Interestingly, the study with the highest degree of overlap was with gene-expression changes reported when *C. elegans* was exposed to *S. aureus*[22] ($P < 4.89 \times 10^{-20}$). We next compared our list of proteins exhibiting differential levels in our study with the proteins identified in other proteomic analyses of *C. elegans* exposed to various types of pathogens (i.e. Gram-negative or Gram-positive bacteria or fungi) (Figure 2.9) [9, 14, 20-23, 25, 109] We found that eighteen proteins whose levels were elevated after pathogen exposure in our study (Figure 2.9a) and six whose levels were diminished (Figure 2.9b), were also found to exhibit similar changes in one or more of the other studies. Only three proteins' levels were reduced upon PA01 exposure in our study but showed higher levels upon pathogen attack in other reports (Figure 2.9c). These results are promising and suggested that some responses to infection are not pathogen specific. The highest degree of overlap (i.e. 27 unique proteins) occurred however, for proteins elevated in the presence of PA01 in our study but lowered levels in the presence of other pathogens (Figure 2.9d). For example, 11 proteins had higher levels after *P. aeruginosa* PA01 exposure in our study but were reduced upon *S. aureus* infection[22] suggesting that worms mount pathogen-specific responses that may involve up- or down-regulation of the same protein dependent upon the pathogen involved. These comparisons substantiated the presence of both general and pathogen-specific responses in the *C. elegans* adult proteome.

2.4 DISCUSSION

Previously, we have demonstrated that age influences the acute response to infection in elderly individuals suffering from community-acquired pneumonia that eventually develop severe sepsis.[115] The human proteome has dynamic changes in response to these infections and the changes are age-related, mostly involving mechanisms related to lipid metabolism, inflammation, and acute-phase response.[115] Despite the considerable differences in size, number of cells, and inherent complexity of the immune system, *C. elegans* has become a valuable model to study host-response to pathogens, especially to understand changes in innate immunity.[124-126] *P. aeruginosa* PA01 is a slow killing, Gram-negative bacterial strain implicated in human infections such as sepsis and pneumonia.[127] Our proteomic studies measure the influence of aging on *C. elegans* exposed to *P. aeruginosa* strain PA01 using shotgun quantitative proteomics techniques. We aged *C. elegans* to Day 1 or day 5 in adulthood, exposed them to pathogen, and then harvested *C. elegans* at 18 hours. The time-point of 18 h was selected to maximize observance of changes related to infection. Minimal media was used to introduce *P. aeruginosa* PA01 to *C. elegans*; this "slow-killing" assay leads to the accumulation of pathogen in the intestine through quorum sensing.[128-130] Hydrogen cyanide is released from *P. aeruginosa* PA01, paralyzes *C. elegans*, and leads to lethal toxicity.[128, 131] Herein, survivorship of *C. elegans* fed on NGM containing *P. aeruginosa* PA01 was significantly lower (i.e., LT_{50} = ~7-10 days compared to 18-20 days) than control *C. elegans* fed on *E. coli* OP50 media which is generally consistent with other studies.[17, 132] However, worms in our study survived longer on *P. aeruginosa* PA01 compared to previous reports.[17, 132] These differences in survivability could be directly related to the upkeep of *C. elegans*; for instance, we plated *C. elegans* to fresh media containing pathogen

every other day. Initial mortality of *C. elegans* exposed to *P. aeruginosa* PA01 differs by several days for Day 1 and Day 5 *C. elegans*. Day 1 *C. elegans* have a lag time of several days prior to large percentages of the population dying whereas Day 5 *C. elegans* began to die more immediately upon *P. aeruginosa* PA01 exposure. This substantiates previous evidences that age diminishes *C. elegans*' ability to effectively fight off the pathogen attack. However, after this period pathogen exposure does not have a long-term effect on the aging of *C. elegans*, as in our experiments Day 1 and Day 5 *C. elegans* exposed to *P. aeruginosa* PA01 have similar lifespans. This is likely due to differences in the innate response of young *C. elegans.*

2.4.1 Pathogen-induced Proteomic Changes in Day 1 and Day 5 Adults are Overlapping but Distinct

As *C. elegans* age, several proteomic and physiological changes occur, including structural disintegration,[107] protein aggregation,[107] and immunosenescence. In order to determine how aging influences the response to infection, we exposed Day 1 and Day 5 adult *C. elegans* to *P. aeruginosa* PA01 for 18 hours and examined their proteomes. We observed that there are general responses to infection that are not age-specific however, a few biological pathways are unique to a given age (Figure 2.10).

The proteome of Day 1 *C. elegans* exposed to *P. aeruginosa* PA01 is notably enriched for developmental and reproduction functions (Appendix A Table A2.7). This is intuitive as Day 1 *C. elegans* are completing larval stage 4 development and commencing egg laying. Cytoskeletal proteins and locomotion were significantly represented in both Day 1 and Day 5 *C. elegans* after pathogen exposure. At Day 5, worms are actively mobile and our data underscores

the importance of pathogen-avoidance behavior for immunological defense in worms during both young and middle-ages.

In Day 5 *C. elegans,* protein folding/unfolding and stress response pathways such as UPR and UPR^{ER} were significantly enriched along with metabolic functions. Upon pathogen exposure, Day 5 adult *C. elegans* elicit an elevated stress response to infection that is not observed in *C. elegans* on OP50. Specifically, we observe elevated levels of heat shock proteins (HSPs) after PA01 exposure. HSPs are chaperones that assist in protein folding,[133] removal of improperly folded proteins,[134] and stress response. Activation of HSPs after pathogen exposure and in aging is evolutionarily conserved, including in worms[135] and is known to occur in other stressful conditions such as oxidative stress[136-137] and after the onset of inflammatory diseases.[138-140] The combination of proteins being produced in response to stress and that are involved in metabolism, show a concerted effort from Day 5 *C. elegans* to counter the effects of pathogen – exposure and elicit an immune response.

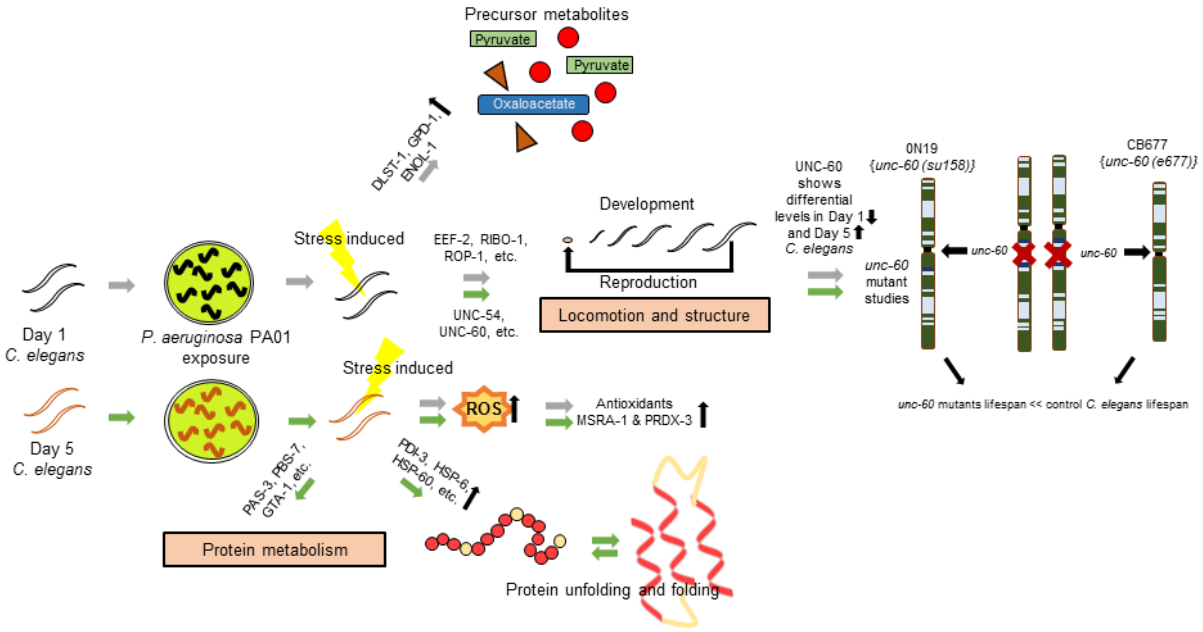

Figure 2.10 Scheme of Day 1 and Day 5 *C. elegans*' Response to *P. aeruginosa* PA01 Exposure. Day 1 (black) and Day 5 (orange) *C. elegans* were exposed to *P. aeruginosa* PA01, resulting in general and age-specific changes. Day 1 adult *C. elegans* (grey arrows) had an increase in the generation of metabolic precursors and energy while Day 5 adult *C. elegans* (green arrows) had significant changes related to protein metabolism and protein folding/unfolding. Both age groups had changes related to development, reproduction, locomotion, and structure. The loss of actin-polymerizing protein, UNC-60, reduces *C. elegans* lifespan and antioxidants MSRA-1 and PRDX-3 reduce increased levels of ROS.

2.4.2 Mutations in unc-60 Reduce Lifespan

Both myofiber structural integrity as well as locomotive ability decline with aging in worms as in humans.[141] Interestingly, one proteins whose levels were altered by both age and pathogen exposure, though oppositely, was the cytoskeletal protein, UNC-60. UNC-60 is an actin-binding structural protein that mediates actin filament depolarization and is expressed in two, tissue-specific isoforms. Since UNC-60 was present at differential levels in both Day 1 and Day 5 aged *C. elegans* exposed to *P. aeruginosa* PA01 (see Results section above), we were interested in how the loss-of-function and protein expression of *unc-60* may alter *C. elegans*' lifespan. Survival curves of mutants CB677 {*unc-60(e677)*} and ON19 {*unc-60(su158)*} unveiled significant decreases in *C. elegans*' lifespan, in comparison to the lifespan of control *C. elegans*. Interestingly, the lifespans of both mutants were similar, even though ON19 is considered to be the more severe mutant.[121] Since UNC-60 is necessary for proper actin assembly in myofibrils,[121, 142] the absence of this protein decreases *C. elegans*' mobility and ability to obtain food, thus causing a premature death. Indeed, the mutants exhibited such a dramatic lifespan shortening under normal conditions that it precluded examining their survival in the presence of PA01. It can be inferred that upon pathogen exposure, similar or even more severe results would be yielded, as *C. elegans* would be unable to avoid the pathogen.

2.4.3 P. aeruginosa PA01 Exposure Causes Elevated Carbonylation of Worm Proteome

The presence of reactive oxygen and nitrogen species, and hence oxidative stress, is known to increase in aging organisms.[143] Antioxidants are critical in immune response as they

help protect against toxic species elicited from defense mechanisms and from the pathogen directly.[144-145] In this study, antioxidant proteins peroxiredoxin-3 (PRDX-3) and methionine sulfoxide reductase 1 (MSRA-1) were elevated in Day 5 *C. elegans* exposed to *P. aeruginosa* PA01 and between Day 1 and Day 5 *C. elegans*, respectively. Elevation of PRDX-3 suggests activation of antioxidant pathways in response to oxidative stress (Table 2.1, Figure 2.8). MSRA-1 levels have been shown to decrease with aging in wild-type *C. elegans*[146], however, our results show higher levels of this protein after pathogen exposure (Table 2.1). This change is supportive of an environment where *C. elegans* is warding off reactive oxygen and nitrogen species through an increased antioxidant response. Elevated levels of protein carbonyls (an indirect marker of oxidative stress) in Day 1 *C. elegans* upon pathogen exposure were observed in this study, very much consistent with the idea that ROS/RNS increases due to *P. aeruginosa* PA01.

Inflammatory processes, antimicrobial activity, and innate immune responses to toxins lead to excess production of reactive oxygen and nitrogen species. However, in Day 5 *C. elegans* the exposure to pathogen did not result in any enhanced levels of oxidative stress. This observation suggests that by Day 5, worms were already experience increased oxidative stress which is not further exacerbated by PA01 infection (Figure 2.11).

2.5 CONCLUSIONS

This study provides new and significant insights into how the proteome of *C. elegans* changes upon *P. aeruginosa* PA01 exposure at different adult ages. Pathogen exposure results in

significant alterations in metabolism, development, reproduction, stress response, protein folding/unfolding, and locomotion pathways. Many of these pathway changes are not unique to *P. aeruginosa* PA01 and are observed at the transcript or protein level when *C. elegans* are exposed to other Gram-negative and Gram-positive pathogens. However, we were able to observe a number of proteins that appear to have *P. aeruginosa* PA01-pathogen specific changes. Additionally, it is clear that the specific pathways that are activated in the proteome in response to pathogen depend on the age of the worms. Day 1 *C. elegans* have general alterations and do not have the confounding effects of aging that can limit their response to the pathogen. Initial survivability of Day 1 *C. elegans* is maintained for a longer period compared to Day 5 *C. elegans* prior to death after *P. aeruginosa* PA01 exposure. It will be very interesting to determine if these and other virulence-related factors identified in our study can be modulated to extend survivability of aged *C. elegans* after pathogen exposure.

3.0 PROTEOMICS ANALYSIS OF VIRULENCE-RELATED FACTORS IN YOUNG AND AGING C. *ELEGANS* EXPOSED TO *PSEUDOMONAS AERUGINOSA* PA01- PART 2*

(*please note, contents of this Chapter are related to the following publication: "King, C.D; Singh, D.; Holden, K.; Govan, A.B.; Keith, S.A.; Ghazi, A., Robinson, R.A.S. *Data in Brief*, **2016**)[147]

3.1 INTRODUCTION

In **Chapter 2**, young and aging *C. elegans* were exposed to an opportunistic pathogen, *P. aeruginosa* PA01 to understand how aging influenced the response of *C. elegans* to infection. These experiments were performed on an LTQ Orbitrap Velos mass spectrometer, which offered high resolution, fast scan rates, and improved fragmentation spectra compared to other state-of-the-art MS instruments.[148] However, only ~1,000 proteins were identified with the use of this instrument in our proteomics platform. The LTQ Orbitrap Velos was upgraded to an Orbitrap Elite mass spectrometer and *C. elegans* samples were re-analyzed in order to take advantage of instrumental improvements. The Elite was improved from the LTQ Orbitrap Velos by including a neutral blocker, enhanced fourier transform (eFT) technology, and a smaller size Orbitrap. These improvements increased the resolution of the instrument to 240,000 and reduced scanning

speeds to 250 ms (Orbitrap) and ~100 ms (ion trap). Samples were prepared in a similar fashion as in **Chapter 2**, except only one biological cohort was applied. Protein from young and aging *C. elegans* exposed to *P. aeruginosa* PA01 and aged-matched controls were digested using trypsin. Peptides were labeled with TMT^6-plex isobaric reagents and fractionated off-line with SCX. Fractions were analyzed by LC – MS/MS and MS^3 and RAW files were searched using PD.

3.2 EXPERIMENTAL PROCEDURES

3.2.1 Protein Digestion

Protein was purified using acetone precipitation and the amount of protein was re-determined with BCA assay. Protein (~80 – 100 µg) was denatured with an extraction buffer (0.2 M Tris, 8 M urea, 10 mM $CaCl_2$, pH 8.0), reduced with 1:40 molar excess of dithiothreitol (DTT) for 2 h at 37 ºC, and then alkylated with 1:80 molar excess of iodoacetamide (IAM) for 2 h on ice. The alkylation reaction was quenched by adding 1:40 molar excess of cysteine and the mixture was incubated at room temperature for 30 min. Tris buffer (0.2 M Tris, 10 mM $CaCl_2$, pH 8.0) was added to dilute the urea concentration to 2 M. Each sample was incubated with bovine TPCK-treated trypsin (Sigma–Aldrich) at 50:1 substrate/enzyme ratio for 24 h at 37 ºC.

3.2.2 TMT Labeling

Digested samples were desalted with an HLB cartridge and dried by centrifugal evaporation. Each sample was labeled with a TMT^6-plex reagent following the manufacturer's protocol (Thermo Scientific). TMT^6 reagents were equilibrated to room temperature, solubilized with 41 µL of acetonitrile, and transferred to peptide samples reconstituted in triethylammonium bicarbonate (TEAB) buffer. After 1 h of incubation (~25 ºC), the reaction was quenched using 5% hydroxylamine. Equimolar amounts of samples were combined such that reagents that generate reporter ions at *m/z* 126:127:128:129:130 correspond to D1 OP50, D1 PA01, D5 OP50, D5 PA01, and the pooled sample, respectively.

3.2.3 Offline SCX Fractionation

SCX fractionation was performed on a PolySulfoethyl A 100 mm x 2.1 mm, 5µm, 200 Å column (The Nest Group, Inc.) with buffers as follows: mobile phase A was 5 mM monopotassium phosphate (25% v/v acetonitrile, pH 3.0), and mobile phase B was 5 mM monopotassium phosphate, 350 mM potassium chloride (25% v/v acetonitrile, pH 3.0). Dried TMT^6– labeled samples were re-suspended in 200 µL of mobile phase A and injected onto the column. The gradient was as follows: 0 – 5 min, 0% B; 5 – 45 min, 0 – 40% B; 45 – 90 min, 40 – 80% B; 90 – 100 min, 80 – 100% B; 100 – 110 min, 100% B; 110 – 121 min, 0% B. Eluent was collected every minute and combined into 20 fractions. Each fraction was desalted using Supel-Tips C18 micropipette tips (Sigma – Aldrich). Fractions were solubilized in 50 µL and filtered with a 0.45 µm filter (Thermo Fisher Scientific).

3.2.4 LC – MS Analyses

Online desalting and reversed-phase chromatography was performed with a Nano liquid chromatography (LC) system equipped with an autosampler (Eksigent). Mobile phases A and B used for reversed phase (RP)-LC separation of peptides were 3% (v/v) acetonitrile with 0.1% formic acid and 100% acetonitrile with 0.1% formic acid, respectively. SCX fractions (10 µL) were loaded onto a trapping column (100 µm i.d. x 2 cm), which was packed in house with C_{18} 200 Å stationary phase material (Michrom Bioresource Inc,) at 3 µL/min in 3% mobile phase B for 3 min. After desalting, the sample was loaded onto an analytical column (75 µm i.d. x 13.2 cm) which was packed in-house with C_{18} 100 Å 3 µm stationary phase material (Michrom Bioresource Inc). The gradient was as follows: 0 – 7 min, 10% mobile phase B; 7 – 67 min, 10 – 30% B; 67 – 75 min, 30 – 60% B; 75 – 77 min, 60 – 90% B; 77 – 82 min, 90% B; 82 – 83 min, 90 – 10% B; 83 – 95 min, 10% B. The LC eluent was analyzed with positive mode nanoflow electrospray using a LTQ Orbitrap Elite mass spectrometer (Thermo Fisher Scientific). Data-dependent acquisition parameters were as follows: the MS survey scan in the Orbitrap (300 – 1800 *m/z*) was 120,000 resolution; the top seven most intense peaks were isolated and fragmented with collision-induced dissociation (CID) in the LTQ (normalized collision energy of 35%). Directly after each tandem MS/MS scan, the most intense fragment ion over the m/z range 200 – 1545 was selected for higher-energy collisional dissociation (HCD) triple staged mass spectrometry (MS^3). The fragment isolation width was set to 4 *m/z*, the MS^3 AGC was 3 x 10^5, the normalized collision energy was 60%, the resolution was 7,500 and the maximum ion time was 250 ms. HCD spectra were recorded in the Orbitrap. Each fraction was subject to duplicate injections.

3.2.5 Data Analyses

RAW files were analyzed with PD 2.1 software (Thermo Scientific) and searched against the Uniprot *C. elegans* database (25,673 sequences). SEQUEST search parameters were as follows: two maximum trypsin mis-cleavages, precursor mass tolerance of 10 ppm, fragment mass tolerance of 0.8 Da; static modifications were TMT six-plex/+229.163 Da (N-terminus, Lys) and carbamidomethyl modification/+57.021 Da (Cys); dynamic modification was oxidation modification/+15.995 Da (Met). Decoy database searching was employed to generate medium ($p<0.05$) and high ($p<0.01$) confidence peptide lists. All the peptides with medium and high confidence were used to identify and quantify proteins. To filter peptides, the following parameters were applied: peptide confidence level of medium or high, peptide rank of 1, and peptide deviation of 10 ppm. Peptides with a PSM (peptide to spectral match) count of 1 were not considered for analysis. The reporter ions (i.e. *m/z* 126 – 130) were identified with the following parameters: most confident centroid and 20 ppm for reporter ion mass tolerance. Furthermore, reporter ion values were normalized 126/130, 127/130, 128/130, and 129/130 and final ratio reporting given as 127/126 and 129/128. Proteins belonging to multiple isoforms were grouped into a single accession number and final ratios were reported.

3.3 RESULTS AND DISCUSSION

In this experiment, *C. elegans* samples from one biological cohort were analyzed using quantitative proteomic techniques to obtain more information about aging and infection.

Previously obtained samples (Figure 3.1) were digested using trypsin, labeled using TMT^6-plex and analyzed using LC – MS/MS and MS^3. To obtain MS information, an Orbitrap Elite MS was used instead of applying an Orbitrap Velos.

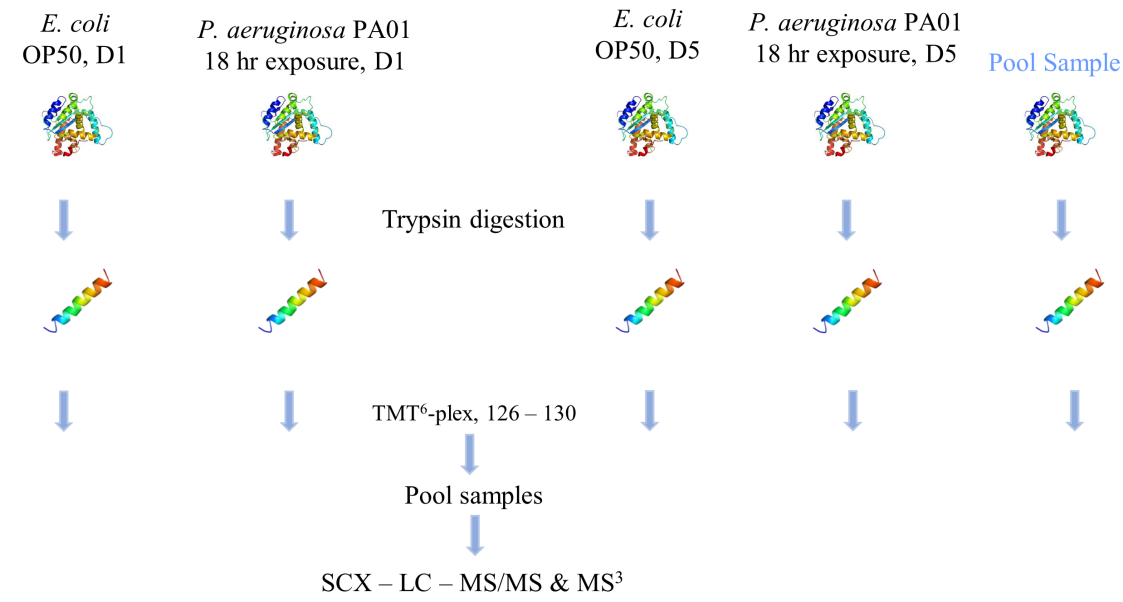

Figure 3.1 Experimental Workflow of Young and Aging *C. elegans* Exposed to *P. aeruginosa* PA01.

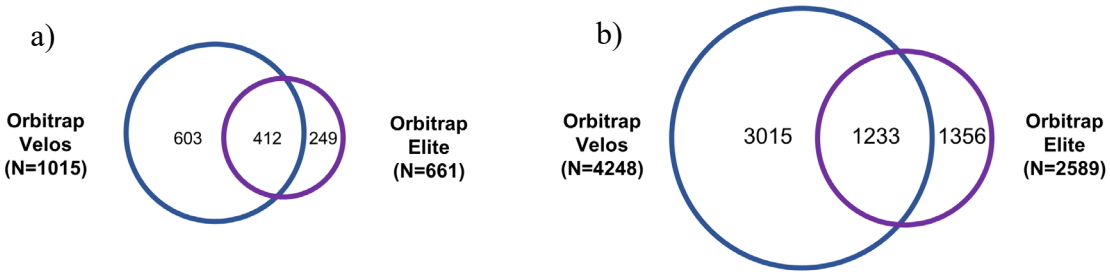

Figure 3.2 a) Protein and b) Peptide Overlap across Orbitrap Velos and Orbitrap Elite Platforms.

From this analysis, 12215 PSMS, corresponding to 2589 unique peptides (Appendix B Table B3.1) and 836 proteins were identified. This number was reduced to 661 proteins when a PSM filter of >1 is applied (Appendix B Table B3.2). Between both datasets, 412 proteins and 1233 peptides were shared across instruments (Figure 3.2); this corresponds to ~40 and 60% of proteins and 29% and 47% of peptides in the Orbitrap Velos and Elite, respectively.

In terms of protein quantification, 416 proteins (i.e. 62%) were quantified in all ratio groups (i.e. 126/130, 127/130, 128/130, and 129/130). In comparison, using a stringent filter (≥2 PSMs per technical replicate) in the Orbitrap Velos data-set (N=897 proteins), 288 proteins (~32%) were quantified. A dramatic increase (~100%) of proteins were quantified between the two instruments. Since one biological cohort was used in the Elite data-set, proteins were not analyzed for statistical – significance; however, general trends about quantified proteins were made.

Among proteins only identified from the Elite (i.e. 249), 134 (i.e. 54%) were also quantified across all ratio groups. Using established fold-change values of >1.4 and <0.7 (**Chapter 2**), quantified proteins that met this criteria were involved in similar biological processes (Appendix B Tables B3.3 – B3.5) as proteins differentially – expressed in **Chapter 2**. Processes related to development, translation, metabolism, reproduction, and cell organization were identified in both young- (D1) and aging (D5) adult *C. elegans* exposed to *P. aeruginosa* PA01 at lower levels (D1 *C. elegans*) or at higher and lower levels (D5 *C. elegans).* Interestingly, proteins related to translation and cell-redox homeostasis were quantified at lower levels in both D1 and D5 *C. elegans* and at higher levels in D5 *C. elegans,* respectively. Within proteins identified across both data-sets (i.e. 412), 123 (i.e. 30%) were also quantified. Protein levels were similar (CV < 0.33) for 51 (i.e. 41%) and 74 (i.e. 60%) proteins in D1 and D5 *C.*

elegans and 28 proteins differentially – expressed in Chapter 2 (i.e. 51%), were also quantified in Elite data-set (Appendix B Table B3.6). This list of proteins included those involved in heat-shock response, protein folding, and metabolism.

Overall, results from data acquired on the Elite MS showed a decrease in proteins identified but an increase in the number of proteins quantified. Decreases in protein identifications are related to analyzing one biological cohort and experimental error. Since one biological cohort was analyzed, it was expected that the overlap between proteins identified and/or quantified across instruments would be lower. In addition, inefficient sample loading may have also contributed to decreased protein identifications. An increase of quantified proteins in the Elite, however, is due to improved instrumental parameters. Faster scan rates and higher sensitivity on the Elite allows more duty cycles to be performed, thus obtaining more quantitative spectra. In addition, the overlap between proteins identified across both instruments shows the ability to reproduce similar datasets across different Orbitrap instruments while the identification of proteins specific to the Elite displays instrument variability.

3.4 CONCLUSIONS

The Elite has many advantages of other Orbitrap hybrid instruments and lower resolution systems including its faster scan rate, higher resolution and improved ion optics. Though usage of this instrument did not increase protein identifications, it provided insight about novel and similar proteins identified previously in **Chapter 2**. It also highlighted the potential benefits of using this instrument for future applications. Addressing issues related to low biological replicate

sampling and experimental error will improve peptide and protein identifications and quantifications in future experiments.

4.0 EVALUATING cPILOT PERFORMANCE OF ORBITRAP INSTRUMENTS TO STUDY THE PERIPHERAL PROTEOME OF ALZHEIMER'S DISEASE

4.1 INTRODUCTION

Alzheimer's disease (AD) is both a neurodegenerative and metabolic disease, characterized by the main pathogenic hallmarks such as senile plaques and the deposition of amyloid beta (Aβ) plaques and neurofibrillary tangles composed of hyperphosphorylated tau. Other features of this disease include metabolic dysfunction,[149] insulin resistance,[150-151] and lower cerebral glucose metabolism.[152] While AD affects the brain, it also has implications in peripheral organs. For example, cardiovascular disease[28, 153-155] is a major risk factor for AD, as well as others such as type-2 diabetes, hypertension, obesity and high cholesterol. These comorbidities suggest that peripheral organs may contribute to disease pathogenesis, therefore a comparative analysis of heart tissues, to others implicated in AD pathogenesis (e.g. brain and liver) may give insight into how these tissues contribute to AD pathogenesis. Specifically, performing an analysis of brain, heart, and liver tissues from 14-month-old amyloid precursor protein/presenilin 1 mice (APP/PS-1) would be beneficial. APP/PS-1, hereafter is referred to as (AD) mice, are a double transgenic strain with mutant APP^{swe} and $PS1^{de9}$ genes.[156] This model presents many aspects of AD, including the formation and aggregation of amyloid-beta plaques and cognitive decline.[157] This model has been used broadly in proteomics to gain insight into the

pathogenesis of AD [84, 158-160] and our laboratory has initial studies in peripheral tissues such as the liver.[2]

Multiplexing becomes an effective approach to study the proteome across tissues. This technique is used within quantitative proteomics to increase sample throughput by analyzing several samples simultaneously in a single MS analysis. Multiplexing can occur at the protein or peptide level and may be executed by metabolic, enzymatic, or chemical reactions. These reactions incorporate unique fluorescent tags[161-162] or heavy isotopes into proteins or peptides from multiple samples, which are pooled and detected by flow cytometry or mass spectrometry. The two major groups of techniques used to multiplex in MS are isotopic labeling and isobaric tagging. Isotopic labeling allows up to five samples to be analyzed simultaneously in cells[71] with stable isotopic labeling with amino acids in cell culture (SILAC) or in mammals with stable isotopic labeling with amino acids in mammals (SILAM).[72] Other techniques incorporate heavy isotopes into proteins with isotope protein coded labels (IPCL)[163] or ^{18}O exchange,[164] or in peptides with acetylation[165] or dimethylation.[71] Isobaric tagging chemically labels proteins or peptides with a tag that, upon fragmentation, provides a unique reporter ion at lower *m/z* values, with an intensity corresponding to the protein concentration. Tandem mass tags (TMT),[77] isobaric tag for relative and absolute quantitation (iTRAQ),[166] and N,N-Dimethyl Leucine (DiLeu)[79] tags can analyze as little as two or four samples, or up to as many as 11- 12- and 21-plex analyses.[167-168] Using these multiplexing strategies has provided insight into disease-state pathology,[84] drug-target studies, and kinetics-based experiments.

Our laboratory[83] and others[74, 86, 88, 91] have pushed the limits of multiplexing with enhanced multiplexing approaches. Combined precursor isotopic labeling and isobaric tagging (cPILOT) uses amine-based chemistry to chemically label N-termini of primary amines and

lysine residues of peptides.[83] The flexibility of this method can be adapted to study oxidative post-translational modifications such as 3-nitrotyrosine, S-nitrosylation, and cysteine-containing peptides.[85, 89] In order to maximize the number of quantified peptides and broaden the types of analyses that can be studied, different sample preparation strategies and data acquisition methods were developed on the LTQ Orbitrap Velos MS instrument. Gas-phase fractionation, two-tiered DDA in MS acquisition, and MS^3 fragmentation were employed to increase the number of dimethylated pairs and reporter ion channels detected and accurately quantified.[116] However, there are some limitations of conducting a cPILOT analysis on an Orbitrap Velos MS. A major challenge is obtaining quantitative information for large numbers of dimethylated pairs and for detecting signal for all reporter ion channels used. One strategy to improve this was to use selective y_1-fragmentation[80] of MS/MS fragments for MS^3. Another strategy is to increase the MS/MS and MS^3 signal by using newer Orbitrap Tribrid instruments[169-170] (Orbitrap Fusion and Orbitrap Fusion Lumos) for MS^3 quantification.[80] These instruments provide multi-notch MS^3 called synchronous precursor selection (SPS), which allows for multiple MS/MS fragment ions to be selected and fragmented, significantly increasing the reporter ion signal.[171] Multi-notch MS^3 increases the number of quantifiable peptides and overall information available about relative protein changes across different samples.

In addition to SPS, the Fusion Lumos has several functions that should improve cPILOT-analysis including faster scan rates, top speed or top N data dependent acquisition options, and targeted mass analysis. The goal here was to evaluate and optimize MS acquisition parameters for cPILOT on a Fusion Lumos and compare data for the same samples on the Orbitrap Velos to Fusion Lumos instruments. Optimized data analysis parameters for cPILOT-labeled peptides on this platform was developed for a system-wide proteomics analysis of AD. Specifically, LC

gradient time, *m/z* isolation window, dynamic exclusion time, targeted analyses nodes, and SPS-n were tested on fractionated and unfractionated samples. An optimized method was applied an AD mouse model to study disease pathogenesis across the brain and periphery (i.e. liver and heart). Protein from six biological replicates of tissues of wild-type (WT) and AD mice were extracted and peptides were labeled by a cPILOT approach. Since there was a total of 36 samples (i.e. six biological replicates, two genotypes and three tissue types), three batches of 12-plex cPILOT experiments were performed. Each batch was separated by offline strong cation exchange (SCX) and online reversed-phase fractionation prior to MS analysis. Samples were ran on the Orbitrap Velos or Fusion Lumos as follows: 1) peptides not subjected to offline fractionation and separated with RPLC coupled to the Fusion Lumos, 2) peptides fractionated by SCX and separated with RPLC coupled to the Fusion Lumos and 3) peptides fractionated by SCX and separated with RPLC coupled to the Orbitrap Velos. Findings from these experiments, including the outcome of parameter testing is discussed. These studies provide insight into the benefits and challenges of using different Orbitrap instruments for cPILOT analysis. More importantly, these studies lay the foundation for using enhanced multiplexing to understand changes in the peripheral and brain proteomes in AD.

4.2 EXPERIMENTAL PROCEDURES

4.2.1 Animal Husbandry and Ethical Statement

APP/PS-1 male mice (B6.Cg-Tg(APPswe, PSEN1dE9)85Dbo/Mmjax, stock no. 005864, genetic background:C57BL/6J) and heterozygous controls were purchased from Jackson Laboratory and housed in the Division of Laboratory Animal Resources at the University of Pittsburgh. All animal protocols were approved by the Institutional Animal Care and Use Committee at the University of Pittsburgh. Mice were fed standard Purina rodent laboratory chow *ad libitum* and kept in a 12 h light/dark cycle. Brain, heart, and liver tissues were harvested from 14-month-old APP/PS-1, referred to as (N = 6) and WT (N = 6) mice and stored at −80 ºC.

4.2.2 Tissue Homogenization, Protein Extraction, and Digestion

Brain, heart, and liver tissues (i.e. 60 – 80 mg) were homogenized (1× PBS w/ 8M urea) with a mechanical homogenizer (MP Biomedicals, LLC) to generate tissue lysates. To extract protein, samples were centrifuged (13,000 rpm, 4 ºC, 15 min) and supernatant was collected. Protein concentration was determined using BCA assay. Protein from brain, heart, and liver tissues (~100 µg) was reduced (DTT 1:40 mol ratio), alkylated (IAA 1:80 mol ratio), quenched (L-cysteine 1:40 mol ratio), and digested with trypsin (1:50 mol ratio) for 24 h. Peptides were desalted using a HLB cartridge (Waters) and dried down using centrifugal evaporation.

4.2.3 cPILOT Labeling

Peptides (~50 µg) were dissolved in 1% acetic acid (0.25 $\mu g \cdot \mu L^{-1}$). Formaldehyde /deuterated formaldehyde (Sigma Aldrich, 8 µL) and sodium cyanoborohydride/-deuteride (Sigma Aldrich, 8 µL) are added to either label peptides with light [$(-CH_3)_2$] or heavy [$(-^{13}CD_3)_2$] dimethyl groups, respectively. Peptides were reacted at room temperature for 10 min with shaking. To quench the reactions, of 1% ammonia (16 µL) was added for 5 min. Dimethylated peptides were re-acidified with 5% formic acid and light and heavy samples, were pooled (Table 4.1), desalted, and dried down by centrifugal evaporation. Desalted dimethylated peptides were dissolved in 100 mM triethyl ammonium bicarbonate (TEAB) buffer and TMT^6-plex reagents were prepared according to the manufacturer's protocol. TMT^6 -plex reagents were added to peptides and reacted at room temperature for 1 h with shaking. cPILOT labeled peptides were quenched with 5% (w/v) hydroxylamine-hydrochloride for 15 min and re-acidified with formic acid. Peptides were then pooled together into a single sample, concentrated, desalted, and dried down an additional time by centrifugal evaporation. Two portions of cPILOT labeled peptides were subjected to SCX fractionation while one portion was dissolved in 0.1% formic acid for instrument analysis (Figure 4.1).

Table 4.1 Experimental Scheme of cPILOT

TMT^6-plex tag	**126 (WT)**	**127 (AD)**	**128 (WT)**	**129 (AD)**	**130 (WT)**	**131 (AD)**
Light DM-Batch 1	Brain	Brain	Heart	Heart	Liver	Liver
Heavy DM-Batch 1	Heart	Heart	Liver	Liver	Brain	Brain
Light DM-Batch 2	Liver	Liver	Heart	Heart	Brain	Brain
Heavy DM-Batch 2	Brain	Brain	Liver	Liver	Heart	Heart
Light DM-Batch 3	Heart	Heart	Brain	Brain	Liver	Liver
Heavy DM-Batch 3	Heart	Heart	Brain	Brain	Liver	Liver

4.2.4 Offline SCX Fractionation

Peptides labeled by cPILOT were fractionated according to the manufacturer's protocol (Protea Biosciences). Briefly, peptides (600 µg) were dissolved in buffer A and loaded onto a pre-activated spin column. Peptides were eluted from the spin column in 8 intervals (room temperature, 6 min, 4000 × g) with increasing ammonium formate solutions (i.e. 20, 40, 60, 80, 100, 150, 250, and 500 mM). Fractionated peptides were dried down by centrifugal evaporation and dissolved in 0.1% formic acid.

4.2.5 Liquid Chromatography and Mass Spectrometry Analyses

Peptides were analyzed using three platforms. 1) Online desalting and reversed-phase liquid chromatography (RP-LC) was performed with a nano-UHPLC system equipped with an autosampler (Dionex, ThermoFisher Scientific). Mobile phases A and B used for separation were (v/v) 0.1% formic acid and 100% ACN with 0.1% formic acid, respectively. Peptides (250 ng) were loaded onto a commercial (Thermo Fisher Scientific) trapping column (75 µm x 2 cm) containing C_{18} (3 µm, 100 Å) at 2 $\mu L \cdot min^{-1}$ in 0.1% formic acid for 10 min. After desalting, the sample was loaded onto an analytical column (100 µm i.d. x 23 cm), which was packed in-house with C_{18} (2.5 µm, 150 Å, Waters). Four gradients were used as follow:

a) 0 – 10 min, 10% mobile phase B; 10 – 67 min, 10 – 30% B; 67 – 75 min, 30 – 60% B; 75 – 77 min, 60 – 90% B; 77 – 82 min, 90% B; 82 – 83 min, 90 – 10% B; 83 – 105 min, 10% B.

b) 0 – 10 min, 10% mobile phase B; 10 – 30 min, 10 – 15% B; 30 – 75 min, 15 – 30% B 75 – 88 min, 30 – 60% B; 88 – 92 min, 60 – 90% B; 92 – 99 min, 90% B; 99 – 100 min, 90 – 10% B; 100 – 120 min, 10% B.

c) 0 – 10 min, 10% mobile phase B; 10 – 30 min, 10 – 15% B; 30 – 100 min, 15 – 30% B 100 – 118 min, 30 – 60% B; 118 – 123 min, 60 – 90% B; 123 – 129 min, 90% B; 129 – 130 min, 90 – 10% B; 130– 150 min, 10% B.

Standard data-dependent acquisition parameters were as follows: the MS survey scan in the Orbitrap (375 – 1500 *m/z*) was 120,000 resolution; the most intense peaks with 3s (Top Speed) were isolated (0.7 *m/z*) and fragmented with collision-induced dissociation (CID) in the ion trap with an NCE of 35%, AGC of 1 x 10^4, dynamic exclusion of 20 s, ppm mass tolerance of 10, maximum IT of 100 ms. Directly after each MS/MS scan, the four most intense fragment ions (over varying *m/z* ranges) were selected for an additional fragmentation (i.e. MS^3) event by HCD and analyzed in the OT (scan range: 100 – 400 *m/z*, isolation width: 2 *m/z,* AGC: 5 x 10^4, NCE: 55%, resolution: 60,000, maximum IT: 118 ms). Other parameters such as precursor selection range, precursor ion exclusion, and isobaric tag loss exclusion were set as default.

Targeted inclusion and exclusion tests were performed using the following nodes: targeted mass, targeted mass difference, targeted isotopic ratio, and targeted mass trigger. In both targeted mass, and targeted mass trigger nodes, a list including *m/z*, z, m, and retention time (targeted mass only) are imported into a list. In targeted mass difference, a mass difference of 8.0444 Da (Heavy DM – Light DM) and 7.0381 Da (Dimethyl 7-Light DM) were listed, the partner intensity range relative to the most intense precursor was set to 70 – 100 %, a subsequent scan was performed on both ions in the pair and the charge state for ions in the pair had to be

similar. For targeted isotopic ratio, similar parameters were added, with the distinction that the predicted isotopic range was set to 70 – 100%.

Parameters including precursor isolation width (experiment 1), dynamic exclusion (experiment 3), targeted analyses (experiment 4), and SPS selection (experiment 5) were tested and varied as such: Experiment 1, 0.7, 2, or 2.5 *m/z*; Experiment 3, 0, 10, or 20 s; Experiment 4, targeted mass, targeted mass difference, targeted isotopic ratio, and targeted mass trigger; Experiment 5,SPS-n of 4, 6, 8 or 10.

(2) Peptides were loaded onto the same commercial trap column as (1). Separation occurred on the same in-house analytical column, but the gradient was adjusted to 1b (see above). An optimized MS data acquisition method was applied. Standard data-dependent acquisition parameters were as follows: the MS survey scan in the OT (375 – 1500 *m/z*) was 120,000 resolution; the most intense peaks with 3s (Top Speed) were isolated (2*m/z*) and fragmented with CID in the ion trap with an NCE of 35%, AGC of 1 x 10^4, dynamic exclusion of 20 s, ppm mass tolerance of 10, maximum IT of 100 ms. Peptide pairs were targeted by using the targeted mass difference node. Directly after each MS/MS scan, the ten most intense fragment ions (over varying *m/z* ranges) were selected for an additional fragmentation (i.e. MS^3) event by HCD and analyzed in the OT (scan range: 100 – 400 *m/z*, isolation width: 2 *m/z,* AGC: 5 x 10^4, NCE: 55%, resolution: 60,000, maximum IT: 118 ms). Other parameters such as precursor selection range, precursor ion exclusion, and isobaric tag loss exclusion were set as default.

(3) Online desalting and RP-LC was performed with a nano-HPLC system equipped with an autosampler (Eksigent). Mobile phases A and B used for RP-LC separation of peptides were 3% (v/v) acetonitrile with 0.1% formic acid and 100% acetonitrile with 0.1% formic acid, respectively. SCX fractions (6 µL) were loaded onto a trapping column (100 µm i.d. x 2 cm),

which was packed in house with C_{18} (3 µm, 200 Å) stationary phase material (Michrom Bioresource Inc,) at 3 µL/min in 3% mobile phase B for 3 min. After desalting, the sample was loaded onto an analytical column (75 µm i.d. x 13.2 cm) which was packed in-house with C_{18} (3 µm, 100 Å) stationary phase material (Michrom Bioresource Inc). The LC eluent was analyzed with positive mode nanoflow electrospray using a LTQ Orbitrap Velos mass spectrometer (Thermo Fisher Scientific). Peptides were loaded onto an in-house trap column (2 cm, 5 µm, 200 Å) for 3 min (3 µL/min) and separated on an in-house analytical column (75 µm, 13.2 cm) with C_{18} (5 µm, 100 Å). The gradient is as follows: 0 – 7 min, 10% mobile phase B; 7 – 27 min, 10 – 15% B; 27 – 102 min, 15 – 20% B; 102 – 122 min, 20 – 30% B; 122 – 132 min, 30 – 60% B; 133 – 137 min, 60 – 80% B; 137 – 150 min, 80% B, 150 – 180, 10% B. Separated peptides were detected using a previously described method[84] on a LTQ Orbitrap Velos. Briefly, data-dependent acquisition parameters were as follows: the MS survey scan in the OT (300 – 1800 *m/z*) was 60,000 resolution; the top 1 – 7 and top 8 – 14 most intense peaks were isolated and fragmented with CID in the LTQ with an NCE of 35%. Directly after each MS/MS scan, the most intense fragment ion (over 200 – 1545 *m/z*) was selected for an additional fragmentation (i.e. MS^3) by HCD (isolation width: 4 *m/z,* AGC: 3 x 10^5, NCE: 60%, resolution: 7500, maximum IT: 250 ms). Each fraction was subject to triplicate injections.

4.2.6 Data Analysis

Raw files were analyzed with PD v. 2.1 and 2.2 software (Thermo Scientific). Spectra were used to obtain sequence information against the Uniprot *M. musculus* database (01/19/2018, 53035 sequences). SEQUEST HT search parameters were as follows: two maximum trypsin

miscleavages, precursor mass tolerance of 15 ppm, fragment mass tolerance of 1 Da; static modifications were either Dimethyl/+28.031 or 36.028/35.070 Da (N-terminus) and carbamidomethyl (Cys) /+57.021 Da; dynamic modifications were TMT six-plex/+229.163 Da (Lys) and oxidation (Met) /+15.995 Da. Decoy database searching was employed to generate medium ($p<0.05$) confidence peptide lists. All peptides with medium confidence were used to identify and quantify proteins. To filter peptides, the following parameters were applied: peptides with a peptide to spectral match (PSM) >1 across biological replicates, peptide confidence level of medium, peptide rank of 1, peptide deviation of 10 ppm, and S/N ≥10. The reporter ions (i.e. *m/z* 126 – 131) were identified with the following parameters: most confident centroid and 30 ppm for reporter ion mass tolerance. Furthermore, reporter ion values were normalized using internal reference scaling.[172]

To identify statistically-significant proteins, a one-way ANOVA was performed in Perseus software.[173] Proteins with a fold-change of >1.2 or <0.83 were further used for bioinformatics analyses in ingenuity pathway analysis (IPA).

4.3 RESULTS

Here, we were interested in determining protein changes across WT and AD mice in multiple tissues in a single experiment. In addition, because of the advantages of enhanced multiplexing offered by cPILOT, insight about changes across biological replicates were also identified. The use of TMT reagents in the cPILOT approach requires sample prefractionation and/or MS data acquisition methods that provide optimal protein coverage and protein

quantification. As with isobaric tagging strategies, cPILOT also becomes limited in the number of proteins that can be quantified compared to the total number of proteins identified. The additional steps of sample tagging and clean-up as well as necessary MS^3 steps for accurate protein quantification[116], require longer instrument duty cycles. Thus, less peptides are sampled and less proteins are quantified. Previously, cPILOT has been utilized on Orbitrap Velos instruments and only recently has the approach been demonstrated on an Orbitrap Fusion Lumos instrument.[91] Due to the improvements in scan rates, sensitivity, fragmentation and detection flexibility, and SPS, the Fusion Lumos dramatically increases the performance of our cPILOT strategy. Below, we describe efforts to systematically test the performance of the Fusion Lumos to study Alzheimer's disease system-wide in a mouse model (Figure 4.1).

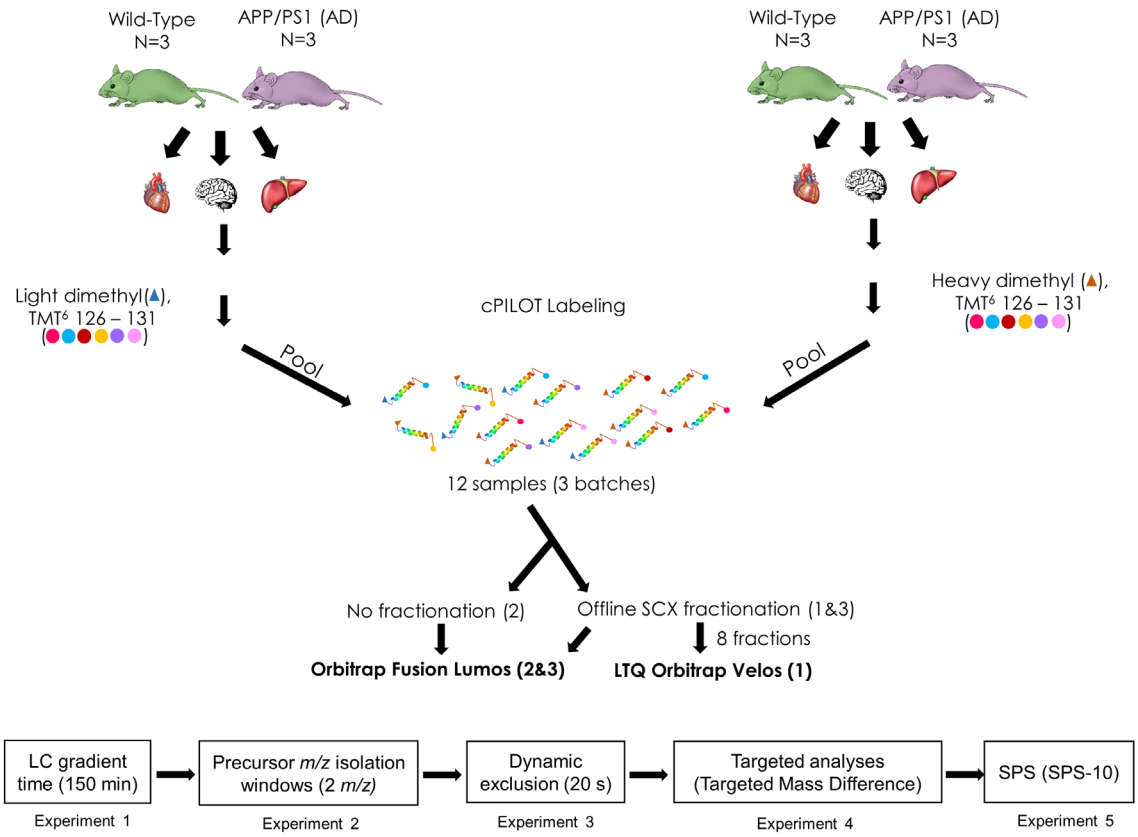

Figure 4.1 Experimental Workflow of AD and WT Brain, Heart, and Liver Tissues. Protein (100 µg) was extracted from brain, heart, and liver tissues from 14-month old AD and WT mice and digested using trypsin. Peptides generated from protein digestion were labeled via cPILOT, pooled, and separated by off-line strong cation exchange (SCX) fractionation and reversed-phase HPLC. Fractions were analyzed on either an LTQ Orbitrap Velos or an Orbitrap Fusion Lumos. Samples not subjected to fractionation were directly separated by reversed-phase HPLC and analyzed on an Orbitrap Fusion Lumos. One sample (not subjected to fractionation) from were used to test the LC gradient time, precursor *m/z* isolation window width, dynamic exclusion, targeted analyses methods, and SPS-N ions.

Specifically, extracted protein from brain, heart, and liver tissues from 14-month old WT (N=6) and AD (N=6) mice was digested with trypsin. To accommodate all tissues and biological replicates, three pooled sample batches were generated (i.e., Batches 1 – 3). Peptides were labeled by using a global cPILOT approach in which peptides are light- or heavy- dimethylated at low buffer pH and then tagged with TMT at high buffer pH. After this dual labeling strategy, peptides were subjected to different analyses methods. Briefly, a portion of Batch 1 peptides were not fractionated and analyzed directly by LC – MS/MS and MS^3 on the Fusion Lumos. Batch 1-3 peptides were fractionated by SCX and analyzed using either the Fusion Lumos or Orbitrap Velos.

Several experimental parameters were evaluated in each analysis method and included those prior to MS introduction and others related to MS acquisition (Figure 4.1). Experiment 1 tested the effects of increasing the LC gradient from 105 to 150 min and Experiment 2 tested different precursor isolation widths from 0.7 to 2.5 *m/z*. Experiment 3 tested various dynamic exclusion times of 0, 10, and 20 s. Experiment 4 tested different "targeted" acquisition methods in the Fusion Lumos, which enable dimethylated pairs to be selectively isolated for MS/MS and further MS^3 steps. Lastly, Experiment 5 evaluated SPS in which the number of MS/MS fragment ions varied from 4 – 10.

An initial demonstration that cPILOT successfully worked in this application of multiple tissues in WT and AD mice is shown in Figure 4.2.

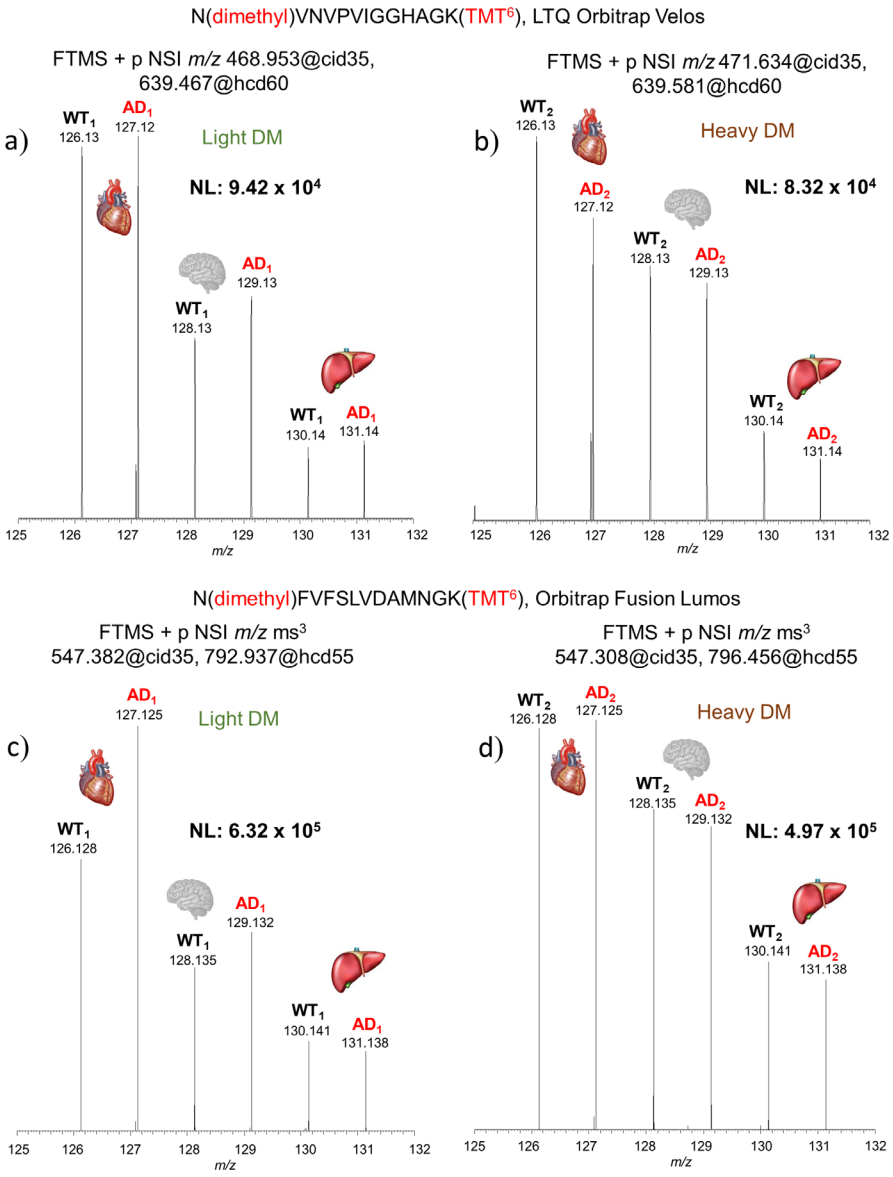

Figure 4.2 Comparison of Reporter Ion Spectra from a) and c) Light and b) and d) Heavy Peptides Labeled by cPILOT Acquired on a) and b) an Orbitrap Fusion Lumos or c)and d) a LTQ Orbitrap Velos MS Platforms. Reporter ions (e.g. 126 – 131) corresponding to peptides N(dimethyl)FVFSLVDAMNGK(TMT^6) and N(dimethyl)VNVPVIGGHAGK(TMT^6) were detected on the Orbitrap Fusion Lumos and LTQ Orbitrap Velos, respectively. Light and heavy dimethylated peptides were detected in both phenotypes and all tissue-types and correspond to Krebs cycle protein malate dehydrogenase. Notably, reporter ion intensities from the Fusion Lumos is ~5 to 6× greater than corresponding intensities from the Orbitrap Velos.

Two peptides that belong to malate dehydrogenase are shown and based on the MS/MS data (*not shown*) these peptides were dimethylated on the N-terminal amines and TMT^6-plex tagged on the lysine residues. The MS^3 spectra for N(dimethyl)VNVPVIGGHAGK(TMT^3) for light (Figure 4.2a) and heavy (Figure 4.2b) dimethylated pairs have reporter ions detected in channels *m/z* 126-131. For this example peptide, the reporter ion signals show that there is no difference in protein level between WT and AD mice for any of the tissues. The enhanced multiplexing afforded by cPILOT allows a quick assessment of the consistency of changes in WT and AD, as well as in the three tissues from multiple biological replicates. The changes for this peptide observed in one biological replicate (Figure 4.2a) are consistent in other replicates (Figure 4.2b and *data not shown*). However, a noticeable difference in signal across tissues is apparent, as malate dehydrogenase has higher levels in heart compared to brain and liver, and in brain compared to liver tissues. This trend is similar for other peptides detected for this protein as shown in Figures 2.4c and 4.2d. It is also apparent that the reporter ion signals are higher from the Fusion Lumos data compared to that from the Orbitrap Velos data.

4.3.1 Evaluation of LC Gradients and Precursor Isolation Windows (Experiments 1 and 2)

It is expected that increasing the LC gradient would improve the number of proteins identified as greater numbers of MS/MS spectra are possible with increased data acquisition time. From analysis method 1, samples were injected multiple times to test LC gradient times of 105, 120, and 150. Upon increasing the gradient, there was an increase of protein (Figure 4.3a) and PSMs (Figure 4.3b) identifications generated from both light and heavy dimethylated peptides. For example, the average number of proteins identified at 105 min (across different

precursor isolation windows) was 863 proteins from light dimethylated peptides which increased to 937, and 1106 with gradients of 120 and 150 min respectively (Figure 4.3a).

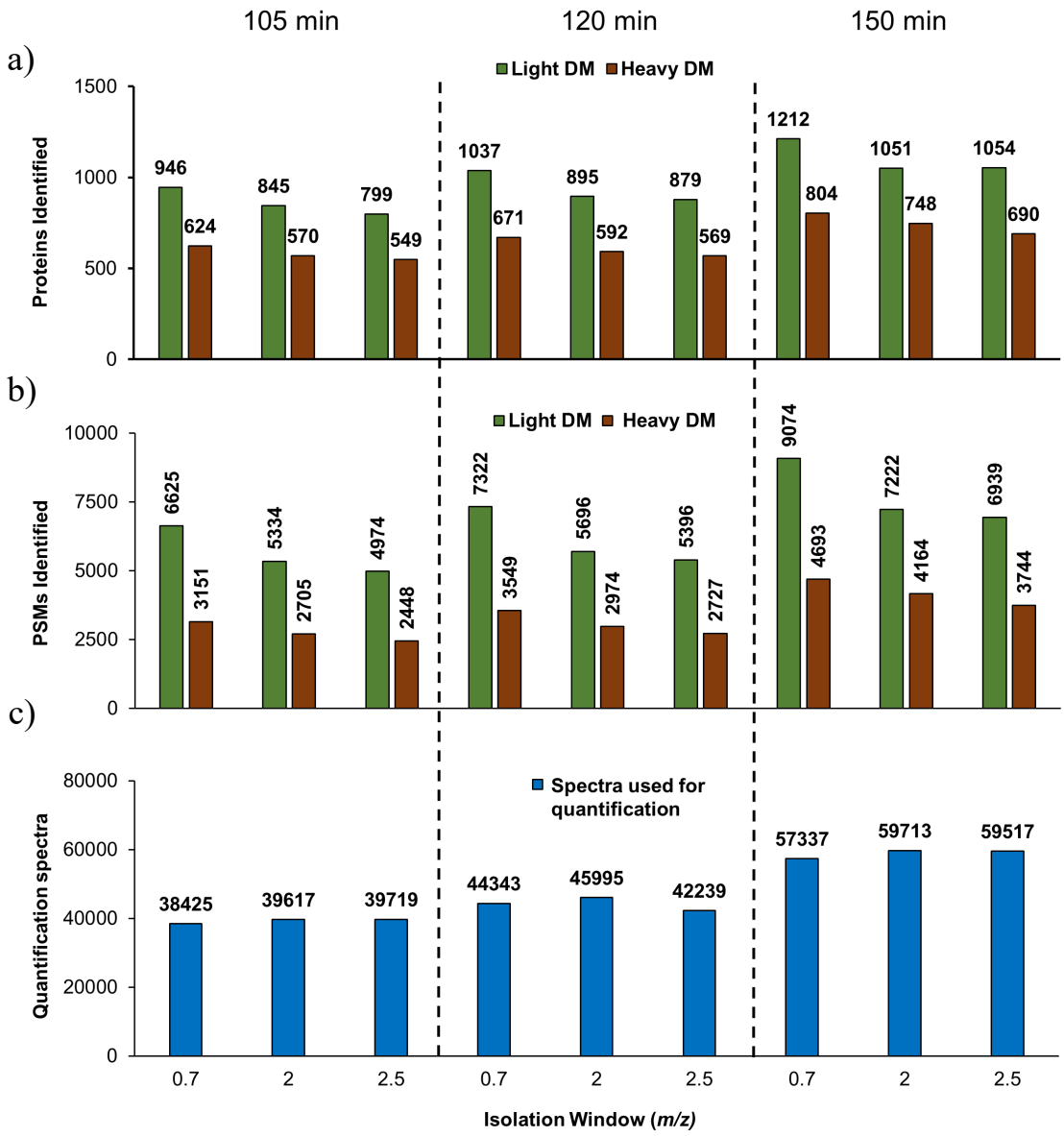

Figure 4.3 Comparison of a) Protein and b) Peptide Identification, and c) Quantified Spectra at 105, 120, and 150 min. Light and heavy dimethylated peptides from a sample not pre-fractionated were identified with increasing LC gradient times of 105, 120, and 150 min and widening precursor *m/z* isolation widths of 0.7, 2.0, and 2.5. a) Protein group, b) unique peptide, and PSM IDs increase with gradient time yet decrease with widening the isolation window. Conversely, widening the isolation window increases the number of c) quantified spectra.

This is a 1.3x increase in identifications obtained by increasing the LC gradient by 45 minutes and is consistent for both light and heavy dimethylated peptides. Higher protein identifications is a direct result of higher numbers of PSMs and peptides being obtained (Figure 4.3b). PSMs and peptides increased by ~400 – 1800 and ~200 – 1200 respectively, as the gradient time increased. The impact of gradient on average numbers of spectra that were quantified also increases by 1.5x from 105 min to 150 min. We anticipate that extended gradient times would allow more spectra to be quantified and hence proteins identified however, there are major considerations with regards to total instrument time. If the experimental design includes multiple batches, sample pre-fractionation, and technical replicates then gradient times that are shorter will be generally preferred. For the remainder of parameter testing Experiments 2-5, we continued with a 150 min gradient time in order to optimize numbers of spectra, peptides, and proteins detected.

For cPILOT analyses it is most critical that both peaks in a light and heavy dimethylated pair are isolated at the precursor stage for MS/MS and subsequent MS^3. This it to accommodate detecting reporter ion signals from all samples present in a batch. The considerations for changing the isolation window are that interfering species can be co-isolated from the precursor MS spectra if the window is too large whereas lower signal intensities for precursors are carried forward into MS/MS if the isolation window is too small. Previously, we evaluated isolation window widths for yeasts with DiLeu[91] and determined that 0.7 *m/z* is appropriate. Here, on the Fusion Lumos we changed the precursor isolation window from *m/z* 0.7 to 2.0 and 2.5. The goal is to minimize co-isolation of precursors but primarily the co-isolation of light and heavy dimethylated peptides while also optimizing the number of pairs selected. Most peptides for this dataset haves charge state of 2 (48%) and 3 (43%). Peptides with a charge state of 1 are rejected

in the data acquisition method and those with higher charge states are observed infrequently (9% for charge state 4-7) in this experiment. Thus, isolation windows of *m/z* 2.5 or less are likely most appropriate for peptides with a charge state of 2, and will need to be even less to accommodate peptides with a charge state of 3. The isolation window in these experiments is also impacted by the fact that heavy dimethylated peptides have a peak that shows up 7 Da from the light dimethylated peak and is often isolated as the precursor peak in the heavy cluster. Increasing isolation windows from *m/z* 0.7 to 2.0 with a gradient time of 150 min resulted in a 13-16% decrease of 1212 and 804 proteins to 1054 and 690 proteins from light and heavy dimethylated peptides, respectively (Figure 4.3a). Peptides and PSMs followed the same trend with increasing isolation windows (Figure 4.3b). On the other hand, the number of quantified spectra increased from 57337 to 59517 (Figure 4.3c) which is likely a result of wider windows leading to more ion signal at the AGC level; such that the instrument duty cycle is a bit faster in this scenario. However it is apparent that even with greater quantified spectra the number of identified peptides and PSMs decreases by 25% from isolation windows of m/z 0.7 to 2.0.

It is expected that increasing the LC gradient would improve the number of proteins identified as greater numbers of MS/MS spectra are possible with increased data acquisition time. From analysis method 1, samples were injected multiple times to test LC gradient times of 105, 120, and 150. Upon increasing the gradient, there was an increase of protein (Figure 4.3a) and PSM (Figure 4.3b) identifications generated from both light and heavy dimethylated peptides. For example, the average number of proteins identified at 105 min (across different precursor isolation windows) was 863 proteins from light dimethylated peptides which increased to 937, and 1106 with gradients of 120 and 150 min respectively (Figure 4.3a). This is a 1.3x increase in identifications obtained by increasing the LC gradient by 45 minutes and is consistent

for both light and heavy dimethylated peptides. Higher protein identifications is a direct result of higher numbers of PSMs and peptides being obtained (Figure 4.3b). PSMs and peptides increased by ~400 – 1800 and ~200 – 1200 respectively, as the gradient time increased. The impact of gradient on average numbers of spectra that were quantified also increases by 1.5x from 105 min to 150 min. We anticipate that extended gradient times would allow more spectra to be quantified and hence proteins identified however, there are major considerations with regards to total instrument time. If the experimental design includes multiple batches, sample pre-fractionation, and technical replicates then gradient times that are shorter will be generally preferred. For the remainder of parameter testing Experiments 2-5, we continued with a 150 min gradient time in order to optimize numbers of spectra, peptides, and proteins detected.

For cPILOT analyses it is most critical that both peaks in a light and heavy dimethylated pair are isolated at the precursor stage for MS/MS and subsequent MS^3. This it to accommodate detecting reporter ion signals from all samples present in a batch. The considerations for changing the isolation window are that interfering species can be co-isolated from the precursor MS spectra if the window is too large whereas lower signal intensities for precursors are carried forward into MS/MS if the isolation window is too small. Here, on the Fusion Lumos we changed the precursor isolation window from *m/z* 0.7 to 2.0 and 2.5. The goal is to minimize co-isolation of precursors but primarily the co-isolation of light and heavy dimethylated peptides while also optimizing the number of pairs selected. Most peptides for this dataset haves charge state of 2 (48%) and 3 (43%). Peptides with a charge state of 1 are rejected in the data acquisition method and those with higher charge states (e.g. 4 – 7) are observed infrequently (9%) in this experiment. Thus, isolation windows of *m/z* 2.5 or less are likely most appropriate for peptides with a charge state of 2, and will need to be even less to accommodate peptides with a charge

state of 3. The isolation window in these experiments is also impacted by the fact that heavy dimethylated peptides have a peak that shows up 7 Da from the light dimethylated peak and is often isolated as the precursor peak in the heavy cluster. Increasing isolation windows from *m/z* 0.7 to 2.0 with a gradient time of 150 min resulted in a 13-16% decrease of 1212 and 804 proteins to 1054 and 690 proteins from light and heavy dimethylated peptides, respectively (Figure 4.3a). PSMs followed the same trend with increasing isolation windows (Figure 4.3b). On the other hand, the number of quantified spectra increased from 57337 to 59517 (Figure 4.3c) which is likely a result of wider windows leading to more ion signal at the AGC level; such that the instrument duty cycle is a bit faster in this scenario. However it is apparent that even with greater quantified spectra the number of identified peptides and PSMs decreases by 25% from isolation windows of *m/z* 0.7 to 2.0.

4.3.2 Dynamic Exclusion (Experiment 3)

Next we conducted an experiment that tested the effects of dynamic exclusion on the number of peptides and proteins identified (Figure 4.4). Precursor isolation width was set to *m/z* 2.0 and the dynamic exclusion varied from 0 to 10 and 20 s. To assess the quality of the proteins that were identified, we evaluated proteins with low, medium, and high confidence as determined from PD. Proteins identified considering only light dimethylated peptides came from a larger percentage (36 to 69%) of low confidence proteins as the dynamic exclusion went from 20 s to 0 s, whereas the percentage of high confidence peptides decreased from 53% to 22%, respectively.

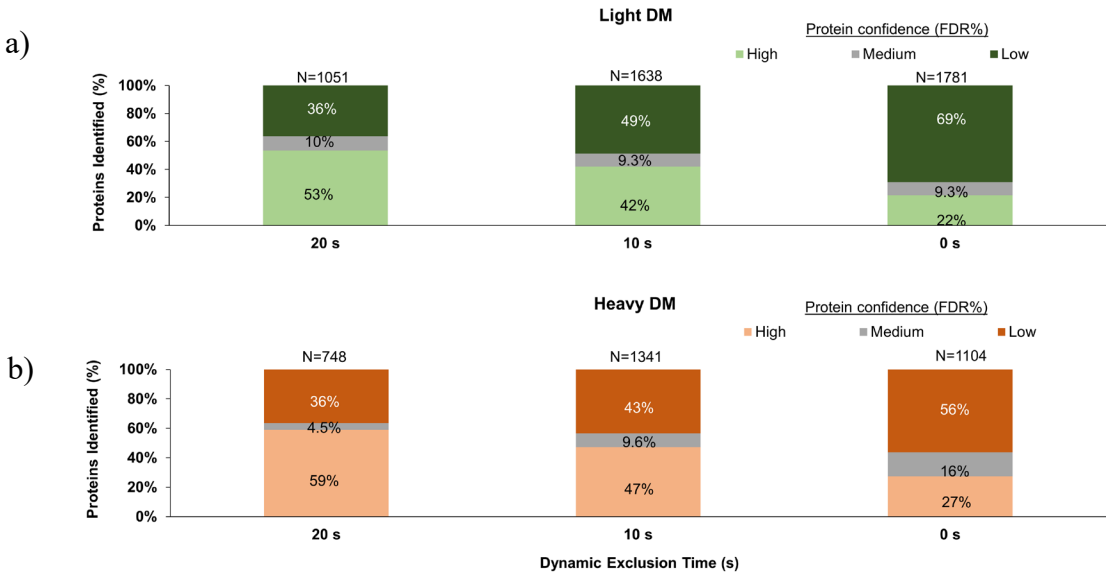

Figure 4.4 Effects of Dynamic Exclusion Times 0, 10, 20 s on Protein Identifications from a) Light and b) Heavy Dimethylated Peptides. Dynamic exclusion times of 0, 10, and 20s was tested to identify if this parameter was necessary. An increase of exclusion time resulted in a decrease of protein identifications, yet an increase (~30%) in high-confident proteins (false discovery rate <1%).

The same trend was observed for proteins identified from heavy dimethylated peptides although the number of total proteins identified was generally lower. Removing dynamic exclusion results in over sampling of the same high abundance peptides and more sporadic sampling of low abundance peptides, leading to higher numbers of low confidence proteins.

4.3.3 Targeted Mass Analyses (Experiment 4)

The above experiments were all conducted with Top Speed (3s) DDA, which is an untargeted method. The Fusion Lumos includes targeted inclusion/exclusion nodes are helpful to increase the number of dimethylated pairs quantified by removing time spent on R-terminal peptides. Among the targeted mass nodes available: targeted mass trigger, targeted mass difference, targeted isotopic ratio, and targeted mass (inclusion and exclusion) methods were tested (Figure 4.5, Table 4.2).

Both targeted mass difference and isotopic ratio searched for pairs based on mass difference or peptide ratios, whereas the other targeted methods used a list of target *m/z*, z, M, and/or retention times with specified information. Dimethylated PSMs (*not shown*), had similar identifications across the first four methods (i.e. 6599 – 7403 PSMs and 1002 – 1106 proteins) whereas a substantial decrease was present in the targeted mass inclusion run (4855 PSMs and 492 protein groups). Among heavy dimethylated peptides (Figure 4.5d), the targeted mass difference method identified 8059 PSMs. The other tests, however, identified ~2-4× (1941 – 4265 PSMs) less PSMs (Table 4.2).

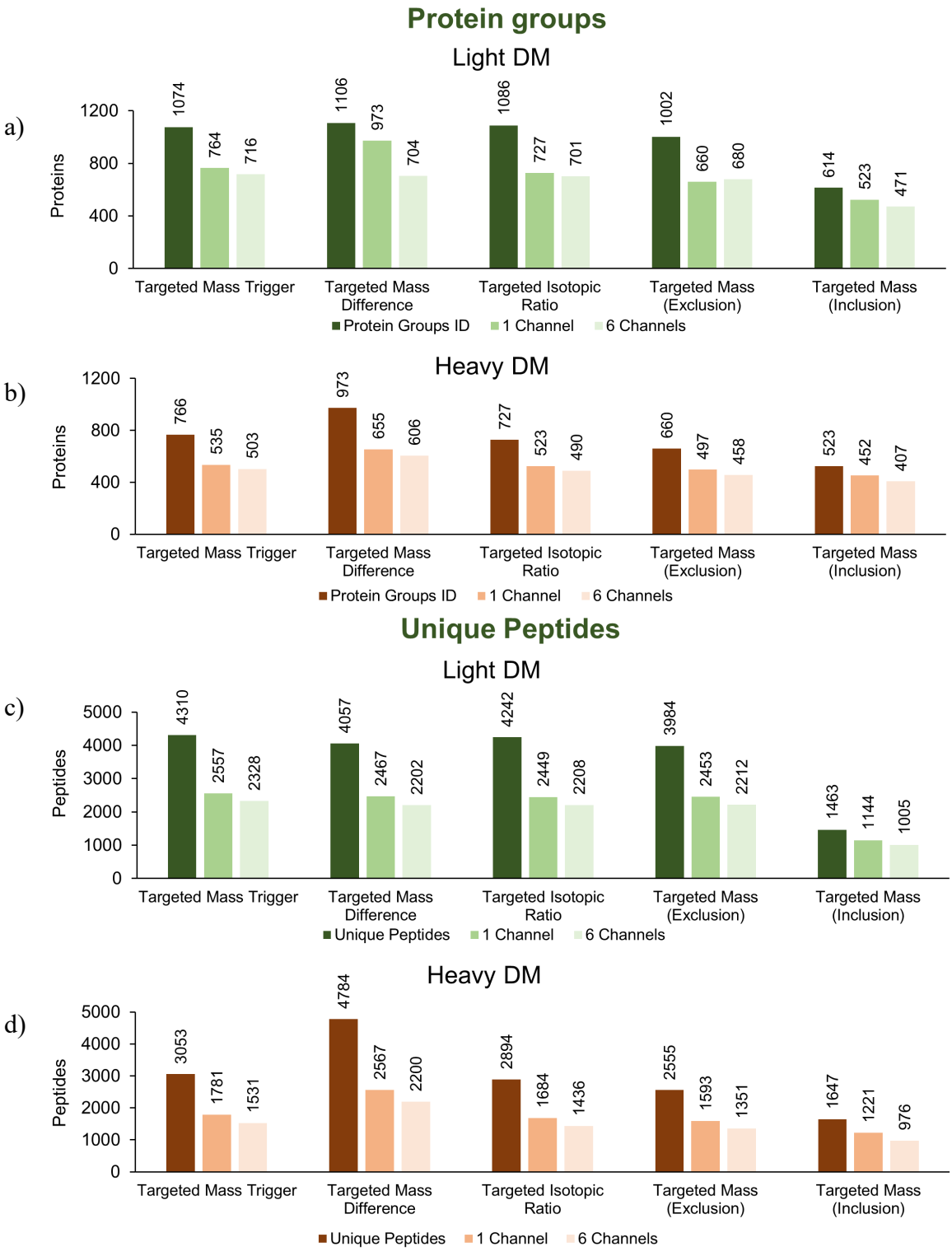

Figure 4.5 Comparison of a) and b) Protein and c) and d) Peptide Identifications of Light and b) Heavy Dimethylated Peptides using Targeted Analyses Methods.

Table 4.2 Effects of Targeted Analyses on the Number of PSMs Quantified (Experiment 4).

Targeted Test	PSMs ID		R (%)[a]		K(%)[b]		TMT-K(%)[c]	
	Light	Heavy	Light	Heavy	Light	Heavy	Light	Heavy
Targeted Mass Trigger	7378	4265	3159 (42.8)	1725 (40.4)	4079 (55.3)	2440 (57.2)	3985 (97.7)	2375 (97.3)
Targeted Mass Difference	7403	8059	3172 (42.8)	3454 (42.8)	4048 (54.7)	4384 (54.4)	3957 (97.7)	4263 (97.2)
Targeted Isotopic Ratio	7078	3890	3061 (43.2)	1577 (43.2)	3878 (54.8)	2228 (54.8)	3795 (97.9)	2169 (97.4)
Targeted Mass (Exclusion)	6599	3498	2536 (38.4)	1199 (34.3)	3934 (59.6)	2197 (59.6)	3854 (98.0)	2146 (97.7)
Targeted Mass (Inclusion)	1744	1941	47 (2.7)	113 (5.8)	1695 (97.2)	1825 (94.0)	1676 (98.9)	1810 (99.2)

[a] The number of PSMs and percentage ending with arginine. [b]The number of PSMs and percentage ending with lysine. [c]The number and percentage of lysine ending peptides that are labeled with TMT-6plex.

In terms of protein quantification, a range of 67-85% of proteins were quantified in at least one channel. This percentage decreased to a range of 62-78% when considering proteins quantified in all six channels. Over 50% of PSMs identified (Table 4.2) contained lysine and ~ 97-99% of those peptides were labeled with TMT. Table 4.2 also shows that the targeted mass inclusion method was most effective at spending the least amount instrument time on R-terminated peptides, otherwise increasing the selectivity of the approach.

Experiment 4 provided insight into which targeted analyses would be helpful in selecting dimethylated peptide pairs during MS acquisition. It was confirmed that targeted mass and targeted mass trigger tests inefficiently increased the quantity of peptide pairs since a) targeted mass inclusion only selected K-terminating peptides on the inclusion list, b) targeted mass exclusion did not remove all R-terminated peptides, and c) targeted mass trigger worked similarly to a and b. Though b) only selected K-terminated peptides, it would not be ideal for global analyses as only selected a fraction of the peptide *m/z* values on the list. Conversely, targeted mass difference and targeted mass isotopic ratio tests were expected to identify and quantify similar amounts of proteins, and thus an increase of dimethylated pairs. However, targeted mass difference identified more light and heavy PSMs combined (15,462) than targeted isotopic ratio (10,966) and greater percentages (70 and 81% vs. 59 and 77%) of light and heavy dimethylated pairs, respectively. Based on these data, the best method for conducting targeted cPILOT experiments for enhancing dimethylated pairs appears to be with targeted mass difference.

4.3.4 Synchronous Precursor Selection (Experiment 5)

Multi-notch MS^3 uses between 2 – 20 fragment ions for quantification, thus increasing the signal present in reporter ion channels in comparison to single-notch MS^3. In experiment 5, a range of 4-10 SPS ions were tested, resulting in similar amounts of proteins being identified and quantified in at least one channel (Table 4.3).

Proteins were considered quantified if the S/N ≥10 for a given reporter ion channel and the minimal signal above the set threshold. Among proteins quantified in six channels, the largest increase (65 – 72%) was present with SPS-10. In terms of peptide quantification (*not shown)*, similar percentages of peptides containing lysine at the C-terminus (~55%) of which ~97-98% were labeled with TMT. While SPS-4 generated the largest number of MS/MS (116,113) and more importantly, quantified spectra (59713) compared to SPS-10, SPS-10 had the greatest number of proteins with data in six channels and was selected for further experiments.

Table 4.3 Effects of SPS Parameters on the Number of Protein IDs (Experiment 5).

SPS-N[b]	Protein Groups		Proteins[c]: 1 Channel (%)		Proteins[d]: 6 Channels (%)		MS/MS Spectra	Quan. Spectra
	Light	Heavy	Light	Heavy	Light	Heavy	Light/Heavy	Light/Heavy
4	1051	748	725 (69)	540 (72)	682 (65)	501 (67)	116113	59713
6	1042	722	729 (70)	517 (72)	707 (68)	492 (68)	116017	59528
8	1077	735	760 (71)	532 (72)	733 (68)	513 (70)	113097	57995
10	1056	702	770 (73)	514 (73)	756 (72)	509 (73)	113266	58131

[a] Isolation window 2 *m/z*. [b] The number of fragment ions used to for synchrous precursor selection (SPS). [c] The number and percentage of proteins quantified in at least one reporter ion channel. [c]The number and percentage of proteins quantified in all reporter (i.e. 126 - 131) ion channels.

4.3.5 Comparisons of Samples Analyzed by Velos and Fusion Lumos Instrumentation

Unfractionated and fractionated samples were compared to identify how differences in Orbitrap instrumentation may affect protein identification and quantification. Across three cPILOT 12-plex batches and three different sample analyses methods, over >600,000 PSMs (Table 4.4) corresponding to >22,000 unique peptides and 6074 protein groups (Figure 4.6) were identified (Appendix C Tables C4.1 – C4.8).

Sample fractionation dramatically increased the number of peptides and proteins identified on the Orbitrap Velos (Appendix C Tables C4.1 and C4.2) and Fusion Lumos (Appendix C Tables C4.3 and C4.4), compared to un-fractionated samples on the Fusion Lumos (Figures 4.6a and 4.6b, Appendix C Tables C4.5 and C4.6). Similarities in protein identifications (Figure 4.6a) range from 19 – 65% with the least overlap occurring between unfractionated and fractionated datasets from different instruments. However, each approach still observed unique proteins. Peptides shared similar behavior across approaches (Figure 4.6b). Overall, 910 proteins were identified in all approaches. Among all 6074 identified proteins, 70% were identified with >2 PSMs (Figure 4.7). Interestingly, a criterion of excluding single PSMs was reconsidered based on the data shown. An observation of six reporter ions shows that the peptide was still present in six different samples. Some vital information may be diagnosed with this criterion. As the number of PSMs increase from 11 – 100, 101 – 1001, and so forth, the number of proteins identified decreases. Among proteins identified by 1 PSM (Figure 4.7c insert), most were quantified in either none or all six reporter ion channels.

Table 4.4 Effects of SCX Fractionation on the Number of Proteins and PSMs Identified.

	SPS-N[a]	Protein Groups[b]	Proteins[c] (%)	PSMS ID	R[d]	K[e]	TMT-K[f]
Batch 1-3, 8 Fractions, Velos	1	2199	142 (14)	374951	133759 (35.7)	236177 (63.0)	234114 (99.1)
Batch 1-3, 0 Fractions, Lumos	10	1848	334 (26)	44620	17851 (40.0)	25959 (58.2)	25498 (98.2)
Batch 1-3, 8 Fractions, Lumos	10	4968	1012 (28)	223286	87840 (39.3)	129797 (58.0)	127791 (98.0)

[a] The number of fragment ions used to for synchrous precursor selection (SPS). [b] The number of proteins identified with more than 1 PSM. [c]The number and percentage of proteins quantified in all reporter (i.e. 126 - 131) ion channels across all experimental groups. [d]The number and percentage of peptides ending with arginine a. [e]The number and percentage of peptides ending with lysine. [f]The number and percentage of lysine ending peptides labeled with TMT-6plex.

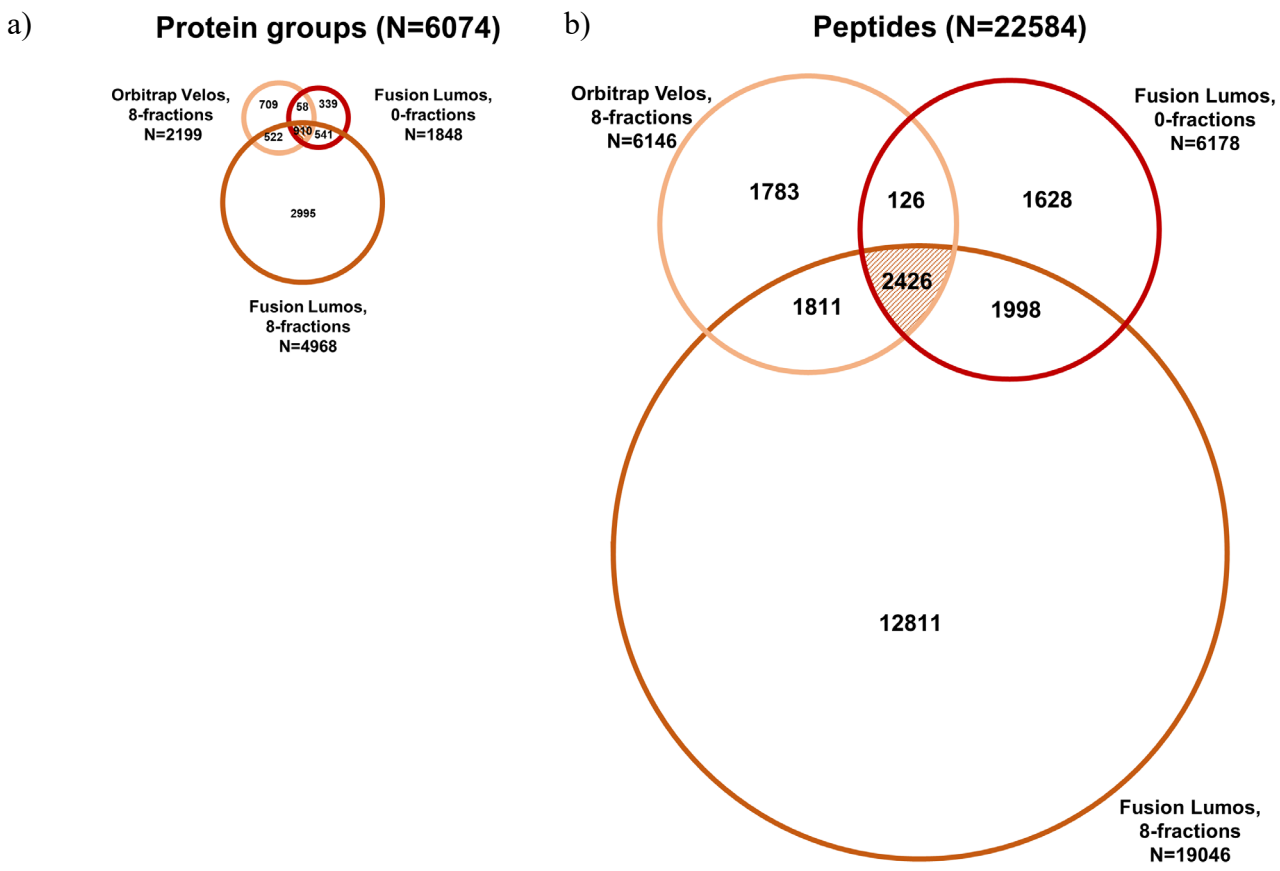

Figure 4.6 Identification of a) Protein and b) Peptide Groups Identified Across Three MS Experiments. a) Proteins identified from 8-fractions on the Orbitrap Velos (N=2199) were compared to proteins identified from 8-fractions on the Fusion Lumos (N=4968) and non-fractionated on the Fusion Lumos (N=1848). Across all three experiments, 6074 proteins were identified, with 910 proteins (~15%) being present in all groups. This total number corresponds to b) 22,584 unique peptides being identified.

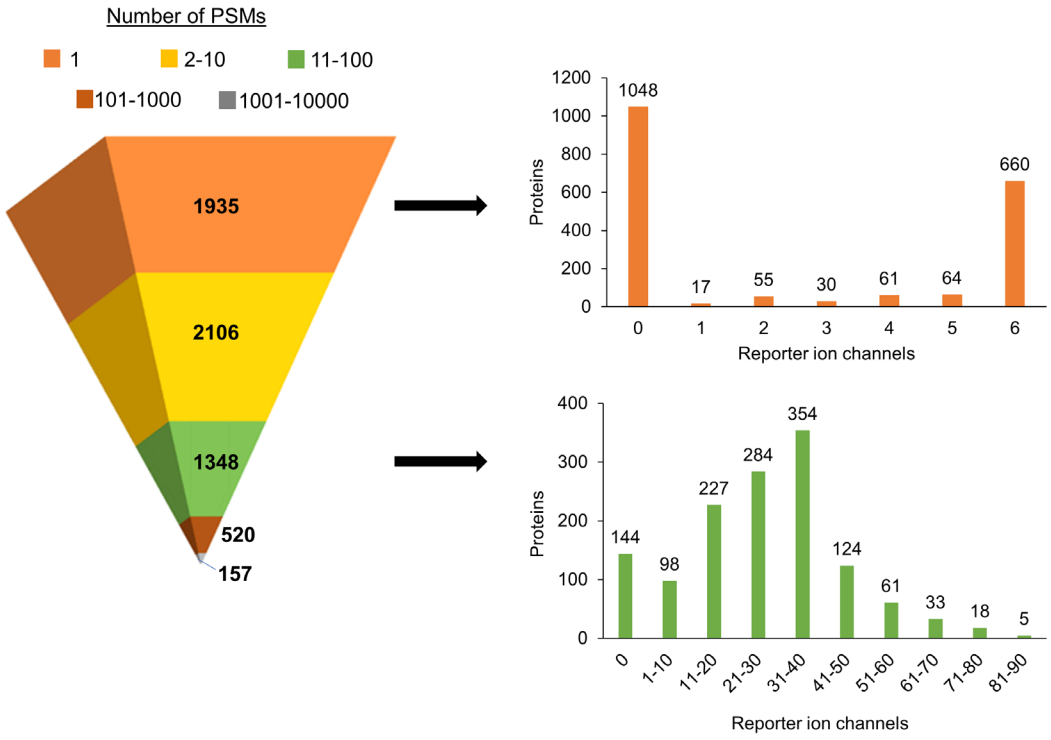

Figure 4.7 Distribution of PSMs within Identified Proteins. Proteins were identified from a range of 1 - >10000 PSMs per protein. Zoomed-in views of proteins identified from 1 PSM (top right) or 11 – 100 PSMs (bottom right), shows that most proteins identified by one 1 PSM were quantified in either 0 or 6 channels and that most proteins identified by 11 – 100 PSMs were quantified in at least two instrumental methods.

Generally, K-terminated peptides were selected ~58 – 63% (Table 4.4) for MS analysis across analysis methods and these peptides had a TMT^6 –plex labeling efficiency of 98% (Table 4.4). To compare reporter ion intensities across MS platforms, protein intensities shared across fractionated datasets (Figure 4.8) were compared. Proteins quantified in both fractionated datasets (N=846), had higher intensities of ~1 order of magnitude from the Fusion Lumos. This increase in reporter ion intensity is due to SPS and higher sensitivity for quantification.

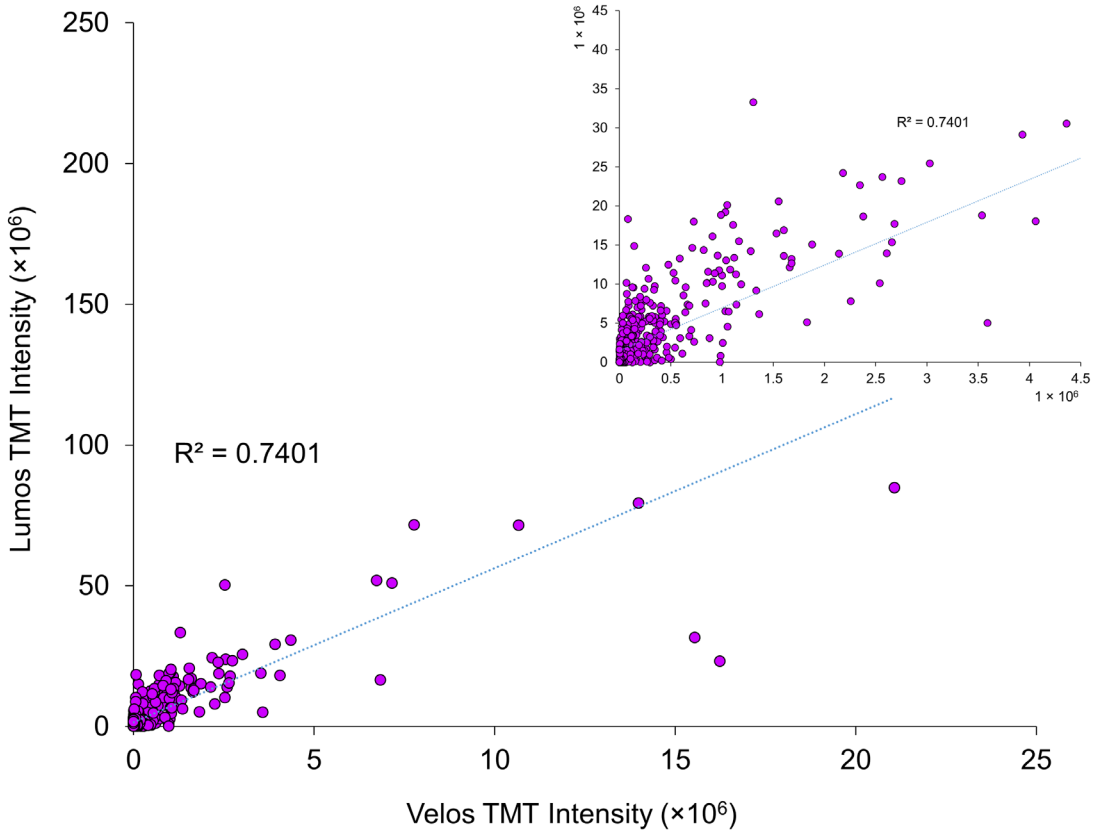

Figure 4.8 Correlation of Reporter-Ion Intensities from Proteins Present in Both Fractionated Datasets. After performing data normalization and statistics, reporter ion intensities corresponding proteins quantified were compared across fractionated datasets (N=846). Protein intensities increased by ~10× (see zoomed-in region) upon quantification by the Fusion Lumos. The reduction of the number of proteins quantified in both datasets is due to the number of proteins quantified from the Orbitrap Velos.

4.3.6 Differentially – Expressed Proteins in AD Brain, Heart, and Liver Tissues

System-wide changes in AD were evaluated in brain, heart, and liver proteins from WT and AD mice (Figure 4.9). Data used for statistical analysis was acquired from the Fusion Lumos. Eighty-five (N=39 brain, N=14 heart, and N=32 liver) varied significantly between AD and WT samples ($p<0.05$) with eight proteins varying substantially ($p<0.001$) in the brain or liver (Figures 4.9a and 4.9c). The most notable changes occurred in Apolipoprotein E in the brain (p=6.14E-6) and proteolytic protein MCG15081 (p=9.67E-5) in the liver.

Proteins that had both a $p<0.05$ and a fold-change of >1.2 or <0.83 (N=23, Table 4.5-bolded) were further analyzed with Ingenuity Pathway Analysis (IPA). Canonical pathways related to cell signaling were significant among brain proteins (Figure 4.10a), where pathways related to biosynthesis, degradation, and fatty acid oxidation were identified among liver proteins (Figure 4.10b). As expected, the molecular function lipid metabolism was also identified in both the brain and liver. Molecular functions related lipid and nucleic metabolism were identified in the heart.

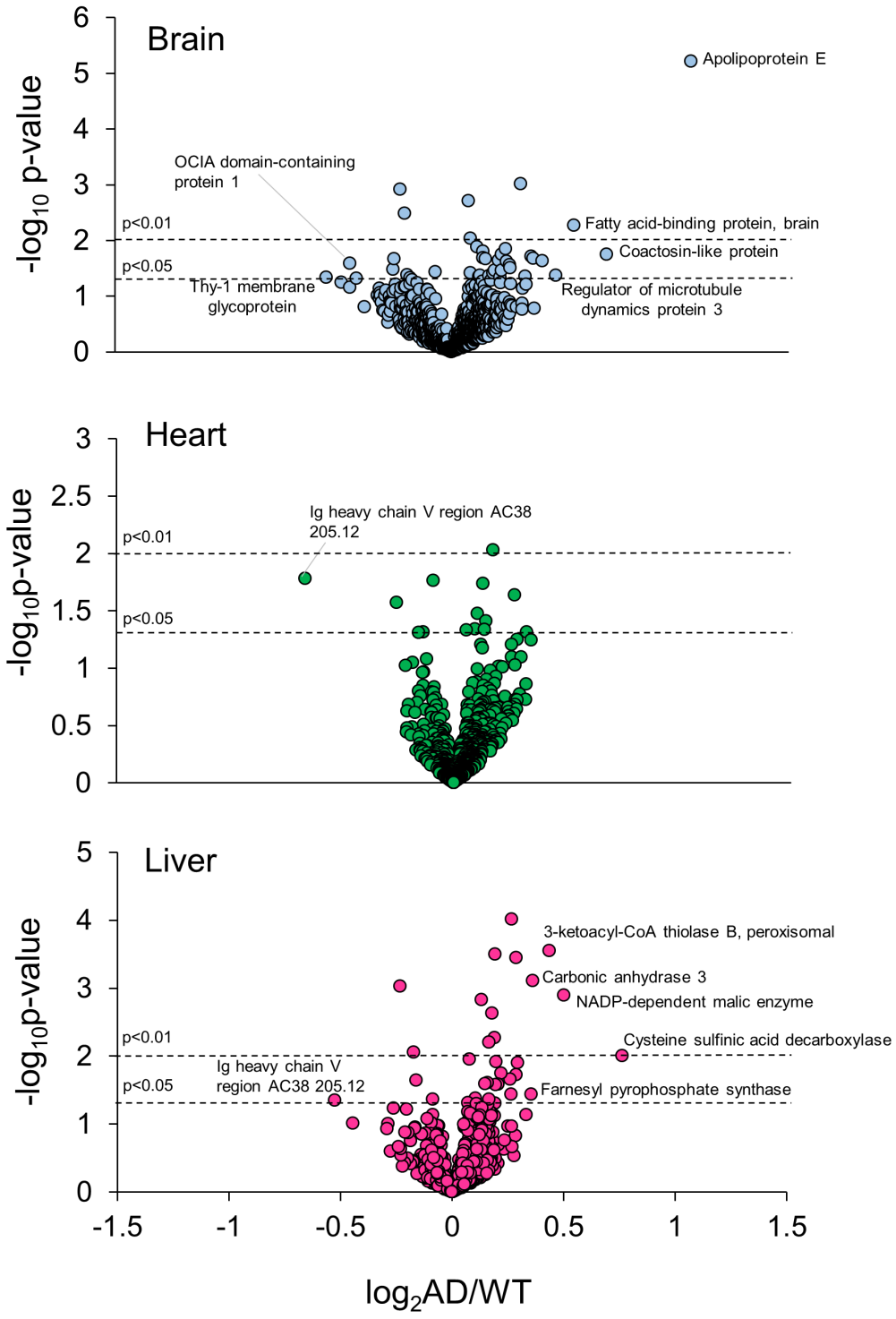

Figure 4.9 Volcano plots of Brain, Heart, and Liver Proteins as a Function of Disease. Normalized and filtered proteins were compared using a one-way-ANOVA. Proteins with a p <0.05 are present above the horizontal line (black) and correspond to a) brain, b) heart, and c) liver tissues.

Table 4.5 Differentially – Expressed Proteins in the Brain, Heart, and/or Liver.

Accession	Protein Description (short)	AD/WT Brain	p-value brain	AD/WT Heart	p-value heart	AD/WT Liver	p-value liver
Q792Y8	**MCG15081**	1.08 ± 0.13	7.70E-02	1.07 ± 0.16	2.90E-01	**1.20 ± 0.089**	**9.67E-05**
A0A075B5P6	Ig mu chain C region (Fragment)	1.00 ± 0.27	9.90E-01	0.89 ± 0.26	2.40E-01	0.82 ± 0.35	9.99E-02
A2AEG6	Glycoprotein m6b, isoform CRA_g	0.80 ± 0.33	9.73E-02	0.92 ± 0.24	-	0.96 ± 0.24	-
A2AWI7	Endophilin-B2	0.99 ± 0.25	7.50E-01	0.94 ± 0.36	-	1.21 ± 0.27	2.94E-01
B0QZN5	Vesicle-associated membrane protein 2	0.80 ± 0.34	8.75E-02	0.90 ± 0.19	-	0.97 ± 0.22	-
B1ATI0	**Aldehyde dehydrogenase**	1.07 ± 0.11	4.60E-01	1.02 ± 0.27	-	**1.22 ± 0.24**	**1.89E-02**
B9EKP8	Sorbin and SH3 domain-containing protein 2	0.83 ± 0.24	1.24E-01	0.97 ± 0.21	6.50E-01	1.13 ± 0.12	-
E9Q0H6	**Fatty acid-binding protein, brain**	**1.46 ± 0.61**	**5.44E-03**	1.02 ± 0.26	8.70E-01	0.98 ± 0.049	8.40E-01
E9Q827	cAMP-regulated phosphoprotein 19	0.82 ± 0.44	2.24E-01	1.03 ± 0.12	8.00E-01	1.08 ± 0.055	6.00E-01
E9QN63	Arf-GAP with SH3 domain, ANK repeat and PH domain-containing protein 1	0.83 ± 0.25	1.02E-01	0.86 ± 0.21	-	1.09 ± 0.093	-
O08532	Voltage-dependent calcium channel subunit alpha-2/delta-1	0.81 ± 0.29	1.81E-01	1.04 ± 0.43	8.30E-01	0.98 ± 0.19	-
O08715	**A-kinase anchor protein 1, mitochondrial**	1.24 ± 0.32	1.36E-01	0.88 ± 0.14	8.90E-02	**1.22 ± 0.084**	**3.59E-04**
O35381	Acidic leucine-rich nuclear phosphoprotein 32 family member A	1.07 ± 0.29	4.50E-01	1.22 ± 0.29	5.66E-02	1.04 ± 0.076	2.60E-01
O88935	Synapsin-1	0.81 ± 0.31	9.65E-02	0.99 ± 0.19	-	1.01 ± 0.087	9.40E-01
P01831	**Thy-1 membrane glycoprotein**	**0.68 ± 0.39**	**4.59E-02**	0.96 ± 0.069	-	1.02 ± 0.083	-
P06330	**Ig heavy chain V region AC38 205.12**	1.24 ± 0.57	-	**0.63 ± 0.18**	**1.66E-02**	**0.70 ± 0.20**	**4.46E-02**
P06801	**NADP-dependent malic enzyme**	1.10 ± 0.21	4.10E-01	1.07 ± 0.18	3.90E-01	**1.42 ± 0.31**	**1.28E-03**
P08226	**Apolipoprotein E**	**2.10 ± 0.38**	**6.14E-06**	1.02 ± 0.12	9.10E-01	1.13 ± 0.079	6.80E-02
P11404	Fatty acid-binding protein, heart	1.02 ± 0.22	-	1.23 ± 0.46	8.01E-02	0.97 ± 0.28	-
P14211	**Calreticulin**	**1.11 ± 0.027**	**2.14E-02**	1.06 ± 0.11	4.70E-01	0.96 ± 0.046	1.90E-01
P16015	**Carbonic anhydrase 3**	1.07 ± 0.20	-	1.01 ± 0.17	9.40E-01	**1.28 ± 0.27**	**7.80E-04**
P18242	**Cathepsin D**	**1.24 ± 0.093**	**9.72E-04**	1.01 ± 0.086	7.90E-01	0.99 ± 0.097	9.10E-01
P26041	Moesin	1.26 ± 0.29	6.22E-02	1.02 ± 0.075	8.80E-01	1.00 ± 0.093	9.70E-01
P34022	Ran-specific GTPase-activating protein	1.07 ± 0.21	4.80E-01	1.21± 0.25	2.27E-01	1.00 ± 0.17	-
P35802	Neuronal membrane glycoprotein M6-a	0.73 ± 0.32	7.02E-02	1.13 ± 0.18	-	1.00 ± 0.12	-
P35980	**60S ribosomal protein L18**	**0.75 ± 0.19**	**4.82E-02**	1.04 ± 0.20	8.60E-01	0.82 ± 0.24	1.20E-01
P43006	Excitatory amino acid transporter 2	0.82 ± 0.56	2.98E-01	0.99 ± 0.16	-	1.04 ± 0.18	-
P46978	Dolichyl-diphosphooligosaccharide--protein glycosyltransferase subunit STT3A	1.15 ± 0.19	2.80E-01	1.25 ± 0.41	1.38E-01	1.00 ± 0.18	9.30E-01
P48036	Annexin A5	1.29 ± 0.60	1.67E-01	1.03 ± 0.086	7.30E-01	1.09 ± 0.12	1.70E-01
P52196	Thiosulfate sulfurtransferase	1.22 ± 0.60	1.57E-01	1.07 ± 0.12	6.50E-01	1.03 ± 0.18	5.10E-01
P54822	Adenylosuccinate lyase	1.20 ± 0.60	1.45E-01	1.02 ± 0.22	8.80E-01	1.00 ± 0.098	9.90E-01
P56382	ATP synthase subunit epsilon, mitochondrial	1.24 ± 0.28	1.74E-01	0.91 ± 0.26	-	1.04 ± 0.21	-
P57759	**Endoplasmic reticulum resident protein 29**	**1.32 ± 0.47**	**2.32E-02**	1.08 ± 0.054	4.50E-01	0.98 ± 0.11	7.20E-01
P61027	Ras-related protein Rab-10	0.95 ± 0.28	6.00E-01	1.10 ± 0.27	-	1.26 ± 0.37	7.36E-02
P62281	40S ribosomal protein S11	0.80 ± 0.26	9.67E-02	0.95 ± 0.28	-	1.07 ± 0.25	5.10E-01
P63037	DnaJ homolog subfamily A member 1	0.98 ± 0.22	8.30E-01	1.21 ± 0.20	1.89E-01	1.04 ± 0.13	6.50E-01
P84091	AP-2 complex subunit mu	0.82 ± 0.31	8.00E-02	1.03 ± 0.18	-	0.99 ± 0.051	8.40E-01
Q06890	**Clusterin**	**1.61 ± 0.81**	**1.79E-02**	0.92 ± 0.20	3.60E-01	0.93 ± 0.075	4.40E-01
Q62277	Synaptophysin	0.80 ± 0.34	1.10E-01	1.05 ± 0.15	-	1.04 ± 0.10	-
Q64176	Carboxylesterase 1E	1.24 ± 0.094	-	0.90 ± 0.24	-	1.22 ± 0.10	1.50E-01
Q6AXD2	Abi2 protein	0.71 ± 0.33	5.67E-02	0.96 ± 0.55	-	1.09 ± 0.20	-
Q6P6I8	Signal-regulatory protein alpha	0.76 ± 0.35	1.57E-01	1.34 ± 0.69	-	1.04 ± 0.093	-
Q71KT5	**Delta(14)-sterol reductase**	0.99 ± 0.22	-	1.09 ± 0.22	-	**1.20 ± 0.27**	**3.65E-02**
Q8BG32	**26S proteasome non-ATPase regulatory subunit 11**	0.97 ± 0.19	7.10E-01	**1.25 ± 0.40**	**4.88E-02**	0.97± 0.074	4.40E-01
Q8CAA7	Glucose 1,6-bisphosphate synthase	0.83 ± 0.32	1.31E-01	1.17 ± 0.28	-	0.95 ± 0.14	-
Q8CBB6	Histone H2B OS	1.18 ± 0.89	-	1.21 ± 0.46	2.08E-01	1.03 ± 0.16	8.40E-01
Q8VCH0	**3-ketoacyl-CoA thiolase B, peroxisomal**	1.05 ± 0.18	-	0.99 ± 0.13	9.40E-01	**1.35 ± 0.26**	**2.80E-04**
Q8VIJ6	Splicing factor, proline- and glutamine-rich	1.12 ± 0.30	2.90E-01	1.25 ± 0.20	1.87E-01	1.01 ± 0.094	9.00E-01
Q91X83	**S-adenosylmethionine synthase isoform type-1**	0.92 ± 0.25	-	1.20 ± 0.27	-	**1.23 ± 0.35**	**1.25E-02**
Q920E5	**Farnesyl pyrophosphate synthase**	1.20 ± 0.23	2.10E-01	0.99 ± 0.22	-	**1.28 ± 0.53**	**3.66E-02**
Q923D2	Flavin reductase (NADPH)	1.21 ± 0.34	1.49E-01	1.05 ± 0.18	6.70E-01	1.05 ± 0.077	1.60E-01
Q99J39	Malonyl-CoA decarboxylase, mitochondrial	1.05 ± 0.16	6.80E-01	1.27 ± 0.45	5.72E-02	0.99 ± 0.23	8.90E-01
Q99LB6	Methionine adenosyltransferase 2 subunit beta	1.06 ± 0.19	4.30E-01	1.22 ± 0.20	1.89E-01	1.09 ± 0.22	3.60E-01
Q99N87	**28S ribosomal protein S5, mitochondrial**	0.80 ± 0.16	7.32E-02	**1.21 ± 0.24**	**2.31E-02**	1.08 ± 0.12	2.60E-01
Q99PL6	UBX domain-containing protein 6	0.96 ± 0.14	6.40E-01	1.02 ± 0.12	9.10E-01	1.20 ± 0.19	2.18E-01
Q9CQI6	**Coactosin-like protein**	**1.28 ± 0.37**	**1.95E-02**	0.90 ± 0.13	-	1.08 ± 0.17	4.30E-01
Q9CRD0	**OCIA domain-containing protein 1**	**0.73 ± 0.23**	**2.62E-02**	0.98 ± 0.40	-	0.73 ± 0.20	9.70E-02
Q9CXS4	Centromere protein V	1.07 ± 0.11	3.70E-01	1.23 ± 0.34	1.69E-01	0.98 ± 0.17	7.70E-01
Q9CYT6	Adenylyl cyclase-associated protein 2	0.83 ± 0.38	1.90E-01	1.03 ± 0.12	7.50E-01	1.00 ± 0.10	-
Q9CZ44	NSFL1 cofactor p47	1.13 ± 0.34	1.60E-01	1.20 ± 0.28	2.49E-01	1.20 ± 0.18	1.09E-01
Q9D0F9	Phosphoglucomutase-1	1.25 ± 0.40	7.34E-02	1.00 ± 0.055	9.90E-01	1.08 ± 0.067	1.40E-01
Q9DAW9	**Calponin-3**	**1.26 ± 0.43**	**4.43E-02**	1.20 ± 0.27	-	1.06 ± 0.39	5.90E-01
Q9QYB8	Beta-adducin	0.81 ± 0.37	1.88E-01	1.27 ± 0.27	-	0.96 ± 0.12	8.10E-01
Q9Z1Q5	**Chloride intracellular channel protein 1**	**1.29 ± 0.34**	**2.10E-02**	1.05 ± 0.069	5.50E-01	1.02 ± 0.087	8.20E-01
Q9Z2Q6	Septin-5	0.81 ± 0.37	1.29E-01	1.00 ± 0.25	9.90E-01	1.00 ± 0.098	-
V9GX76	Unconventional myosin-VI	1.20 ± 0.26	6.12E-02	0.93 ± 0.16	-	1.04 ± 0.19	7.70E-01

Differentially - expressed proteins have p<0.05 and AD/WT of >1.20 or <0.83 brain, heart, and liver tissues and are in **bold.**

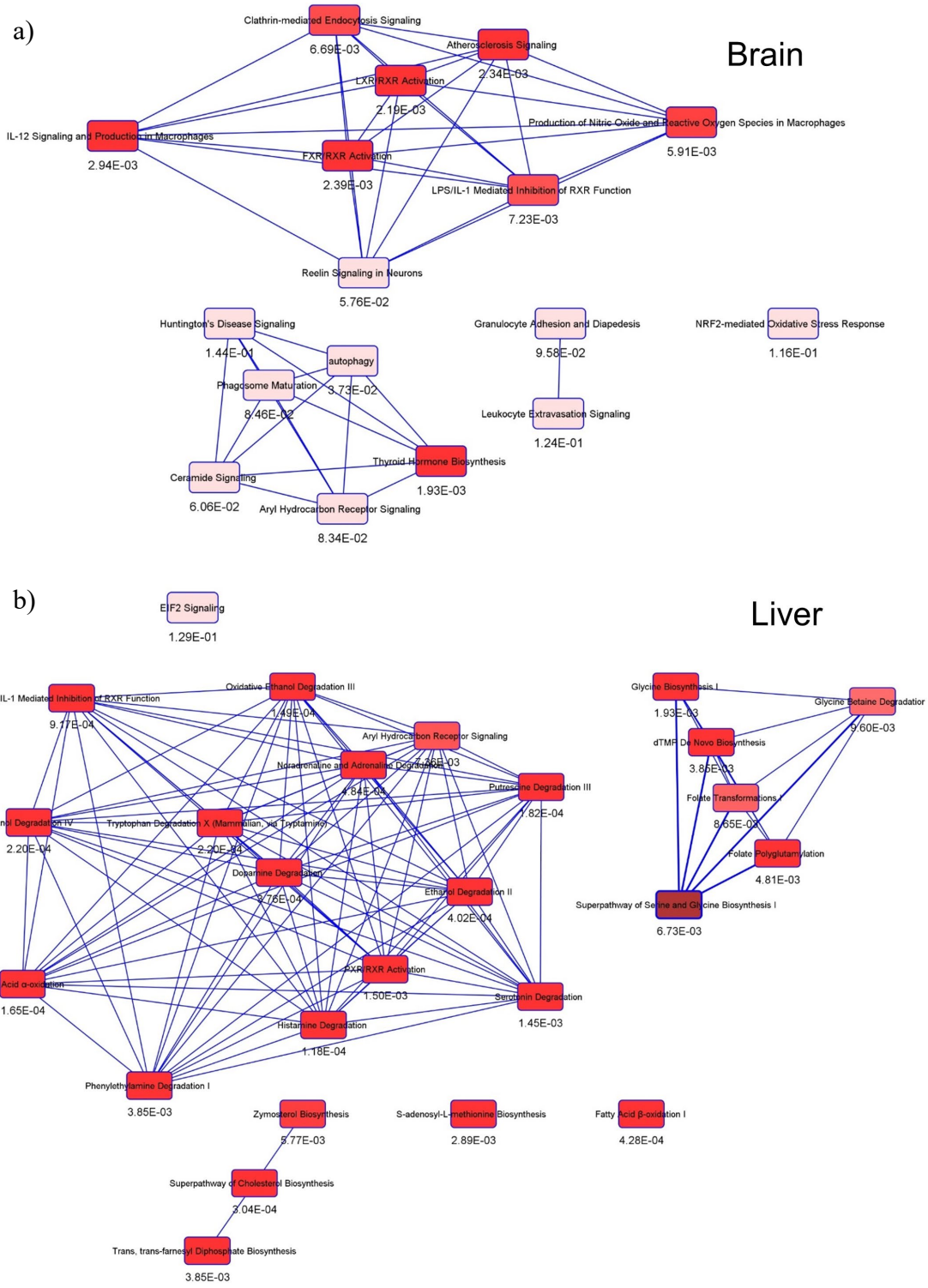

Figure 4.10 Canonical Pathways of Statistically-Significant Proteins in a) Brain and b) Liver Tissues. Pathways related to cell signaling, metabolism, and cell development were identified by IPA in the a) brain and b) liver.

4.4 DISCUSSION

The most biological information is gained from cPILOT experiments when quantitative information is obtained from all samples. To achieve this goal, high labeling efficiencies are necessary, both light and heavy dimethylated pairs must both be selected for tandem MS analysis, and selected peptides must generate reporter ion intensities above the minimum threshold. On the Orbitrap Velos platform, quantitative information was gained from all samples by 1) implementing offline SCX fractionation, 2) applying a two-tiered DDA method to select both high- and low abundant peptides and 3) using longer LC gradients and MS^3 quantification. The tradeoffs of this two-tiered DDA approach are, increased sample and data analysis times and due to single-notch MS^3, missing reporter ion channels. The Fusion Lumos dramatically improved the performance of the cPILOT analysis and increased the number quantified dimethylated peptide pairs.

4.4.1 cPILOT Method Optimization Experiments (Fusion Lumos)

To modify cPILOT analysis for the Fusion Lumos, the LC gradient time, precursor isolation window, dynamic exclusion time, targeted analyses, and SPS-N were varied. These experiments identified and quantified similar amounts of proteins without SCX fractionation, in comparison to the Orbitrap Velos. This was due to a number of factors, including the improved analytical separation of peptides, increased scanning speed of both the Orbitrap and ion trap mass analyzers and the improved resolution of identified peptides. Fractionated peptides were analyzed on both the Orbitrap Velos and Fusion Lumos to have a more direct instrument

comparison. Between these two datasets, the Fusion Lumos generated more proteins and peptides identifications. Overall, targeted mass difference and SPS-N parameters were most critical for improving the effectiveness of cPILOT analysis on the Fusion Lumos. The targeted mass difference function specifies the number of precursors within a group by the difference in mass, thus selecting one peak within the peptide pair or both peptides in the pair. This function increased the number of light and heavy dimethylated pairs overlap to ~70 – 80% across all sample channels, thus increasing the percentage of proteins which have quantitative information. In addition, the use of SPS-MS^3 improved the percentage of proteins quantified in all channels by ~20%, in comparison to the Orbitrap Velos thus improving the ability to quantify less abundant proteins.

Challenges related to analyzing cPILOT on the Fusion Lumos were related to the selection of peptide pairs and quantifying low abundant peptides. Light dimethylated peptides were selected for isolation and fragmentation more frequently than heavy dimethylated peptides. This is problematic as not fragmenting both peaks in a pair reduces the amount of information that can be learned. In addition, lower abundance proteins have more missing reporter ion channels or low S/N reporter ions. Overall, it was extremely worthwhile to evaluate different instrumental parameter methods for cPILOT. This gave the foundation of the AD study herein where proteome changes across tissues types and disease were investigated.

4.4.2 AD Pathogenesis from Brain, Heart, and Liver Tissues

cPILOT was applied to AD brain, heart, and liver tissues to understand the contribution of the periphery to AD pathogenesis. Canonical pathways identified (Figure 4.10), including

clathrin-mediated endocytosis signaling (Figure 4.10a) and cholesterol biosynthesis (Figure 4.10b) are known to occur in AD.[174-176] Differentially – expressed proteins apolipoprotein E and clusterin, proteins well-known in AD brain pathogenesis,[177-178] were higher in expression in the brain in this study. In the liver, mostly metabolic proteins, including aldehyde dehydrogenase, 3-ketoacyl-CoA thiolase-B, peroxisomal, and NADP-dependent malic enzyme were higher in AD mice compared to WT. These proteins are involved in glycolysis/gluconeogenesis and the Krebs cycle and may contribute to dysregulated metabolism identified in AD.[179-180] In the heart, 28s ribosomal protein S5, mitochondrial, and 26S proteasome non-ATPase regulatory subunit 11 are related to protein synthesis and folding were higher in AD mice. Immunoglobulin protein, Ig heavy chain V region AC38 205.12, was lower in AD mice in both heart and liver tissues, and may be involved in eliciting an immune response.[181] Proteins related to electron transport and metabolism were at higher levels in the heart which has been related to mitochondrial dysfunction.[182] In addition, proteins related to metabolism, protein folding, peptide synthesis, and oxidative stress were higher in the in the brain and liver of AD mice compared to WT.

Across tissues, quantified proteins (Figure 4.11) in both WT and AD were mostly present in all tissues. MA plots of quantified tissues show that proteins across tissues have a wide range of changes (Figure 4.12) with ratios >4-fold. Interestingly, brain vs. liver proteins (in both WT and AD) have the widest range of change, though it expected that these tissues would behave in a similar fashion.

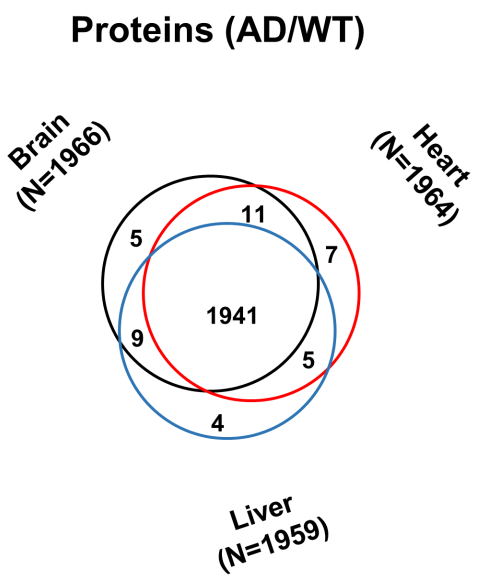

Figure 4.11 Comparison of Quantified Brain, Heart, and Liver Proteins.

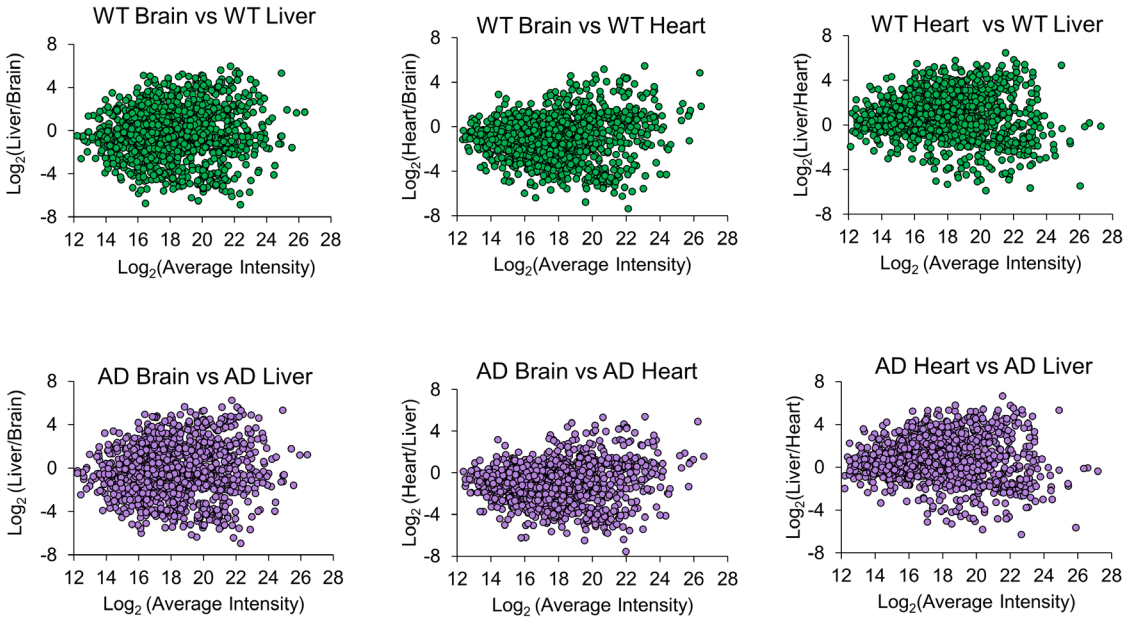

Figure 4.12 MA plots of Quantified Brain, Heart, and Liver Proteins.

4.5 CONCLUSIONS

These experiments have provided insight into 1) cPILOT performance on two Orbitrap instruments and 2) understanding the peripheral proteome of AD. Successful cPILOT analysis on the Fusion Lumos was achieved by using longer LC gradients, targeted mass difference, a wider precursor isolation window, and increase of SPS ions to identify more dimethylated peptide pairs and to increase the percentage of quantified data. With both the Orbitrap Velos and Fusion Lumos capable of cPILOT analysis, this multiplexing strategy is versatile and can be applied to a host of Orbitrap MS platforms and experimental studies. As a function of disease, an increase of metabolic processes, including carbohydrate, lipid, and peptide metabolism occurs across tissues, with the most prominent changes occurring in the brain and liver. Though there was minimal overlap in the number of statistically – significant proteins across tissues, the similarity of molecular functions may indicate that AD pathogenesis occurs similarly across these tissues, but with different mechanisms.

5.0 PROTEOMICS ANALYSIS OF HUMAN POSTMORTEM TISSUES IN ALZHEIMER'S DISEASE

5.1 INTRODUCTION

Alzheimer's disease (AD) is a neurodegenerative disorder that results in cognitive decline. Classical hallmarks of this disease include the deposit of amyloid beta (Aβ) plaques and neurofibrillary tangles. It is also a metabolic disorder that causes lower cerebral glucose metabolism,[183-185] dysregulated lipid metabolism,[149, 186-187] and increased insulin resistance.[188-190] These changes are well-defined in the brain, but are also present in the periphery. Altered metabolic processes in skin fibroblasts[191] and mitochondrial dysfunction in lymphocytes[192] suggests that the periphery may be involved in AD pathogenesis. One peripheral tissue that has been implicated in AD is the liver. This tissue is responsible for protein synthesis, detoxification, and metabolizing molecules. It is also responsible for degrading and clearing Aβ peptides.[193-195] The proteomics analysis of liver tissues from amyloid precursor protein/presenilin-1 (APP/PS-1) mice in our laboratory,[84] identified changes related to carbohydrate and fatty – acid metabolism, transcription and translation, and redox signaling. These pathways highlight that AD is a metabolic disorder. Another tissue that may be involved in AD pathogenesis is the heart. This organ is a part of the circulatory system and pumps blood, which provides oxygen and nutrients to tissues. Cardiovascular disease (CVD) risk factors, including hypercholesterolemia,

hypertension, diabetes, obesity, and smoking are also risk-factors in AD.[154] Pre-clinical markers of CVD (e.g. intima media thickness,[196] carotid plaques,[196-197] lacunae,[198-199] and white matter lesions[200-201]) are also more prevalent in AD. One hypothesis is that CVD risk factors cause brain hypoperfusion, which results in cognitive decline and increases the chances of developing AD.[202] Generally though, the molecular mechanisms of how the heart may contribute to AD pathogenesis are still poorly understood.[28, 203-205]

Proteomics analyses of peripheral cells and tissues have been performed on ante-/post-mortem samples from humans and model organisms. Plasma,[206] cerebrospinal fluid,[207] and blood derived lymphocytes[192] have been studied, identifying inflammatory and metabolic proteins related to AD progression. Post-mortem proteomics analyses of tissues have been performed using brain regions (e.g. hippocampus,[208] cortical samples,[209] olfactory bulb,[210] prefrontal cortex,[211] and temporal neocortex[212]), and result in changes related to immune response, metabolism, and apoptosis. Proteomics analyses of peripheral tissues in AD have been limited to mouse models. In these studies, splenocytes[213] and liver[84] samples were studied in 14-month-old APP/PS-1 mice, resulting in changes in glucose metabolism, electron transport, and oxidative phosphorylation. Most recently, a multi-tissue analysis was performed, comparing brain, heart, and liver tissues from this model (**Chapter 4**). APP/PS-1 is a human double transgenic mouse model which develops amyloid-beta plaques and has cognitive decline with increasing age.[156]

Here, we designed a translational study to obtain a more direct understanding of how the periphery may be involved in AD pathogenesis. Brain (superior frontal gyrus), heart, and liver tissues from AD (Braak stages IV and V) and cognitively normal (CN) controls were analyzed using quantitative proteomics techniques. The SFG is a part of the frontal lobe and is responsible for higher cognitive function, working memory, and impulse responses.[214-215]

Combined precursor isotopic labeling and isobaric tagging (cPILOT), an enhanced multiplexing strategy has been implemented.[80, 83, 91] This method allows up to 24 samples to be analyzed simultaneously[91], thus increasing sample throughput while decreasing instrumental analysis time. Similarities and differences across both disease-state and tissue-type have been directly compared within one experiment. Results from these experiments provide insight into understanding how the periphery contributes to late – onset AD, thus revealing similarities and differences across these tissues response to disease.

5.2 EXPERIMENTAL PROCEDURES

5.2.1 Tissue Harvesting and Ethical Statement

Frozen human brain (superior frontal gyrus), heart, and liver tissues were collected post-mortem from 3 AD patients and 3 cognitively normal control subjects (Table 1). The AD cases were neuropathologically diagnosed as CERAD-NP definite AD, Braak stages IV and V. All samples were obtained from Banner Sun Health Research Institute (Sun city, AZ). Samples were collected 3-5 hours post-mortem, frozen, and stored at -80 ^{o}C prior to sample handling. The collection of brain, heart, and liver tissues and the conducted research had been approved by the Institutional Review Board at Vanderbilt University.

Table 5.1 AD and CN Subject Clinical and Neuropathological Data.

patient	case	gender	race	age	Braak stage
1	control	male	Caucasian	79	II
2	control	male	Caucasian	74	I
3	control	male	Caucasian	87	III
4	AD	male	Caucasian	77	IV
5	AD	male	Caucasian	87	V
6	AD	male	Caucasian	73	IV

5.2.2 Tissue Homogenization, Protein Extraction, and Digestion

Brain, heart, and liver tissues were homogenized with a mechanical homogenizer (Fastprep 24) to generate tissue lysates. To extract protein, samples were centrifuged (13,000 rpm, 4 ^{o}C, 15 min) and supernatant were collected. Protein concentration was determined using BCA assay. Protein from brain, heart, and liver tissues (~100 µg) was reduced (DTT 1:40 mol ratio), alkylated (IAA 1:80 mol ratio), quenched (L-cysteine 1:40 mol ratio), and digested with trypsin/lys-c (1:100 mol ratio) for 8 h. Peptides were desalted using a HLB cartridge and dried down using centrifugal evaporation. Prior to labeling by cPILOT, peptide concentration was determined by using BCA assay.

5.2.3 cPILOT Labeling

Peptides (~50 µg) were dissolved in 1% acetic acid (0.25 $\mu g \cdot \mu L^{-1}$). Formaldehyde /deuterated formaldehyde (Sigma Aldrich, 8 µL) and sodium cyanoborohydride/-deuteride (Sigma Aldrich, 8 µL) are added to either label peptides with light [$(-CH_3)_2$] or heavy [$(-^{13}CD_3)_2$] dimethyl groups, respectively. Peptides were reacted at room temperature for 10 min with shaking. To quench the reactions, of 1% ammonia (16 µL) was added for 5 min. Dimethylated peptides were re-acidified with 5% formic acid and light and heavy samples, were pooled (Table 5.2), desalted, and dried down by centrifugal evaporation. Desalted dimethylated peptides were dissolved in 100 mM triethyl ammonium bicarbonate (TEAB) buffer and TMT^{6}-plex reagents were prepared according to the manufacturer's protocol. TMT^{11}-plex reagents were added to peptides (Table 5.2) and reacted at room temperature for 1 h with shaking. Peptides labeled by

cPILOT were quenched with 5% (w/v) hydroxylamine-hydrochloride for 15 min and re-acidified with formic acid. Peptides were then pooled together into a single sample, concentrated, desalted, and dried down an additional time by centrifugal evaporation.

Table 5.2 Experimental Scheme of cPILOT

TMT^{11}-plex tag	126	127n	127c	128n	128c	129n	129c	130n	130c	131n	131c
Light DM	Pool 1	CN Liver 1	AD Liver 1	CN Liver 2	AD Heart 2	CN Heart 3	AD Heart 3	CN Brain 1	AD Brain 1	CN Brain 2	Pool 2
Heavy DM	Pool 1	CN Heart 1	AD Heart 1	CN Heart 2	AD Liver 2	CN Liver 3	AD Liver 3	AD Brain 2	CN Brain 3	AD Brain 3	Pool 2

5.2.4 Offline SCX Fractionation

Peptides were fractionated according to the manufacturer's protocol (Protea Biosciences). Briefly, peptides (600 µg) were dissolved in buffer A and loaded onto a pre-activated spin column. Peptides were eluted off the spin column in 8 intervals (room temperature, 6 min, 4000 × g) with increasing ammonium formate solutions (i.e. 20 mM, 40 mM, 60 mM, 80 mM, 100 mM, 150 mM, 250 mM, and 500 mM). Fractionated peptides were dried down by centrifugal evaporation and dissolved in 0.1% formic acid.

5.2.5 Liquid Chromatography and Mass Spectrometry Analyses

Online desalting and reversed-phase chromatography was performed with a nano-UHPLC system equipped with an autosampler (Dionex, ThermoFisher Scientific). Mobile phases A and B used for separation were (v/v) 0.1% formic acid and 100% ACN with 0.1% formic acid,

respectively. Peptides (250 ng) were loaded onto a trapping column (100 µm i.d. x 2 cm), which was packed in house with C_{18} (3 µm, 200 Å) stationary phase material (Michrom Bioresource Inc,) at 3 µL*min^{-1} in 2% ACN with 0.1% FA for 7 min. After desalting, the sample was loaded onto an analytical column (100 µm i.d. x 25 cm), which was packed in-house with C_{18} (2.5 µm, 150 Å, Waters). The gradient was as follows: 0 – 10 min, 10% mobile phase B; 10 – 30 min, 10 – 15% B; 30 – 75 min, 15 – 30% B 75 – 88 min, 30 – 60% B; 88 – 92 min, 60 – 90% B; 92 – 99 min, 90% B; 99 – 100 min, 90 – 10% B; 100 – 120 min, 10% B.

Standard data-dependent acquisition parameters were as follows: the MS survey scan in the OT (375 – 1500 *m/z*) was 120,000 resolution; the most intense peaks with 3s (Top Speed) were isolated (2 *m/z*) and fragmented with collision-induced dissociation (CID) in the ion trap with an NCE of 35%, AGC of 1 x 10^4, dynamic exclusion of 20 s, ppm mass tolerance of 10, maximum IT of 100 ms. Peptide pairs were targeted by using the targeted mass difference node. Two precursors were listed for the targeted group. In addition, a mass difference of 8.0444 Da (Heavy DM – Light DM) and 7.0381 Da (Dimethyl 7 – Light DM) were listed, the partner intensity range relative to the most intense precursor was set to 70 – 100 %, a subsequent scan was performed on both ions in the pair, and the charge state for ions in the pair had to be the similar. Directly after each MS/MS scan, the ten most intense fragment ions (over varying *m/z* ranges) were selected for an additional fragmentation (i.e. MS^3) event by HCD and analyzed in the OT (scan range: 100 – 400 *m/z*, isolation width: 2 *m/z,* AGC: 5 x 10^4, NCE: 55%, resolution: 60,000, maximum IT: 118 ms). Other parameters such as precursor selection range, precursor ion exclusion, and isobaric tag loss exclusion were set as default. Each fraction was subject to triplicate injections.

5.2.6 Data Analysis

Raw files were analyzed with PD v. 2.2 software (Thermo Scientific). Spectra were used to obtain sequence information against the Uniprot *H. Sapiens* database (06/27/18, 20319 sequences). SEQUEST HT search parameters were as follows: two maximum trypsin miscleavages, precursor mass tolerance of 15 ppm, fragment mass tolerance of 1 Da; static modifications were either light or heavy/dimethyl 7Da Dimethyl/+28.031 or 36.028/35.070 Da (N-terminus) and carbamidomethyl modification/+57.021 Da (Cys); dynamic modifications were TMT eleven-plex/+229.163 Da (Lys) and oxidation modification/+15.995 Da (Met). Decoy database searching was employed to generate medium ($p<0.05$) confidence peptide lists. All peptides with medium confidence were used to identify and quantify proteins. To filter peptides, the following parameters were applied: peptides with a PSM (peptide to spectral match) >1 across biological replicates, peptide confidence level of medium, peptide rank of 1, peptide deviation of 10 ppm, and S/N ≥10. The reporter ions (i.e. *m/z* 126 – 131) were identified with the following parameters: most confident centroid and 30 ppm for reporter ion mass tolerance. Furthermore, reporter ion values were normalized using internal reference scaling. Proteins with only N=3 biological replicates were used for normalization.

To identify statistically-significant proteins, a one-way ANOVA was performed in Perseus software. Proteins with a p-value <0.05 and a fold-change of >1.2 or <0.83 were further used for bioinformatics analyses. Statistically – significant proteins were searched against databases in ingenuity pathway analysis (IPA) to identify significant-pathways.

5.3 RESULTS

Here, we designed a quantitative proteomics experiment (Figure 5.1) to better understand molecular mechanisms in the heart and liver that may contribute to AD progression. These tissues were compared to the brain, which is well-studied in AD, to understand similarities and differences across brain and peripheral tissues in AD. Protein from brain, heart, and liver post-mortem tissues and cognitively normal controls (N=3) were extracted and digested using trypsin/lys-c. Peptides from eighteen samples and four pooled samples were labeled (Table 5.2) at the N-terminus with light or heavy dimethylated groups and at lysine residues with TMT^{11}-plex (cPILOT). Labeled peptides were then pre-fractionated using SCX and analyzed by LC – MS/MS and MS^3.

This analysis identified 136,084 PSMs corresponding to 14,892 unique peptides and 3085 proteins (Appendix D Tables D5.1 and D5.2). Proteins quantified (Figure 5.2a) in all tissues (2082, 67%) had a tremendous overlap (~99%) in brain (N=2095), heart (N=2091), and liver (N=2091) tissues. A marginal overlap of quantified proteins was present among brain and liver (N=7), heart and liver (N=1) and heart and brain (N=6). In addition, a minimal portion of proteins were only quantified in one tissue-type, suggesting that most proteins were present across all tissues.

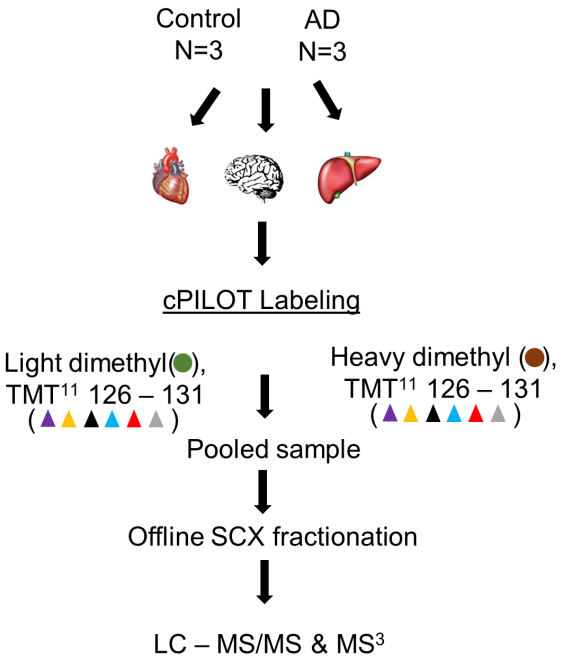

Figure 5.1 Experimental Workflow of Human Post-Mortem AD and CN Brain, Heart, and Liver Tissues.

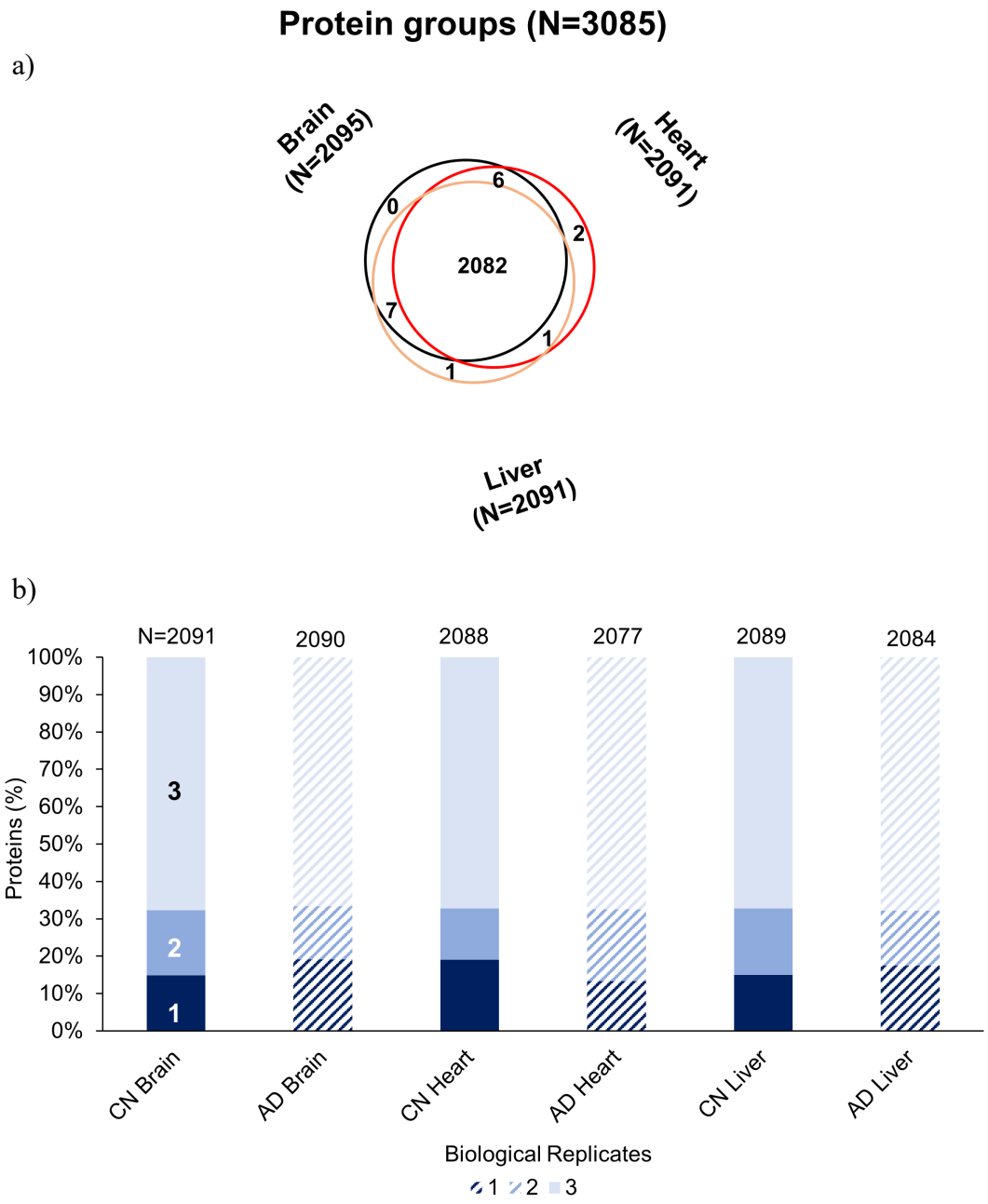

Figure 5.2 Protein Quantification of Brain, Heart, and Liver Tissues a) across all and b) each Biological Replicate. Proteins identified (N=3085) were quantified in most tissues (N=2082), with a slight increase in the brain (N=2095). In addition, >60% of proteins were quantified in all biological replicates.

Quantified proteins had a TMT-reporter intensity above the minimal threshold in either CN or AD tissue. Among quantified proteins, >60% were quantified in all biological replicates (Figure 5.2b) whereas 15 – 20% were quantified in one biological replicate. This range is not specific to one tissue type or genotype, as higher percentages of proteins quantified in one biological replicate is present in both AD and CN from all tissues.

5.3.1 Hierarchical Clustering Patterns of Quantified Brain, Heart, and Liver Tissues

Quantified proteins across CN and AD brain, heart, and liver tissues (N=3 biological replicates) were visualized to identify similar and different clustering patterns across tissue and disease state. With a stringent filter applied (average coefficient of variation <0.33 across all tissues), quantified proteins that met this criteria (N=147) were clustered (Figure 5.3). CN and AD tissues clustered together (i.e. CN and AD brain, CN and AD heart, and CN and AD liver), highlighting potential differences across tissues. In the top region (Figure 5.3, zoom-in top), proteins are at higher levels in the heart and liver, whereas they are at lower levels in the brain. CN and AD levels in the region also had similar changes across these tissues. Example proteins in this region that follow this trend include metabolic proteins aldehyde dehydrogenase and isocitrate dehydrogenase (NADP), mitochondrial. In the middle region (Figure 5.3, zoom-in *not shown*), proteins were present at slightly higher levels in the heart, while at lower levels in the brain and liver. This region includes several proteins involved in electron transport, including cytochrome c oxidase, subunit 7c and cytochrome b-c1 complex subunit 1. Lastly, in the bottom region (Figure 5.3, zoom-in bottom), proteins in the brain are at higher levels while proteins in

both the heart and liver are at lower levels. Proteins that follow this trend include syntaxin binding protein-1 (STXBP-1) and tubulin alpha 1A chain.

In both brain (Figure 5.4a) and heart (Figure 5.4b) tissues, protein distributions are similar, with comparable numbers of proteins changing at both higher and lower levels in AD. In the liver (Figure 5.4c), however, there was a larger percentage of proteins that changed at lower levels in AD compared to CN.

Figure 5.3 Hierarchical Clustering Across CN and AD Brain, Heart, and Liver Tissues. Proteins quantified with a CV<0.33 across all samples (N=147) were clustered using Clustvis[216] and input with ln transformed values.

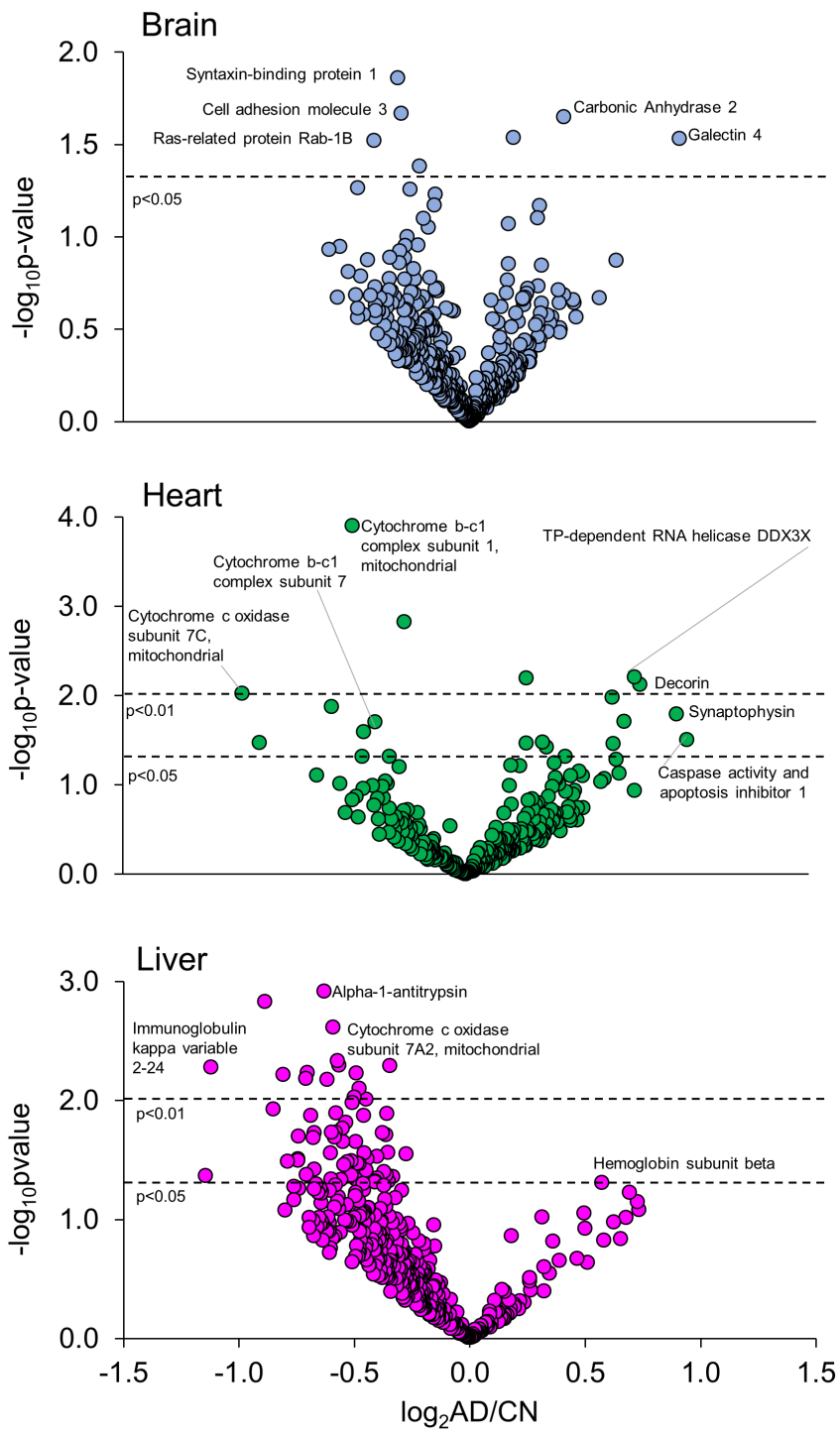

Figure 5.4 Volcano Plots of Brain, Heart, and Liver Tissues. Protein distributions across a) brain, b) heart, c) liver tissues. Volcano plots display proteins with a fold change of >1.2 or <0.83 and a p value <0.05 (horizontal lines) were statistically – significant.

Among proteins that had a significant fold-change as a function of disease (AD/CN >1.2 or < 0.83), some interesting trends were present. In the brain, few proteins met this criteria, whereas in the heart and liver, many proteins were expressed at lower or higher levels. Tissue samples, per biological replicate, originated from the same person, therefore a system-wide analysis of these tissues could be profiled. Selected proteins differentially – expressed in AD compared to CN (in at least one tissue) were compared across tissues (Figure 5.5). Both cAMP-dependent protein kinase type II-beta regulatory subunit (CAAP-1, Figure 5.5a) and syntaxin-binding protein 1 (STXBP-1, Figure 5.5b) were quantified at higher levels in the brain and at lower levels in both the heart and liver. In both proteins, AD levels compared to CN were lower in the brain (CAAP-1: 0.88 ± 0.64, STXBP-1: 0.81± 0.054) while higher in the heart (CAAP-1: 1.96 ± 0.94, STXBP-1: 1.27 ± 0.69). In the liver, these proteins were at either higher (1.47 ± 0.88) or lower (0.79 ± 0.29) levels. In hemoglobin protein beta (HBB, Figure 5.5c), proteins were at higher levels in the brain (1.24 ± 0.23) while at lower levels in the liver (0.77 ± 0.21); in the heart, proteins levels were more abundant than in the liver, but at similar levels in AD compared to CN (1.08 ± 0.38). Lastly, in both cytochrome b-c1 complex subunit 1, mitochondrial (Figure 5.5d) and thioredoxin-related transmembrane protein 4 (Figure 5.5e), Protein levels in AD compared to CN were lower in both the brain (UQCRC1: 0.82 ± 0.17, TMX-4: 0.77 ± 0.34) and liver (UQCRC1: 0.79 ± 0.24, TMX-4: 0.68 ± 0.088. However, AD levels in the heart were at either lower (UQCRC1 0.71 ± 0.034) or higher (1.35 ± 0.19) levels.

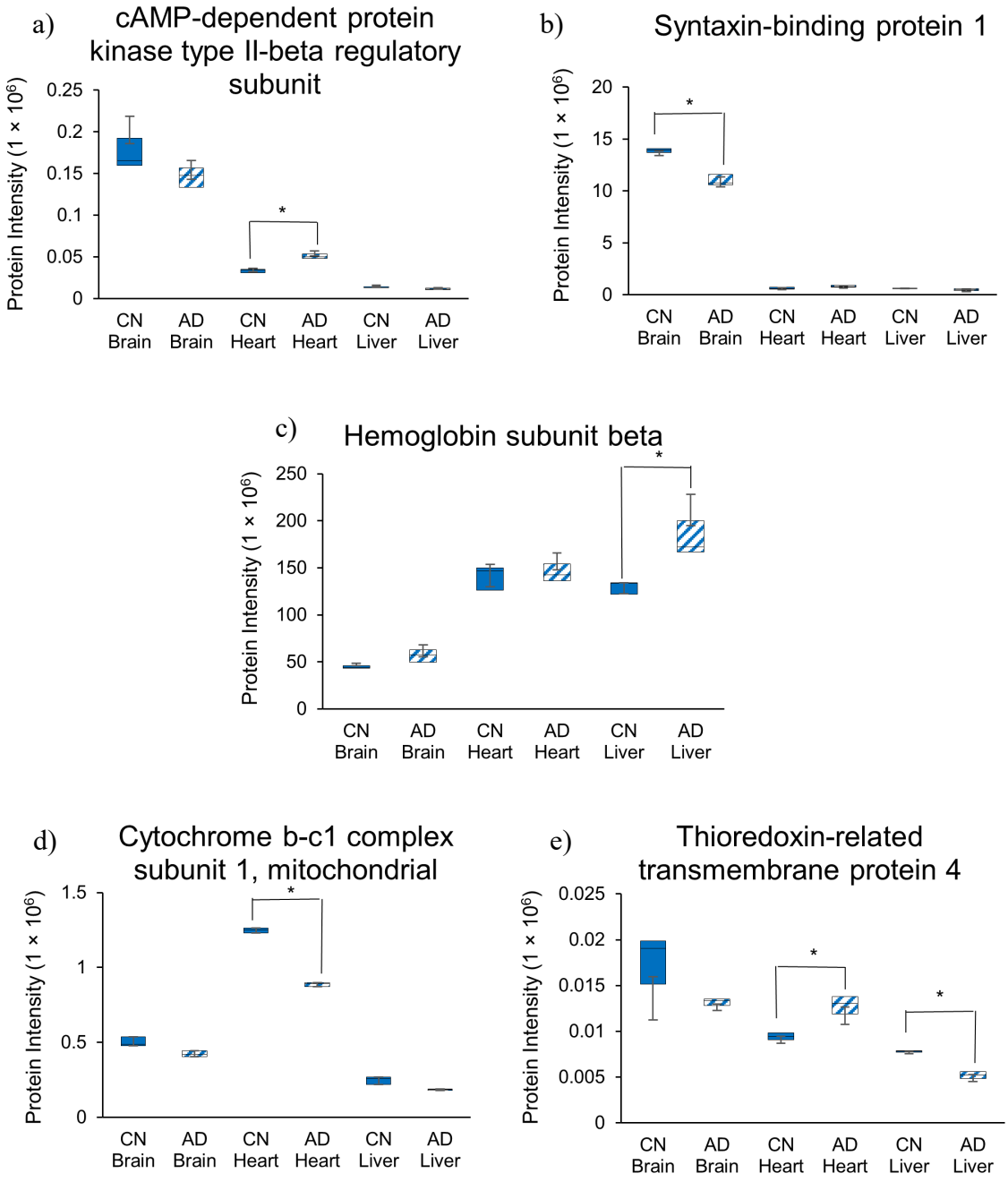

Figure 5.5 Trends of Statistically – Significant Proteins in Brain, Heart, and Liver Tissues. Whisker plots of statistically – significant proteins ($p<0.05$) involved in apoptosis, electron transport, and other processes are compared.

Table 5.3 Differentially – Expressed Proteins in the Brain, Heart, and/or Liver.

Accession	Protein Description (short)	AD/CN Brain	p-value brain	AD/CN Heart	p-value heart	AD/CN Liver	p-value liver
P61981	14-3-3 protein gamma	0.98 ± 0.065	0.84	**1.28 ± 0.20**	**0.038**	0.85 ± 0.20	0.61
Q6NVY1	3-hydroxyisobutyryl-CoA hydrolase, mitochondrial	0.99 ± 0.060	0.97	1.46 ± 1.4	0.50	**0.78 ± 0.089**	**0.020**
P25398	40S ribosomal protein S12	0.95 ± 0.11	0.71	0.99 ± 0.41	0.96	**0.73 ± 0.050**	**0.039**
P08708	40S ribosomal protein S17	1.20 ± 0.39	0.38	1.07 ± 0.59	0.78	**0.70 ± 0.054**	**0.010**
P23396	40S ribosomal protein S3	0.97 ± 0.15	0.79	1.16 ± 0.74	0.76	**0.78 ± 0.060**	**0.013**
P18124	60S ribosomal protein L7	1.02 ± 0.51	0.95	1.13 ± 0.78	0.78	**0.69 ± 0.054**	**0.035**
Q02952	A-kinase anchor protein 12	1.16 ± 0.019	0.46	1.11 ± 0.41	0.56	**0.78 ± 0.15**	**0.042**
P02763	Alpha-1-acid glycoprotein 1	0.85 ± 0.67	0.66	0.90 ± 0.14	0.76	**0.77 ± 0.064**	**0.019**
P01009	Alpha-1-antitrypsin	0.83 ± 0.35	0.67	1.32 ± 0.56	0.49	**0.54 ± 0.082**	**0.0015**
P63010	AP-2 complex subunit beta	0.78 ± 0.25	0.24	1.14 ± 0.49	0.51	**0.78 ± 0.16**	**0.048**
O14617	AP-3 complex subunit delta-1	0.96 ± 0.21	0.82	0.91 ± 0.029	0.64	**0.71 ± 0.069**	**0.022**
O00571	ATP-dependent RNA helicase DDX3X	0.90 ± 0.12	0.30	**1.67 ± 0.39**	**0.0062**	0.52 ± 0.38	0.21
P02730	Band 3 anion transport protein	0.72 ± 0.33	0.28	**1.26 ± 0.16**	**0.033**	1.31 ± 0.35	0.22
O75531	Barrier-to-autointegration factor	0.69 ± 0.34	0.36	1.04 ± 0.68	0.92	**0.63 ± 0.22**	**0.038**
P35613	Basigin	0.93 ± 0.15	0.46	0.83 ± 0.24	0.26	**0.73 ± 0.14**	**0.028**
P19022	Cadherin-2	0.62 ± 0.18	0.21	1.35 ± 0.44	0.12	**0.60 ± 0.18**	**0.020**
O75746	Calcium-binding mitochondrial carrier protein Aralar1	1.10 ± 0.16	0.24	**0.73 ± 0.14**	**0.048**	0.56 ± 0.46	**0.42**
Q9HB71	Calcyclin-binding protein	0.83 ± 0.32	0.46	1.01 ± 0.33	0.98	**0.66 ± 0.16**	**0.019**
P31323	cAMP-dependent protein kinase type II-beta regulatory subunit	0.81 ± 0.25	0.22	**1.56 ± 0.16**	**0.010**	0.82 ± 0.19	0.16
P00918	Carbonic anhydrase 2	**1.33 ± 0.20**	**0.022**	1.13 ± 0.12	0.54	1.25 ± 0.47	0.25
Q9H8G2	Caspase activity and apoptosis inhibitor 1	0.88 ± 0.64	0.80	**1.96 ± 0.94**	**0.031**	1.47 ± 0.88	0.48
P35221	Catenin alpha-1	0.89 ± 0.23	0.68	1.36 ± 0.78	0.29	**0.76 ± 0.087**	**0.030**
Q8N126	Cell adhesion molecule 3	**0.82 ± 0.11**	**0.021**	1.14 ± 3.0	0.85	0.42 ± 0.86	0.19
Q00610	Clathrin heavy chain 1	0.83 ± 0.16	0.10	1.14 ± 0.55	0.56	**0.76 ± 0.16**	**0.045**
P53618	Coatomer subunit beta	0.88 ± 0.30	0.66	1.03 ± 0.38	0.86	**0.70 ± 0.092**	**0.042**
P10643	Complement component C7	0.90 ± 0.58	0.69	0.92 ± 0.50	0.78	**0.57 ± 0.034**	**0.0061**
P31930	Cytochrome b-c1 complex subunit 1, mitochondrial	0.82 ± 0.17	0.11	**0.71 ± 0.034**	**0.00012**	0.77 ± 0.24	0.14
P14927	Cytochrome b-c1 complex subunit 7	0.85 ± 0.20	0.17	**0.76 ± 0.11**	**0.020**	0.63 ± 0.14	0.05
P09669	Cytochrome c oxidase subunit 6C	0.95 ± 0.094	0.45	0.79 ± 0.25	0.18	**0.50 ± 0.066**	**0.032**
P14406	Cytochrome c oxidase subunit 7A2, mitochondrial	0.99 ± 0.36	0.96	0.76 ± 0.17	0.17	**0.66 ± 0.052**	**0.0024**
P15954	Cytochrome c oxidase subunit 7C, mitochondrial	0.86 ± 0.21	0.31	**0.51 ± 0.092**	**0.0094**	0.70 ± 0.21	0.23
P07585	Decorin	0.94 ± 0.63	0.87	**1.70 ± 0.41**	**0.0075**	1.38 ± 0.97	0.49
Q9UI17	Dimethylglycine dehydrogenase, mitochondrial	1.36 ± 1.5	0.61	1.08 ± 1.0	0.82	**0.62 ± 0.086**	**0.013**
P11532	Dystrophin OS	0.60 ± 0.20	0.27	1.18 ± 0.80	0.67	**0.68 ± 0.21**	**0.046**
Q15075	Early endosome antigen 1	1.25 ± 0.64	0.51	1.15 ± 0.68	0.75	**0.45 ± 0.18**	**0.043**
Q6UWR7	Ectonucleotide pyrophosphatase/phosphodiesterase family member	1.09 ± 0.29	0.70	0.78 ± 0.015	0.14	**0.69 ± 0.12**	**0.033**
Q9BY44	Eukaryotic translation initiation factor 2A	0.96 ± 0.37	0.81	0.99 ± 0.79	0.97	**0.61 ± 0.11**	**0.0066**
Q16658	Fascin	0.91 ± 0.24	0.50	1.33 ± 0.66	0.35	**0.79 ± 0.059**	**0.0051**
P30043	Flavin reductase (NADPH)	1.18 ± 0.37	0.23	**1.20 ± 0.14**	**0.034**	1.18 ± 0.11	0.50
P56470	Galectin-4	**1.88 ± 0.24**	**0.029**	1.39 ± 1.6	0.51	1.04 ± 0.92	0.92
Q9UEY8	Gamma-adducin	1.04 ± 0.21	0.81	0.98 ± 0.40	0.91	**0.67 ± 0.061**	**0.0046**
P68871	Hemoglobin subunit beta	1.24 ± 0.23	0.23	1.08 ± 0.38	0.58	**1.49 ± 0.21**	**0.049**
Q5SSJ5	Heterochromatin protein 1-binding protein 3	1.03 ± 0.24	0.81	0.95 ± 0.33	0.78	**0.73 ± 0.10**	**0.010**
Q99729	Heterogeneous nuclear ribonucleoprotein A/B	1.02 ± 0.61	0.94	0.96 ± 0.36	0.85	**0.72 ± 0.085**	**0.034**
O60506	Heterogeneous nuclear ribonucleoprotein Q	0.93 ± 0.11	0.59	0.87 ± 0.58	0.60	**0.71 ± 0.12**	**0.034**
Q9UJM8	Hydroxyacid oxidase 1	1.48 ± 1.9	0.45	0.98 ± 1.1	0.96	**0.66 ± 0.15**	**0.028**
A0A0C4DH68	Immunoglobulin kappa variable 2-24	0.74 ± 0.43	0.41	0.57 ± 0.25	0.08	**0.46 ± 0.16**	**0.0053**
Q14894	Ketimine reductase mu-crystallin	1.07 ± 0.49	0.73	0.58 ± 0.38	0.29	**0.65 ± 0.084**	**0.0012**
Q6P1M0	Long-chain fatty acid transport protein 4	0.90 ± 0.14	0.50	1.33 ± 1.3	0.39	**0.68 ± 0.12**	**0.017**
Q15046	Lysine--tRNA ligase	1.17 ± 0.49	0.38	0.99 ± 0.37	0.96	**0.67 ± 0.14**	**0.020**
P11279	Lysosome-associated membrane glycoprotein 1	1.12 ± 0.12	0.14	1.01 ± 0.35	0.95	**0.77 ± 0.15**	**0.040**
P40926	Malate dehydrogenase, mitochondrial	0.95 ± 0.024	0.25	0.94 ± 0.28	0.68	**0.73 ± 0.15**	**0.031**
P55157	Microsomal triglyceride transfer protein large subunit	1.37 ± 1.17	0.46	1.22 ± 1.6	0.74	**0.79 ± 0.014**	**0.044**
P27816	Microtubule-associated protein 4	0.97 ± 0.21	0.77	1.15 ± 0.38	0.34	**0.67 ± 0.11**	**0.019**
Q9UPY8	Microtubule-associated protein RP/EB family member 3	0.89 ± 0.49	0.59	**0.54 ± 0.094**	**0.034**	0.48 ± 0.40	0.09
Q02978	Mitochondrial 2-oxoglutarate/malate carrier protein	0.90 ± 0.066	0.26	**0.67 ± 0.064**	**0.013**	1.11 ± 0.13	0.68
Q9Y276	Mitochondrial chaperone BCS1	0.98 ± 0.33	0.89	0.96 ± 0.64	0.89	**0.71 ± 0.087**	**0.0059**
Q9NXA8	NAD-dependent protein deacylase sirtuin-5, mitochondrial	0.81 ± 0.31	0.59	0.99 ± 0.72	0.99	**0.60 ± 0.12**	**0.032**
Q6PIU2	Neutral cholesterol ester hydrolase 1	0.88 ± 0.19	0.23	**1.20 ± 0.092**	**0.0064**	0.71 ± 0.25	0.20
Q0ZGT2	Nexilin	1.13 ± 0.60	0.68	0.87 ± 0.16	0.31	**0.71 ± 0.21**	**0.046**
P06748	Nucleophosmin	0.89 ± 0.26	0.66	**1.57 ± 0.37**	**0.035**	0.69 ± 0.31	0.29
P40855	Peroxisomal biogenesis factor 19	1.01 ± 0.21	0.94	1.10 ± 0.69	0.78	**0.71 ± 0.087**	**0.0094**
Q9UPV7	PHD finger protein 24	0.66 ± 0.23	0.23	1.39 ± 1.9	0.63	**0.61 ± 0.19**	**0.042**
O15212	Prefoldin subunit 6	1.20 ± 0.46	0.48	**1.62 ± 0.60**	**0.019**	0.77 ± 0.16	0.38
P07237	Protein disulfide-isomerase	1.31 ± 1.3	0.65	1.07 ± 0.063	0.83	**0.60 ± 0.063**	**0.031**
Q15084	Protein disulfide-isomerase A6	0.91 ± 0.46	0.73	0.96 ± 0.42	0.82	**0.63 ± 0.0090**	**0.021**
Q15404	Ras suppressor protein 1	0.89 ± 0.21	0.43	1.32 ± 0.35	0.09	**0.69 ± 0.16**	**0.015**
Q9H0U4	Ras-related protein Rab-1B	**0.75 ± 0.11**	**0.030**	1.12 ± 0.47	0.65	0.69 ± 0.22	0.075
Q00266	S-adenosylmethionine synthase isoform type-1	1.78 ± 2.5	0.51	1.07 ± 1.0	0.92	**0.65 ± 0.14**	**0.0067**
P67775	Serine/threonine-protein phosphatase 2A catalytic subunit alpha	1.01 ± 0.13	0.94	**0.73 ± 0.070**	**0.025**	0.84 ± 0.075	0.35
Q13813	Spectrin alpha chain, non-erythrocytic 1	0.86 ± 0.23	0.34	1.19 ± 0.44	0.42	**0.70 ± 0.17**	**0.032**
Q01082	Spectrin beta chain, non-erythrocytic 1	0.84 ± 0.19	0.27	1.05 ± 0.27	0.70	**0.72 ± 0.11**	**0.0080**
P63208	S-phase kinase-associated protein 1	0.91 ± 0.13	0.20	1.00 ± 0.36	0.98	**0.68 ± 0.15**	**0.022**
Q9GZT3	SRA stem-loop-interacting RNA-binding protein, mitochondrial	0.69 ± 0.17	0.27	1.09 ± 0.60	0.72	**0.55 ± 0.13**	**0.012**
Q9UJZ1	Stomatin-like protein 2, mitochondrial	1.05 ± 0.34	0.77	**0.79 ± 0.082**	**0.048**	1.18 ± 0.23	0.56
P08247	Synaptophysin	0.85 ± 0.14	0.50	**1.90 ± 0.62**	**0.016**	0.69 ± 0.40	0.31
P61764	Syntaxin-binding protein 1	**0.81 ± 0.054**	**0.014**	1.27 ± 0.69	0.36	0.79 ± 0.29	0.24
Q9Y490	Talin-1	1.06 ± 0.46	0.75	1.00 ± 0.34	1.0	**0.73 ± 0.091**	**0.013**
Q9H1E5	Thioredoxin-related transmembrane protein 4	0.77 ± 0.34	0.26	**1.35 ± 0.19**	**0.048**	**0.68 ± 0.088**	**0.0050**
Q92544	Transmembrane 9 superfamily member 4	0.99 ± 0.41	0.97	1.43 ± 1.0	0.30	**0.67 ± 0.12**	**0.013**
P49755	Transmembrane emp24 domain-containing protein 10	1.05 ± 0.46	0.82	1.40 ± 0.73	0.25	**0.63 ± 0.089**	**0.019**
Q92973	Transportin-1	1.00 ± 0.13	0.98	1.00 ± 0.32	0.99	**0.78 ± 0.13**	**0.028**
P61088	Ubiquitin-conjugating enzyme E2 N	1.01 ± 0.14	0.85	1.02 ± 0.18	0.83	**0.83 ± 0.067**	**0.028**
P61960	Ubiquitin-fold modifier 1	0.85 ± 0.19	0.48	1.19 ± 1.4	0.75	**0.75 ± 0.081**	**0.048**
Q9Y4I1	Unconventional myosin-Va	0.68 ± 0.42	0.33	1.06 ± 0.53	0.75	**0.66 ± 0.23**	**0.046**
P54289	Voltage-dependent calcium channel subunit alpha-2/delta-1	0.86 ± 0.20	0.29	1.07 ± 0.88	0.83	**0.61 ± 0.066**	**0.0058**
O75083	WD repeat-containing protein 1	0.89 ± 0.13	0.47	1.02 ± 0.44	0.95	**0.75 ± 0.17**	**0.048**

*Differentially - expressed proteins have p<0.05 and AD/WT of >1.20 or <0.83 brain, heart, and liver tissues and are in **bold.**

5.3.2 Canonical pathways Associated with Differentially – Expressed Proteins

Differentially – expressed proteins (p value <0.05 and AD/CN >1.2 or <0.83) in the brain (N=5), heart (N=20), and liver (N=62) were searched in IPA to identify significant canonical pathways, molecular functions, and cellular components. As there were few significant brain proteins, no pathways were identified, however, molecular functions related to the cell signaling and interaction, assembly and organization, and survival and death were identified. In the heart (Figure 5.6), the most significant pathways were related to oxidative phosphorylation and mitochondrial dysfunction whereas in the liver (Figure 5.7) pathways related to elongation factor 2 signaling and unfolded protein response were identified. Significant molecular functions across these tissues were related to cell function and protein synthesis, with specific functions related to molecular transport in the heart and RNA damage and repair in the liver. With a relaxed filter (i.e. AD/CN >1.2 or <0.83 only), the pathway mitochondrial dysfunction and molecular function protein synthesis was significant across all tissues. Proteins in the heart and liver, furthermore, had an increase of similar molecular functions, including those related to cell assembly and organization and molecular transport. In addition, this relaxed filter identified 18 proteins related to Alzheimer's disease at higher (e.g. Synaptophysin, STXBP-1, and CAAP-1) or lower (e.g. superoxide dismutase [Mn], mitochondrial, alpha-1 antichymotrypsin, and vacuolar protein sortin-associated protein 35: VPS-35) levels in the heart. In the brain, proteins related to amyloidosis (N=12) were at higher (e.g. gelsolin and microtubule-associated protein 2) or lower (e.g. STXBP-1) levels and in the liver (N=25), proteins (e.g. eukaryotic translation initiation factor 2A, VPS-35, and signal transducer and activator of transcription 3) associated with the same disease (N=25) were mainly at lower levels.

Heart

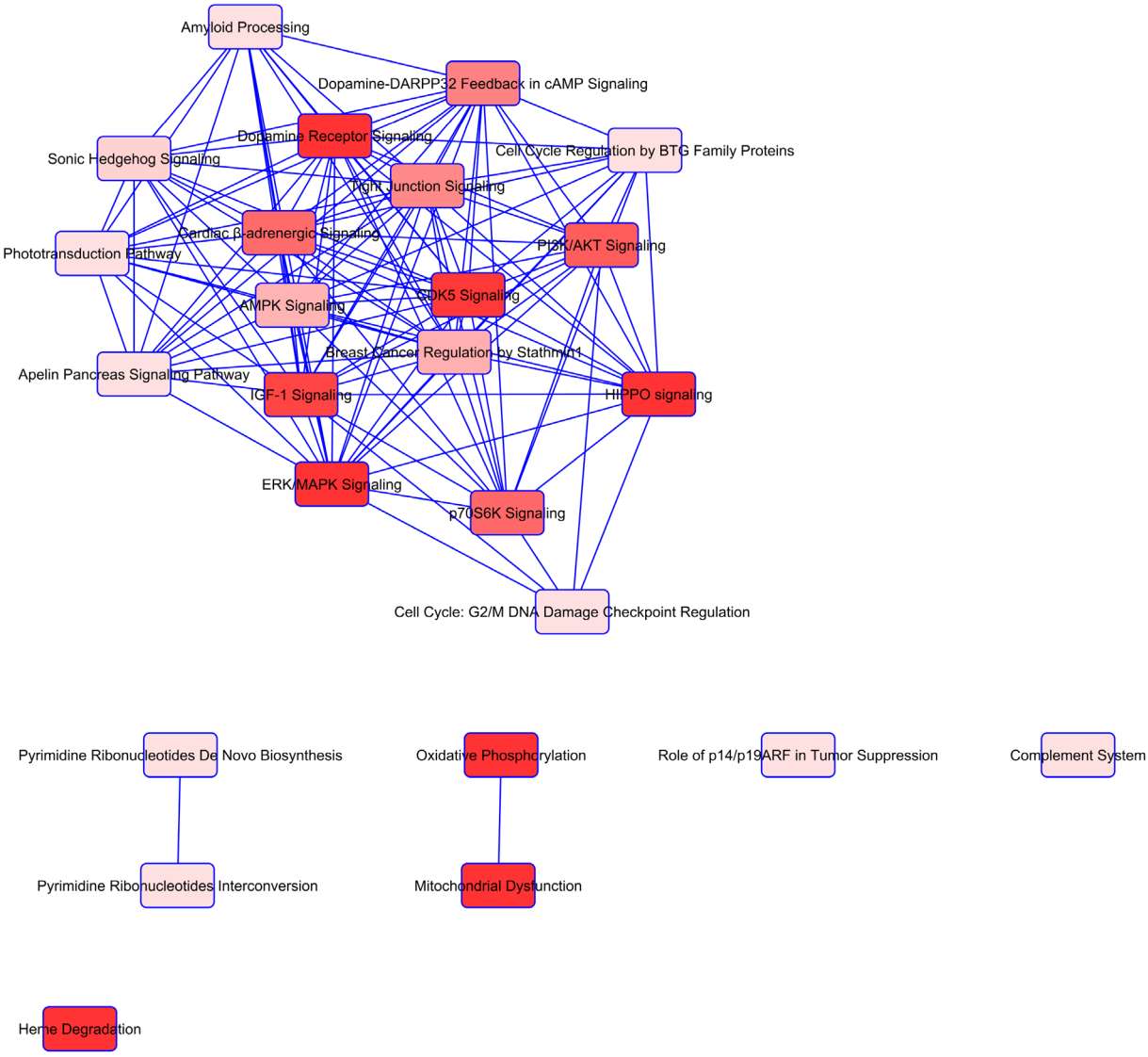

Figure 5.6 Canonical Pathways of Statistically – Significant Heart Proteins.

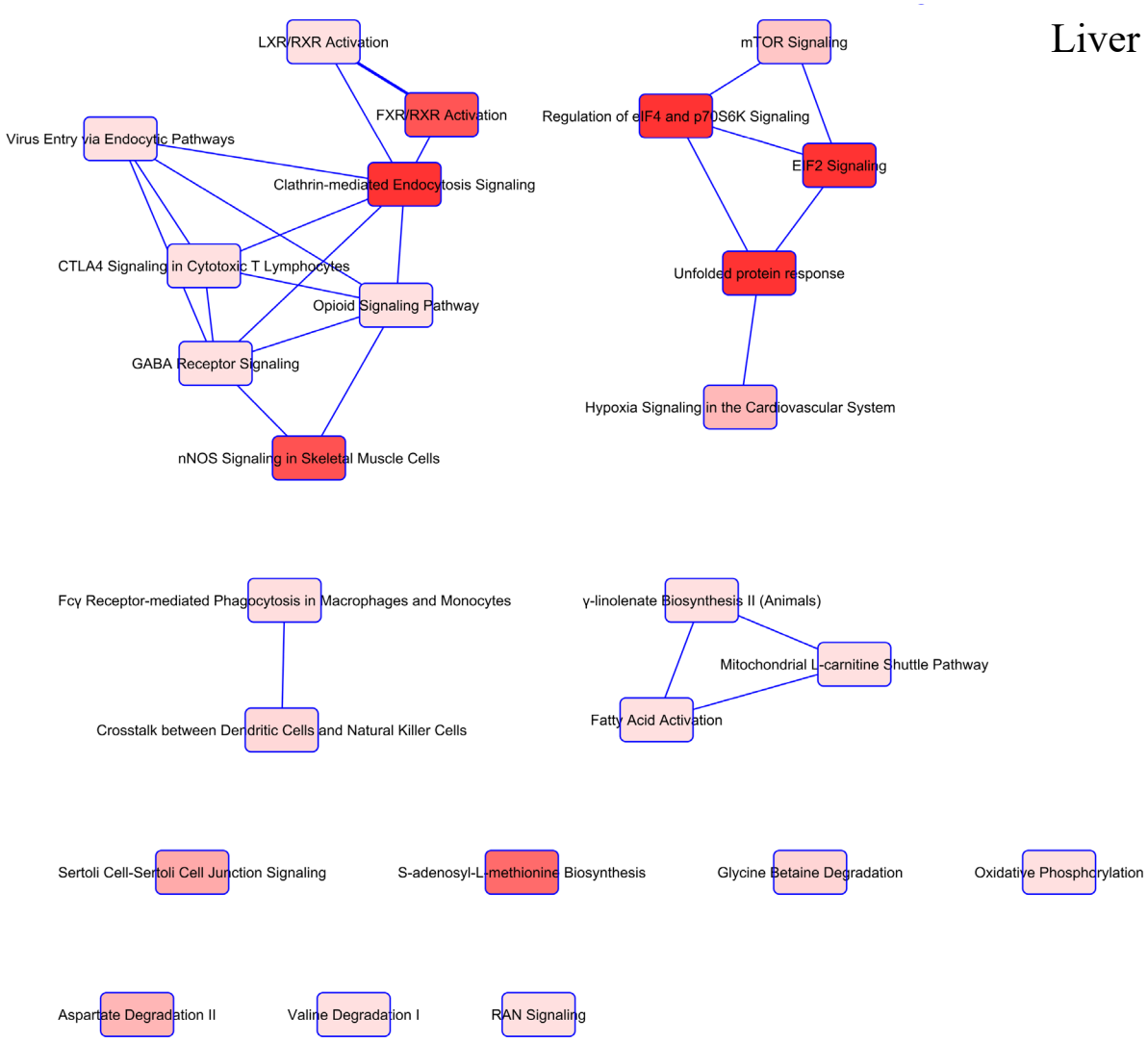

Figure 5.7 Canonical Pathways of Statistically – Significant Liver Proteins.

5.4 DISCUSSION

Recently, we studied AD pathogenesis in brain, heart, and liver tissues in a 14-month-old APP/PS-1 mouse model (**Chapter 4**), in which changes related to energy metabolism were identified across tissues. Biological processes identified from brain and liver proteins overlapped with pathways related to carbohydrate and lipid metabolism, whereas heart proteins were related to protein translation. While that study provided some insight into the contribution of liver and heart peripheral tissues to AD progression, limitations were evident. The APP/PS-1 mouse model is based on early-onset AD, therefore, it does not directly correlate to changes occurring in late-onset AD. This model includes the presence of Aβ plaques, however, it does not have the presence of neurofibrillary tangles. To bridge this gap in understanding, postmortem human brain (superior frontal gyrus), heart, and liver tissues from AD (N=3, Braak stages IV and V) and cognitively normal (CN) controls (N=3) were analyzed using quantitative proteomics. Tissue samples were each from one person, therefore system-wide changes were able to be followed within each individual and across biological replicates. Using cPILOT allowed all samples to be uniquely labeled and subsequently analyzed simultaneously. This reduced potential experimental error and analysis time while increasing sample throughput. In addition, a single analysis allows for direct comparison of all tissues within one experimental analysis therefore, changes occurring across disease state and tissue-type can be compared.

Factors to take into consideration during sample preparation are related to tissue homogenization and protein concentration. Different homogenization times were necessary to extract protein from tissues. Since the heart is a muscular organ, it require additional intervals to fully homogenize. Once samples were homogenized, protein was diluted to perform a protein

concentration assay. As the tissues varied in concentration, dilutions were adjusted in order to successfully determine protein amounts.

5.4.1 Protein Clustering Across Brain, Heart, and Liver Tissues

Proteins that were quantified in all biological replicates and that had an average CV<0.33, were compared to determine similarities across both disease-state and tissue-type. A few notable trends were present across AD and CN tissues, including regions where 1) brain proteins were at lower levels than both the liver and heart (Figure 5.3, zoom-in top), 2) heart proteins were present at higher levels than both the brain and liver (Figure 5.3, middle region), and 3) brain proteins were present at higher levels in comparison to both the liver and heart (Figure 5.3, zoom-in bottom). In the top region, all biological processes were related to metabolism, specifically, catabolic processes involved in glycolysis, the Krebs cycle, amino acid, lipid, and alcohol metabolism. Interestingly proteins involved in translation and protein folding were also grouped together. Ribosomal and other translational proteins are known to decrease in the brain as a function of AD progression and proteins in this group behave similarly.[217-218] Conversely, these levels increased in the heart after disease which may imply that AD progression does not affect the ability of the heart to synthesize proteins. Similar to the top region, proteins in the middle region (*not shown)* were also mainly involved in metabolism with an increase of proteins related to electron transport. Several electron transport proteins (i.e. cytochrome c and cytochrome b) are differentially – expressed in the heart, which has not been previously reported in AD. Dysfunctions in this part of energy metabolism are related to mitochondrial dysfunction.[182, 219] In the bottom region, however, biological processes were

mostly related to transport, localization, and cell function. Transport proteins clathrin heavy chain 1 (CLTC) and vacuolar protein sorting-associated protein-35 (VPS-35) are involved in transporting type-1 transmembrane proteins (e.g. APP and β-site APP cleaving enzyme, BACE) between the cell surface, endosome and trans-golgi network, and are critical to maintaining normal cell function.[174] VPS-35, specifically, is present in the brain at high levels in cognitively normal individuals while declining during AD progression; in this study, VPS-35 was present at levels two times higher in both the heart and the liver of AD, but at slight lower levels in the brain.

5.4.2 Differentially – Expressed Post-Mortem Brain and Peripheral Tissues

In this experiment, samples from the superior frontal gyrus were kindly provided (Banner Sun Health Research Institute), to benchmark changes as a function of disease to heart and liver tissues. In AD, differentially – expressed proteins were related to several types of cellular molecular functions. Rab 1 and syntaxin binding protein 1 are involved in protein transport[174, 220-221] and binding and changed significantly at higher levels in AD. The lack of significant proteins from brain tissues may indicate minor AD pathology in this region during Braak stage IV. SFG has not been reported to change drastically in AD.[222] However, as this region is involved in executive functions, conditions such as frontal temporal dementia (FTD) or frontal variant AD (fvAD) may have elicited a more profound response.[223-225]

In the heart, several proteins related to oxidative phosphorylation, mitochondrial dysfunction, and cell signaling were differentially – expressed. Cytochrome proteins, which are involved in electron transport, were significant at lower levels in AD. Complications in the

electron transport chain are hypothesized to contribute cardiovascular disease[226] and in AD, it may contribute to disease pathogenesis by causing an increase of mitochondrial dysfunction. Transport proteins in the solute carrier family (e.g. SLC4A-1, SLC25A-12, SLC25A-11) changed significantly at higher (SLC4A-1) or lower (SLC25A-12 and SLC25A-11) levels. As protein transport is necessary for protein function and has been noted to be dysregulated in AD, they may contribute to mitochondrial dysfunction.[174] Lastly, proteins involved in apoptosis and immunity, including CAAP-1, dead-box helicase, nucleophosmin, and serine/threonine-protein phosphatase 2A catalytic subunit alpha were differentially – expressed in AD. Dysregulated apoptosis has been implicated in AD.[227] Overall, the identification of significant proteins CAAP-1 and Synaptophysin-1 was especially interesting, as these proteins have been implicated previously in AD pathogenesis.[228-230]

Differentially – expressed liver proteins were related to signaling and unfolded protein response. Some proteins in these pathways included clathrin-related transport proteins alpha-1-acid glycoprotein 1 (ORM-1), alpha-1-antitrypsin (SERPIN-A1), AP-2 complex subunit beta (AP-2B), and CLTC-1, which were at lower levels in AD. Clathrin-mediated endocytosis is involved in transporting transmembrane proteins to and from the endosome and dysregulation has been implicated in AD.[174] Proteins involved in translation or protein folding were also significant at lower levels in liver tissues. As protein synthesis and folding is known to be dysregulated in AD brain pathology, these changes in the liver may be evident of similar patterns present across these tissues.

Across tissues, significant changes were most evident in comparisons of brain vs. heart and brain vs. liver. In both AD and CN tissues, differentially – expressed proteins were mostly involved in transport and localization. In comparison, few proteins changed significantly in liver

vs. heart and were involved in electron transport, carbohydrate metabolism, transport, and protein translation. The lack of significant changes between liver and heart tissues may note similarities between the behavior of these tissues in both AD and healthy states.

5.5 CONCLUSIONS

A comparative analysis across brain, heart, and liver tissues was performed to understand how peripheral liver and heart tissues are involved in AD pathogenesis. In the heart, a decrease of electron transport activity along with an increase of protein binding and apoptosis occurs. In the liver, a decrease of many pathways including translation, protein folding, and transport were present. Though few differentially – expressed proteins overlapped across the tissues, there were similarities in the pathways. A similar trend was also seen in **Chapter 4**, which analyzed a mouse model of AD. In that dataset, most proteins were also only significant in one tissue. When comparing statistically – significant proteins across both organisms, there was minimal overlap. Among the 354 proteins that were quantified in both datasets, several proteins had similar fold-change values in AD compared to WT (mouse) or CN (human), however, the number of differentially – expressed proteins varied. This resulted in statistically – significant proteins only being present in one organism type. In the future, a larger batch of samples will be tested to gain more information about changes in the periphery and validate the findings herein.

6.0 SUMMARY AND FUTURE DIRECTIONS

6.1 SUMMARY

Here, multiplexing techniques have been employed across several organisms to understand aging, infection and Alzheimer's disease (AD). In each analysis, multiplexing was used to analyze several samples simultaneously, thus improving sample throughput by reducing sample analysis time and potential experimental error. In **Chapter 2,** multiplexing efforts allowed for the direct comparison of young and aging adult *Caenorhabditis elegans (C. elegans)* exposed to the opportunistic pathogen *Pseudomonas aeruginosa* (*P. aeruginosa* strain PA01). Each population had unique and shared responses to infection including pathways related to metabolism, development, locomotion and structure. In addition, both *C. elegans* exposed to *P. aeruginosa* PA01 and aging *C. elegans* presented higher levels of oxidative stress. To assess the performance of a higher performing instrument, *C. elegans* samples were ran on an Orbitrap Elite mass spectrometer in **Chapter 3.** Less proteins and peptides were identified from the more advanced instrument (i.e. the Elite) thus leading us to propose that a combination of factors that were not in reference of the instrument, including limited sample and experimental error, may have contributed to a decrease of *C. elegans* proteins identified. In order to analyze >12 samples, a different multiplexing technique, combined precursor isotopic labeling and isobaric tagging (cPILOT) was employed in **Chapter 4,** to understand brain, heart, and liver proteomes from

amyloid precursor protein/presenilin-1 (APP/PS-1) mice. With using both Orbitrap Velos and Fusion Lumos MS platforms, changes heavily involved in metabolism were identified across tissues as a function of disease. In addition, an optimized method to analyze cPILOT samples was developed on the Fusion Lumos, which was also applied in **Chapter 5.** In this chapter, a similar analysis was performed as in **Chapter 4**. Peripheral (i.e. heart and liver) and brain proteomes of AD and cognitively normal (CN) post-mortem tissues were analyzed by using cPILOT. Interestingly, changes related to transport, protein translation and folding, apoptosis and immunity, and metabolism were found to be significant, highlighting ways the periphery may be involved in AD pathogenesis.

Overall, findings from this work highlight the usage of multiplexing and its applications to infection and disease-related biological problems.

6.2 FUTURE DIRECTIONS

Future analyses of cPILOT include studying oxidative modifications. In **Chapter 2**, one of the most defined changes of young- and aging adult *C. elegans* exposed to pathogen was the presence of oxidative stress. Oxidative stress is accompanied by oxidative modifications to proteins, which can impair structure and ultimately protein function. To understand oxidative modifications in *C. elegans*, an *in vivo* oxidation model was applied. Fast photochemical oxidation of proteins (FPOP) is a hydroxyl radical foot printing method that uses a pulsed laser for the photolysis of hydrogen peroxide.[231] This technique irreversibly modifies amino acids and can cross cell membranes. Recently, FPOP has been demonstrated to label cells *in vivo* (IC-

FPOP/IV-FPOP), successfully modifying most (i.e. 16) amino acids.[232-233] In this application, *C. elegans* are labeled by IV-FPOP and is compared to control and *C. elegans* oxidized by hydrogen peroxide (control oxidation). This application requires testing three factors (i.e. FPOP, control oxidation, control) such that an experiment containing three biological replicates and two technical replicates increases the total number of samples for analysis to eighteen. Currently, samples are analyzed individually, which requires extensive sample preparation and analysis time. To increase the throughput of this experiment, *C. elegans* samples labeled by IV-FPOP can be further labeled by cPILOT.

A preliminary proof-of-concept study has been employed to tests the combination of cPILOT and FPOP. Similar to experiments in **Chapters 4 and 5**, protein was extracted from *C. elegans* homogenate and digested with trypsin. Peptides were labeled by light- or heavy dimethylation at the N-terminus and TMT^{10}-plex tags at lysine residues. A pooled sample was fractionated by SCX and analyzed by LC – MS/MS and MS^3 on an Orbitrap Fusion Lumos. Raw data generated was searched in PD and results were analyzed manually to calculate FPOP oxidations. Preliminary data identified over >180,000 PSMs, corresponding to 2682 proteins (Table 6.1). Most lysine terminated light- and heavy-dimethylated peptides were labeled by TMT (i.e. 98%) and >60% of proteins (i.e. 67 and 65%) were quantified in all channels. Additionally, 560 proteins had oxidative modifications, of which 484 proteins (i.e. 86%) were also quantified by cPILOT.

Table 6.1 Protein and Peptide Results of a FPOP-cPILOT Experiment.

	Protein Groups	Protein Groups (10 channels, %)[a]	PSMs ID	R (%)[b]	K (%)[c]	TMT-K (%)[d]
Light DM	2334	1553 (66.5%)	88528	18322 (20.7)	69393 (78.4)	67811 (97.7)
Heavy DM	2193	1426 (65.0%)	92077	17652 (19.2)	73398 (79.7)	71726 (97.7)

[a] The number and percentage of proteins quantified across all reporter ion channels (i.e. 126-131). [b]The number and percentage of peptides ending with arginine. [c]The number and percentage of peptides ending with lysine. [d]The number and percentage of lysine ending peptides labeled with TMT^{10}-plex.

Aspects of this experiment to take into consideration are related to data analysis. As samples are labeled by both FPOP and cPILOT, search parameters have to be adjusted for both sets of modifications. Proteins labeled by FPOP can have several types of oxidative modifications, including carbonylation (+14 Da), oxidation (+16), dioxidation (+32), and trioxidation (+47)[232]; peptides labeled by cPILOT are modified at the N-terminus by light or heavy dimethylation (+28.032 or +36.036/35.070) and at lysine residues by TMT^{10}-plex (+229.163). This results in extended search times (i.e. 12 – 24 h). In order to search efficiently, both sets of parameters were combined into several nodes, thus reducing searching time to (9 – 16 h).

Overall, this proof-of-concept experiment showed that IV-FPOP samples could successfully be labeled by cPILOT. This is advantageous as it allows proteome-wide structural biology to be conducted in this model organism in a high-throughput manner. Future applications (Figure 6.1) include labeling young-adult *C. elegans* exposed to pathogen and wild-type controls with IV-FPOP and multiplexing with cPILOT. As an additional factor (i.e. disease-state) could be added to this experiment and the minimal number of samples could double to 36. This will require at least two cPILOT batches or a 36-plex cPILOT platform. The gain in experimental throughput will be accompanied by an increase in the complexity of sample preparation and data analysis. It will be imperative to handle samples properly and perform labeling of cPILOT samples in intervals to ensure similar labeling times. Once data is searched in PD, result files can be merged into one dataset and data can be analyzed (i.e. data normalization, statistical tests, and bioinformatics analyses). This application and others of cPILOT will show the versatility of this multiplexing strategy and its ability to address a wide variety of biological problems. Moreover,

such an experiment will allow us to better understand the impact of oxidative stress upon exposure to *P. aeruginosa* PA01 infection to *C. elegans.*

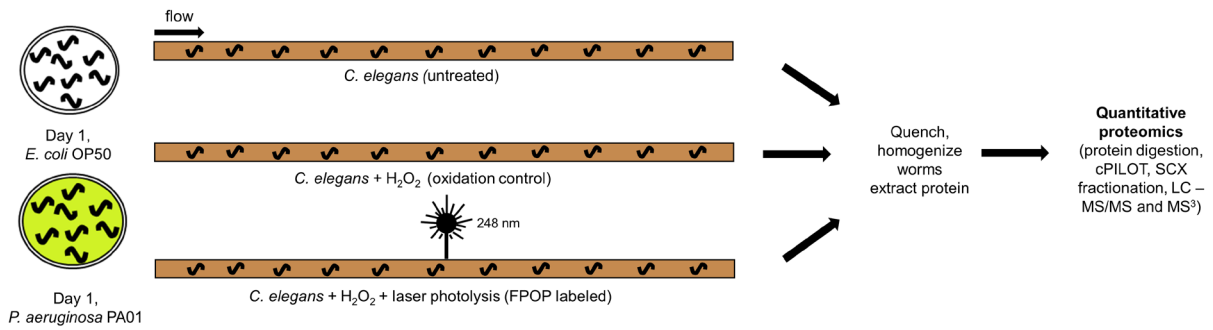

Figure 6.1 Proposed Experimental Workflow of Labeling *C. elegans* with *in vivo* FPOP and cPILOT.

APPENDIX A

Appendix A Table A2.1 Pathogenicity Assays 150

Appendix A Table A2.2 Peptides Identified in *C. elegans* upon *P. aeruginosa* PA01 Exposure by TMT^6……...Attached File

Appendix A Table A2.3 Proteins Identified in *C. elegans* upon *P. aeruginosa* PA01 Exposure by TMT^6……...Attached File

Appendix A Table A2.4 Peptides Identified in *C. elegans* upon *P. aeruginosa* PA01 Exposure by Dimethylation Labeling……...Attached File

Appendix A Table A2.5 Proteins Identified in *C. elegans* upon *P. aeruginosa* PA01 Exposure by Dimethylation Labeling……...Attached File

Appendix A Table A2.6 Proteins Whose Levels are Altered in *C. elegans* upon *P. aeruginosa* PA01 Exposure (Technical Replicates)……Attached File

Appendix A Table A2.7 Biological Processes (GO) of Proteins Whose Levels are Altered in Day 1 Adult *C. elegans* upon *P. aeruginosa* PA01 Exposure……..Attached File

Appendix A Table A2.8 Biological Processes (GO) of Proteins Whose Levels are Altered in Day 5 Adult *C. elegans* upon *P. aeruginosa* PA01 Exposure……..Attached File

Appendix A Table A2.9 Effect of *unc-60* Mutation on N2 Lifespan…….Attached File

Appendix A Table A2.10 Protein Overlap between *C. elegans* Exposed to PA01 vs. Other Pathogens…….Attached File

Appendix A Table A2.1 Pathogenicity Assays

Day 1 (Biological Replicate 1)				
Bacteria	Mean	±SE	n	P-value (vs. OP50)
E. coli OP50	18.5	0.3	65/71	N/A
P. aeruginosa PA01	14.4	0.2	80/84	<0.0001

Day 1 (Biological Replicate 2)				
Bacteria	Mean	±SE	n	P-value (vs. OP50)
E. coli OP50	18.7	0.42	39/44	N/A
P. aeruginosa PA01	11.2	0.58	41/49	0

Day 5 (Biological Replicate 1)				
Bacteria	Mean	±SE	n	P-value (vs. OP50)
E. coli OP50	18.6	0.2	97/108	N/A
P. aeruginosa PA01	10.4	0.08	90/90	<0.0001

Day 5 (Biological Replicate 2)				
Bacteria	Mean	±SE	n	P-value (vs. OP50)
E. coli OP50	21.9	0.65	36/46	N/A
P. aeruginosa PA01	11.7	0.67	37/46	0

APPENDIX B

Appendix B Table B3.1 Peptides Identified in *C. elegans* upon *P. aeruginosa* PA01 Exposure by TMT^6 on an Orbitrap Elite Platform……...Attached File

Appendix B Table B3.2 Proteins Identified in *C. elegans* upon *P. aeruginosa* PA01 Exposure by TMT^6 on an Orbitrap Elite Platform……Attached File

Appendix B Table B3.3 Biological Processes (GO) of Proteins Quantified at Lower Levels in Day 1 Adult C. elegans upon *P. aeruginosa* PA01 Exposure……..Attached File

Appendix B Table B3.4 Biological Processes (GO) of Proteins Quantified at Higher Levels in Day 5 Adult C. elegans upon *P. aeruginosa* PA01 Exposure……..Attached File

Appendix B Table B3.5 Biological Processes (GO) of Proteins Quantified at Lower Levels in Day 5 Adult C. elegans upon *P. aeruginosa* PA01 Exposure……..Attached File

Appendix B Table B3.6 Proteins Quantified in Day 1 and Day 5 Adult C. elegans upon *P. aeruginosa* PA01 Exposure (Velos and Elite)…….Attached File

APPENDIX C

Appendix C Table C4.1 Peptides Identified from Brain, Heart, and Liver Tissues (Batches 1 – 3, 8 Fractions, Orbitrap Velos)…….Attached File

Appendix C Table C4.2 Proteins Identified from Brain, Heart, and Liver Tissues (Batches 1 – 3, 8 Fractions, Orbitrap Velos)…….Attached File

Appendix C Table C4.3 Peptides Identified from Brain, Heart, and Liver Tissues (Batches 1 – 3, 8 Fractions, Fusion Lumos)……..Attached File

Appendix C Table C4.4 Proteins Identified from Brain, Heart, and Liver Tissues (Batches 1 – 3, 8 Fractions, Fusion Lumos)……..Attached File

Appendix C Table C4.5 Peptides Identified from Brain, Heart, and Liver Tissues (Batches 1 – 3, 0 Fractions, Fusion Lumos)……..Attached File

Appendix C Table C4.6 Proteins Identified from Brain, Heart, and Liver Tissues (Batches 1 – 3, 0 Fractions, Fusion Lumos)……..Attached File

Appendix C Table C4.7 Peptides Identified from Brain, Heart, and Liver Tissues (Batches 1 – 3, Combined Experiments)……...Attached File

Appendix C Table C4.8 Proteins Identified from Brain, Heart, and Liver Tissues (Batches 1 – 3, Combined Experiments)……...Attached File

APPENDIX D

Appendix D Table D5.1 Peptides Identified from Brain, Heart, and Liver Tissues...Attached File

Appendix D Table D5.2 Proteins Identified from Brain, Heart, and Liver Tissues...Attached File

REFERENCES

1. King, C. D.; Singh, D.; Holden, K.; Govan, A. B.; Keith, S. A.; Ghazi, A.; Robinson, R. A. S., Proteomic Identification of Virulence-Related Factors in Young and Aging *C. elegans* Infected with *Pseudomonas aeruginosa*. *Journal of Proteomics* **2018,** *181*, 92-103.

2. King, C. D.; Dudenhoeffer, J. D.; Gu, L.; Evans, A. R.; Robinson, R. A. S., Enhanced Sample Multiplexing of Tissues using Combined Precursor Isotopic Labeling and Isobaric Tagging (cPILOT). *Journal of Visualized Experiments* **2017,** (123), 10.3791/55406.

3. Shaw, A. C.; Goldstein, D. R.; Montgomery, R. R., Age-dependent Dysregulation of Innate Immunity. *Nature Reviews. Immunology* **2013,** *13* (12), 875-887.

4. Jagger, A.; Shimojima, Y.; Goronzy, J. J.; Weyand, C. M., Regulatory T Cells and the Immune Aging Process: A Mini-Review. *Gerontology* **2014,** *60* (2), 130-137.

5. Panda, A.; Qian, F.; Mohanty, S.; van Duin, D.; Newman, F. K.; Zhang, L.; Chen, S.; Towle, V.; Belshe, R. B.; Fikrig, E.; Allore, H. G.; Montgomery, R. R.; Shaw, A. C., Age-Associated Decrease in TLR Function in Primary Human Dendritic Cells Predicts Influenza Vaccine Response. *The Journal of Immunology* **2010,** *184* (5), 2518-2527.

6. Fulop, T.; Le Page, A.; Fortin, C.; Witkowski, J. M.; Dupuis, G.; Larbi, A., Cellular Signaling in the Aging Immune System. *Current Opinion in Immunology* **2014,** *29*, 105-111.

7. Hauser, A. R. a. R., J., *Severe Infections caused by Pseudomonas aeruginosa: Perspectives on Critical Care Infectious Disease*. Kluwer Academic Publishers: Norwell, MA, 2003.

8. Powell, J. R.; Ausubel, F. M., Models of *Caenorhabditis elegans* Infection by Bacterial and Fungal Pathogens. In *Innate Immunity*, Ewbank, J.; Vivier, E., Eds. Humana Press: 2008; Vol. 415, pp 403-427.

9. Irazoqui, J. E.; Troemel, E. R.; Feinbaum, R. L.; Luhachack, L. G.; Cezairliyan, B. O.; Ausubel, F. M., Distinct Pathogenesis and Host Responses during Infection of *C. elegans* by *P. aeruginosa* and *S. aureus*. *PLoS Pathog* **2010,** *6*, e1000982.

10. Tan, M.-W.; Rahme, L. G.; Sternberg, J. A.; Tompkins, R. G.; Ausubel, F. M., *Pseudomonas aeruginosa* Killing of *Caenorhabditis elegans* used to Identify *P. aeruginosa* Virulence Factors. *Proceedings of the National Academy of Sciences* **1999,** *96* (5), 2408-2413.

11. Tan, M.-W.; Ausubel, F. M., *Caenorhabditis elegans*: a Model Genetic Host to Study *Pseudomonas aeruginosa* Pathogenesis. *Current Opinion in Microbiology* **2000,** *3* (1), 29-34.

12. Mallo, G. V.; Kurz, C. L.; Couillault, C.; Pujol, N.; Granjeaud, S.; Kohara, Y.; Ewbank, J. J., Inducible Antibacterial Defense System in C. elegans. *Current Biology* **2002,** *12* (14), 1209-1214.

13. Murphy, C. T.; McCarroll, S. A.; Bargmann, C. I.; Fraser, A.; Kamath, R. S.; Ahringer, J.; Li, H.; Kenyon, C., Genes that Act Downstream of DAF-16 to Influence the Lifespan of *Caenorhabditis elegans*. *Nature* **2003,** *424* (6946), 277-283.

14. Troemel, E. R.; Chu, S. W.; Reinke, V.; Lee, S. S.; Ausubel, F. M.; Kim, D. H., p38 MAPK Regulates Expression of Immune Response Genes and Contributes to Longevity in C. elegans *PLOS Genetics* **2006,** *2* (11), e183.

15. Youngman, M. J.; Rogers, Z. N.; Kim, D. H., A Decline in p38 MAPK Signaling Underlies Immunosenescence in *Caenorhabditis elegans*. *PLOS Genetics* **2011,** *7* (5), e1002082.

16. Schulenburg, H.; Kurz, C. L.; Ewbank, J. J., Evolution of the Innate Immune System: The Worm Perspective. *Immunol Rev* **2004,** *198*, 36-58.

17. Tan, M. W.; Mahajan-Miklos, S.; Ausubel, F. M., Killing of *Caenorhabditis elegans* by *Pseudomonas aeruginosa* used to Model Mammalian Bacterial Pathogenesis. *Proceedings of the National Academy of Sciences of the United States of America* **1999,** *96* (2), 715-20.

18. Shapira, M.; Hamlin, B. J.; Rong, J.; Chen, K.; Ronen, M.; Tan, M.-W., A Conserved Role for a GATA Transcription Factor in Regulating Epithelial Innate Immune Responses. *Proceedings of the National Academy of Sciences* **2006,** *103* (38), 14086-14091.

19. Engelmann, I.; Griffon, A.; Tichit, L.; Montañana-Sanchis, F.; Wang, G.; Reinke, V.; Waterston, R. H.; Hillier, L. W.; Ewbank, J. J., A Comprehensive Analysis of Gene Expression Changes Provoked by Bacterial and Fungal Infection in *C. elegans*. *PLoS ONE* **2011,** *6* (5), e19055.

20. Pujol, N.; Zugasti, O.; Wong, D.; Couillault, C.; Kurz, C. L.; Schulenburg, H.; Ewbank, J. J., Anti-Fungal Innate Immunity in *C. elegans* Is Enhanced by Evolutionary Diversification of Antimicrobial Peptides. *PLoS Pathog* **2008,** *4* (7), e1000105.

21. Bolz, D. D., Tenor, J.L., Aballay, A., A Conserved PMK-1/p38 MAPK is Required in *Caenorhabditis elegans* Tissue-Specific Immune Response to *Yersinia pestis* Infection. *Journal of Biological Chemistry* **2010,** *285* (14), 10832-10840.

22. Bogaerts, A.; Beets, I.; Temmerman, L.; Schoofs, L.; Verleyen, P., Proteome Changes of *Caenorhabditis elegans* upon a *Staphylococcus aureus* Infection. *Biol Direct* **2010,** *5*, 11.

23. Simonsen, K. T.; Møller-Jensen, J.; Kristensen, A. R.; Andersen, J. S.; Riddle, D. L.; Kallipolitis, B. H., Quantitative Proteomics Identifies Ferritin in the Innate Immune Response of *C. elegans*. *Virulence* **2011,** *2* (2), 120-130.

24. Durai, S.; Singh, N.; Kundu, S.; Balamurugan, K., Proteomic Investigation of *Vibrio alginolyticus* Challenged *Caenorhabditis elegans* Revealed Regulation of Cellular Homeostasis Proteins and their Role in Supporting Innate Immune System. *PROTEOMICS* **2014,** *14* (15), 1820-1832.

25. Vigneshkumar, B.; Durai, S.; Kundu, S.; Balamurugan, K., Proteome Analysis Reveals Translational Inhibition of *Caenorhabditis elegans* Enhances Susceptibility to *Pseudomonas aeruginosa* PAO1 Pathogenesis. *Journal of Proteomics* **2016**.

26. Treitz, C.; Cassidy, L.; Höckendorf, A.; Leippe, M.; Tholey, A., Quantitative Proteome Analysis of *Caenorhabditis elegans* upon Exposure to Nematicidal *Bacillus thuringiensis*. *Journal of Proteomics* **2015,** *113* (0), 337-350.

27. Association, A. s., 2018 Alzheimer's Disease Facts and Figures. *Alzheimer's & Dementia* **2018,** *14* (3), 367-429.

28. Stampfer, M. J., Cardiovascular Disease and Alzheimer's Disease: Common Links. *Journal of Internal Medicine* **2006,** *260* (3), 211-223.

29. Skoog, I.; Nilsson, L.; Persson, G.; Lernfelt, B.; Landahl, S.; Palmertz, B.; Andreasson, L. A.; Odén, A.; Svanborg, A., 15-year Longitudinal Study of Blood Pressure and Dementia. *The Lancet* **1996,** *347* (9009), 1141-1145.

30. Baglietto-Vargas, D.; Shi, J.; Yaeger, D. M.; Ager, R.; LaFerla, F. M., Diabetes and Alzheimer's Disease Crosstalk. *Neuroscience & Biobehavioral Reviews* **2016,** *64*, 272-287.

31. Valente, T.; Gella, A.; Fernàndez-Busquets, X.; Unzeta, M.; Durany, N., Immunohistochemical Analysis of Human Brain Suggests Pathological Synergism of Alzheimer's Disease and Diabetes Mellitus. *Neurobiology of Disease* **2010,** *37* (1), 67-76.

32. Bomfim, T. R.; Forny-Germano, L.; Sathler, L. B.; Brito-Moreira, J.; Houzel, J.-C.; Decker, H.; Silverman, M. A.; Kazi, H.; Melo, H. M.; McClean, P. L.; Holscher, C.; Arnold, S. E.; Talbot, K.; Klein, W. L.; Munoz, D. P.; Ferreira, S. T.; De Felice, F. G., An Anti-Diabetes Agent Protects the Mouse Brain from Defective Insulin Signaling caused by Alzheimer's Disease–Associated Aβ Oligomers. *The Journal of Clinical Investigation* **2012,** *122* (4), 1339-1353.

33. Zigman, W. B., Atypical Aging in Down Syndrome. *Developmental Disabilities Research Reviews* **2013,** *18* (1), 51-67.

34. Mendez, M. F., Early-Onset Alzheimer Disease. *Neurologic clinics* **2017,** *35* (2), 263-281.

35. Williamson, J.; Goldman, J.; Marder, K. S., Genetic Aspects of Alzheimer Disease. *The neurologist* **2009,** *15* (2), 80-86.

36. Thordardottir, S.; Kinhult Ståhlbom, A.; Almkvist, O.; Thonberg, H.; Eriksdotter, M.; Zetterberg, H.; Blennow, K.; Graff, C., The Effects of Different Familial Alzheimer's Disease Mutations on APP Processing *in vivo*. *Alzheimer's research & therapy* **2017,** *9* (1), 9.

37. Balin, B. J.; Hudson, A. P., Etiology and Pathogenesis of Late-Onset Alzheimer's Disease. *Current Allergy and Asthma Reports* **2014,** *14* (3), 417.

38. Sperling, R. A.; Aisen, P. S.; Beckett, L. A.; Bennett, D. A.; Craft, S.; Fagan, A. M.; Iwatsubo, T.; Jack, C. R.; Kaye, J.; Montine, T. J.; Park, D. C.; Reiman, E. M.; Rowe, C. C.; Siemers, E.; Stern, Y.; Yaffe, K.; Carrillo, M. C.; Thies, B.; Morrison-Bogorad, M.; Wagster, M.

V.; Phelps, C. H., Toward Defining the Preclinical Stages of Alzheimer's Disease: Recommendations from the National Institute on Aging-Alzheimer's Association Workgroups on Diagnostic Guidelines for Alzheimer's Disease. *Alzheimer's & Dementia* **2011,** *7* (3), 280-292.

39. Petersen, R. C.; Smith, G. E.; Waring, S. C.; Ivnik, R. J.; Tangalos, E. G.; Kokmen, E., Mild Cognitive Impairment: Clinical Characterization and Outcome. *Archives of Neurology* **1999,** *56* (3), 303-308.

40. Petersen, R. C., Mild Cognitive Impairment. *Continuum* **2016,** *22* (2), 404-418.

41. Albert, M. S.; DeKosky, S. T.; Dickson, D.; Dubois, B.; Feldman, H. H.; Fox, N. C.; Gamst, A.; Holtzman, D. M.; Jagust, W. J.; Petersen, R. C.; Snyder, P. J.; Carrillo, M. C.; Thies, B.; Phelps, C. H., The Diagnosis of Mild Cognitive Impairment due to Alzheimer's Disease: Recommendations from the National Institute on Aging-Alzheimer's Association Workgroups on Diagnostic Guidelines for Alzheimer's Disease. *Alzheimer's & Dementia* **2011,** *7* (3), 270-279.

42. Mura, T.; Proust-Lima, C.; Jacqmin-Gadda, H.; Akbaraly, T. N.; Touchon, J.; Dubois, B.; Berr, C., Measuring Cognitive Change in Subjects with Prodromal Alzheimer's Disease. *Journal of neurology, neurosurgery, and psychiatry* **2014,** *85* (4), 363-370.

43. Terry, R. D. a.; Davies, P., Dementia of the Alzheimer Type. *Annual Review of Neuroscience* **1980,** *3* (1), 77-95.

44. Rathore, S.; Habes, M.; Iftikhar, M. A.; Shacklett, A.; Davatzikos, C., A Review on Neuroimaging-Based Classification Studies and Associated Feature Extraction Methods for Alzheimer's Disease and its Prodromal Stages. *NeuroImage* **2017,** *155*, 530-548.

45. Vemuri, P.; Jack, C. R., Jr., Role of Structural MRI in Alzheimer's Disease. *Alzheimer's research & therapy* **2010,** *2* (4), 23.

46. Wang, K.; Liang, M.; Wang, L.; Tian, L.; Zhang, X.; Li, K.; Jiang, T., Altered Functional Connectivity in Early Alzheimer's Disease: A Resting-State fMRI Study. *Human Brain Mapping* **2007,** *28* (10), 967-978.

47. Mosconi, L.; Tsui, W. H.; Herholz, K.; Pupi, A.; Drzezga, A.; Lucignani, G.; Reiman, E. M.; Holthoff, V.; Kalbe, E.; Sorbi, S.; Diehl-Schmid, J.; Perneczky, R.; Clerici, F.; Caselli, R.; Beuthien-Baumann, B.; Kurz, A.; Minoshima, S.; de Leon, M. J., Multicenter Standardized 18F-FDG PET Diagnosis of Mild Cognitive Impairment, Alzheimer's Disease, and Other Dementias. *Journal of Nuclear Medicine* **2008,** *49* (3), 390-398.

48. Mosconi, L.; Tsui, W.-H.; De Santi, S.; Li, J.; Rusinek, H.; Convit, A.; Li, Y.; Boppana, M.; de Leon, M. J., Reduced Hippocampal Metabolism in MCI and AD. *Automated FDG-PET image analysis* **2005,** *64* (11), 1860-1867.

49. Chartier-Hariln, M.-C.; Parfitt, M.; Legrain, S.; Pérez-Tur, J.; Brousseau, T.; Evans, A.; Berr, C.; Vldal, O.; Roques, P.; Gourlet, V.; Fruchart, J.-C.; Delacourte, A.; Rossor, M.; Amouyel, P., Apolipoprotein E, ε4 Allele as a Major Risk Factor for Sporadic Early and Late-Onset forms of Alzheimer's Disease: Analysis of the 19q13.2 Chromosomal Region. *Human Molecular Genetics* **1994,** *3* (4), 569-574.

50. Farrer, L. A.; Cupples, L.; Haines, J. L.; et al., Effects of Age, Sex, and Ethnicity on the Association between Apolipoprotein E Genotype and Alzheimer Disease: A Meta-Analysis. *JAMA* **1997,** *278* (16), 1349-1356.

51. Liu, C.-C.; Liu, C.-C.; Kanekiyo, T.; Xu, H.; Bu, G., Apolipoprotein E and Alzheimer Disease: Risk, Mechanisms and Therapy. *Nature reviews. Neurology* **2013,** *9* (2), 106-118.

52. Fenn, J. B.; Mann, M.; Meng, C. K.; Wong, S. F.; Whitehouse, C. M., Electrospray Ionization–Principles and Practice. *Mass Spectrometry Reviews* **1990,** *9* (1), 37-70.

53. Koichi, T.; Hiroaki, W.; Yutaka, I.; Satoshi, A.; Yoshikazu, Y.; Tamio, Y.; T., M., Protein and Polymer Analyses up to m/z 100 000 by Laser Ionization Time-of-Flight Mass Spectrometry. *Rapid Communications in Mass Spectrometry* **1988,** *2* (8), 151-153.

54. Hillenkamp, F.; Karas, M.; Beavis, R. C.; Chait, B. T., Matrix-Assisted Laser Desorption/Ionization Mass Spectrometry of Biopolymers. *Analytical Chemistry* **1991,** *63* (24), 1193A-1203A.

55. Zubarev, R. A.; Horn, D. M.; Fridriksson, E. K.; Kelleher, N. L.; Kruger, N. A.; Lewis, M. A.; Carpenter, B. K.; McLafferty, F. W., Electron Capture Dissociation for Structural Characterization of Multiply Charged Protein Cations. *Analytical Chemistry* **2000,** *72* (3), 563-573.

56. Syka, J. E. P.; Coon, J. J.; Schroeder, M. J.; Shabanowitz, J.; Hunt, D. F., Peptide and Protein Sequence Analysis by Electron Transfer Dissociation Mass Spectrometry. *Proceedings of the National Academy of Sciences of the United States of America* **2004,** *101* (26), 9528.

57. Dongré, A. R.; Somogyi, Á.; Wysocki, V. H., Surface-induced Dissociation: An Effective Tool to Probe Structure, Energetics and Fragmentation Mechanisms of Protonated Peptides. *Journal of Mass Spectrometry* **1996,** *31* (4), 339-350.

58. Yu, Q.; Shi, X.; Feng, Y.; Kent, K. C.; Li, L., Improving Data Quality and Preserving HCD-Generated Reporter Ions with EThcD for Isobaric Tag-Based Quantitative Proteomics and Proteome-Wide PTM Studies. *Analytica Chimica Acta* **2017,** *968*, 40-49.

59. Cooks, R. G., Special Feature: Historical. Collision-Induced Dissociation: Readings and Commentary. *Journal of Mass Spectrometry* **1995,** *30* (9), 1215-1221.

60. Mitchell-Wells, J.; McLuckey, S. A., Collision-Induced Dissociation (CID) of Peptides and Proteins. In *Methods in Enzymology*, Academic Press: 2005; Vol. 402, pp 148-185.

61. Cox, J.; Mann, M., MaxQuant Enables High Peptide Identification rates, individualized p.p.b.-range mass accuracies and proteome-wide protein quantification. *Nature Biotechnology* **2008,** *26*, 1367.

62. MacLean, B.; Tomazela, D. M.; Shulman, N.; Chambers, M.; Finney, G. L.; Frewen, B.; Kern, R.; Tabb, D. L.; Liebler, D. C.; MacCoss, M. J., Skyline: an Open Source Document Editor for Creating and Analyzing Targeted Proteomics Experiments. *Bioinformatics (Oxford, England)* **2010,** *26* (7), 966-968.

63. Chelius, D.; Bondarenko, P. V., Quantitative Profiling of Proteins in Complex Mixtures Using Liquid Chromatography and Mass Spectrometry. *Journal of Proteome Research* **2002,** *1* (4), 317-323.

64. Liu, H.; Sadygov, R. G.; Yates, J. R., A Model for Random Sampling and Estimation of Relative Protein Abundance in Shotgun Proteomics. *Analytical Chemistry* **2004,** *76* (14), 4193-4201.

65. Wang, W.; Zhou, H.; Lin, H.; Roy, S.; Shaler, T. A.; Hill, L. R.; Norton, S.; Kumar, P.; Anderle, M.; Becker, C. H., Quantification of Proteins and Metabolites by Mass Spectrometry without Isotopic Labeling or Spiked Standards. *Analytical Chemistry* **2003,** *75* (18), 4818-4826.

66. Wiener, M. C.; Sachs, J. R.; Deyanova, E. G.; Yates, N. A., Differential Mass Spectrometry: A Label-Free LC−MS Method for Finding Significant Differences in Complex Peptide and Protein Mixtures. *Analytical Chemistry* **2004,** *76* (20), 6085-6096.

67. Griffin, N. M.; Yu, J.; Long, F.; Oh, P.; Shore, S.; Li, Y.; Koziol, J. A.; Schnitzer, J. E., Label-free, Normalized Quantification of Complex Mass Spectrometry Data for Proteomic Analysis. *Nature Biotechnology* **2009,** *28*, 83.

68. Megger, D. A.; Bracht, T.; Meyer, H. E.; Sitek, B., Label-free Quantification in Clinical Proteomics. *Biochimica et Biophysica Acta (BBA)- Proteins and Proteomics* **2013,** *1834* (8), 1581-1590.

69. Li, Z.; Adams, R. M.; Chourey, K.; Hurst, G. B.; Hettich, R. L.; Pan, C., Systematic Comparison of Label-Free, Metabolic Labeling, and Isobaric Chemical Labeling for Quantitative Proteomics on LTQ Orbitrap Velos. *Journal of Proteome Research* **2012,** *11* (3), 1582-1590.

70. Langen, H. F., M.; Evers, S.; Wipf, B.; Berndt, P., In *From Genome to Proteome, 3rd Siena 2D Electrophoresis Meeting*, Wiley-VCH: Weinheim, Germany, Siena, 1998.

71. Ong, S.-E.; Blagoev, B.; Kratchmarova, I.; Kristensen, D. B.; Steen, H.; Pandey, A.; Mann, M., Stable Isotope Labeling by Amino Acids in Cell Culture, SILAC, as a Simple and Accurate Approach to Expression Proteomics. *Molecular & Cellular Proteomics* **2002,** *1* (5), 376-386.

72. Wu, C. C.; MacCoss, M. J.; Howell, K. E.; Matthews, D. E.; Yates, J. R., Metabolic Labeling of Mammalian Organisms with Stable Isotopes for Quantitative Proteomic Analysis. *Analytical Chemistry* **2004,** *76* (17), 4951-4959.

73. Hebert, A. S.; Merrill, A. E.; Bailey, D. J.; Still, A. J.; Westphall, M. S.; Strieter, E. R.; Pagliarini, D. J.; Coon, J. J., Neutron-Encoded Mass Signatures for Multiplexed Proteome Quantification. *Nature Methods* **2013,** *10* (4), 332-334.

74. Merrill, A. E.; Hebert, A. S.; MacGilvray, M. E.; Rose, C. M.; Bailey, D. J.; Bradley, J. C.; Wood, W. W.; El Masri, M.; Westphall, M. S.; Gasch, A. P.; Coon, J. J., NeuCode Labels for Relative Protein Quantification. *Molecular & Cellular Proteomics* **2014,** *13* (9), 2503-2512.

75. Zhang, R.; Sioma, C. S.; Wang, S.; Regnier, F. E., Fractionation of Isotopically Labeled Peptides in Quantitative Proteomics. *Analytical Chemistry* **2001,** *73* (21), 5142-5149.

76. Koehler, C. J.; Arntzen, M. Ø.; de Souza, G. A.; Thiede, B., An Approach for Triplex-Isobaric Peptide Termini Labeling (Triplex-IPTL). *Analytical Chemistry* **2013,** *85* (4), 2478-2485.

77. Thompson, A.; Schäfer, J.; Kuhn, K.; Kienle, S.; Schwarz, J.; Schmidt, G.; Neumann, T.; Hamon, C., Tandem Mass Tags: A Novel Quantification Strategy for Comparative Analysis of Complex Protein Mixtures by MS/MS. *Analytical Chemistry* **2003,** *75* (8), 1895-1904.

78. Ross, P. L.; Huang, Y. N.; Marchese, J. N.; Williamson, B.; Parker, K.; Hattan, S.; Khainovski, N.; Pillai, S.; Dey, S.; Daniels, S.; Purkayastha, S.; Juhasz, P.; Martin, S.; Bartlet-Jones, M.; He, F.; Jacobson, A.; Pappin, D. J., Multiplexed Protein Quantitation in Saccharomyces cerevisiae Using Amine-reactive Isobaric Tagging Reagents. *Molecular & Cellular Proteomics* **2004,** *3* (12), 1154-1169.

79. Xiang, F.; Ye, H.; Chen, R.; Fu, Q.; Li, L., N,N-Dimethyl Leucines as Novel Isobaric Tandem Mass Tags for Quantitative Proteomics and Peptidomics. *Analytical Chemistry* **2010,** *82* (7), 2817-2825.

80. Evans, A. R.; Robinson, R. A. S., Global Combined Precursor Isotopic Labeling and Isobaric Tagging (cPILOT) Approach with Selective MS3 Acquisition. *PROTEOMICS* **2013,** *13* (22), 3267-3272.

81. Goshe, M. B.; Smith, R. D., Stable Isotope-Coded Proteomic Mass Spectrometry. *Current Opinion in Biotechnology* **2003,** *14* (1), 101-109.

82. Filer, C. N., Isotopic Fractionation of Organic Compounds in Chromatography. *Journal of Labelled Compounds and Radiopharmaceuticals* **1999,** *42* (2), 169-197.

83. Robinson, R. A. S.; Evans, A. R., Enhanced Sample Multiplexing for Nitrotyrosine-Modified Proteins Using Combined Precursor Isotopic Labeling and Isobaric Tagging. *Analytical Chemistry* **2012,** *84* (11), 4677-4686.

84. Evans, A. R.; Gu, L.; Guerrero, R.; Robinson, R. A. S., Global cPILOT Analysis of the APP/PS-1 Mouse Liver Proteome. *PROTEOMICS – Clinical Applications* **2015,** *9* (9-10), 872-884.

85. Gu, L.; Evans, A. R.; Robinson, R. A. S., Sample Multiplexing with Cysteine-Selective Approaches: cysDML and cPILOT. *Journal of The American Society for Mass Spectrometry* **2015,** *26* (4), 615-630.

86. Dephoure, N.; Gygi, S. P., Hyperplexing: A Method for Higher-Order Multiplexed Quantitative Proteomics Provides a Map of the Dynamic Response to Rapamycin in Yeast. *Science Signaling* **2012,** *5* (217), rs2-rs2.

87. Braun, C. R.; Bird, G. H.; Wühr, M.; Erickson, B. K.; Rad, R.; Walensky, L. D.; Gygi, S. P.; Haas, W., Generation of Multiple Reporter Ions from a Single Isobaric Reagent Increases Multiplexing Capacity for Quantitative Proteomics. *Analytical Chemistry* **2015,** *87* (19), 9855-9863.

88. Everley, R. A.; Kunz, R. C.; McAllister, F. E.; Gygi, S. P., Increasing Throughput in Targeted Proteomics Assays: 54-Plex Quantitation in a Single Mass Spectrometry Run. *Analytical Chemistry* **2013,** *85* (11), 5340-5346.

89. Gu, L.; Robinson, R. A. S., High-Throughput Endogenous Measurement of S-Nitrosylation in Alzheimer's Disease using Oxidized Cysteine-Selective cPILOT. *Analyst* **2016,** *141* (12), 3904-3915.

90. Gu, L.; Robinson, R. A. S., Proteomic Approaches to Quantify Cysteine Reversible Modifications in Aging and Neurodegenerative Diseases. *Proteomics. Clinical applications* **2016,** *10* (12), 1159-1177.

91. Frost, D. C.; Rust, C. J.; Robinson, R. A. S.; Li, L., Increased N,N-Dimethyl Leucine Isobaric Tag Multiplexing by a Combined Precursor Isotopic Labeling and Isobaric Tagging Approach. *Analytical Chemistry* **2018,** *90* (18), 10664-10669.

92. Shanley, D. P.; Aw, D.; Manley, N. R.; Palmer, D. B., An evolutionary perspective on the mechanisms of immunosenescence. *Trends in Immunology* **2009,** *30* (7), 374-381.

93. Poland, G. A.; Ovsyannikova, I. G.; Kennedy, R. B.; Lambert, N. D.; Kirkland, J. L., A Systems Biology Approach to the Effect of Aging, Immunosenescence and Vaccine Response. *Current Opinion in Immunology* **2014,** *29*, 62-68.

94. West, L. A.; Cole, S.; Goodkind, D.; He, W., 65+ in the United States: 2010. In *Current Population Reports*, Bureau, U. S. C., Ed. U.S. Government Printing Office, 2014; pp 23-212.

95. Larbi, A.; Rymkiewicz, P.; Vasudev, A.; Low, I.; Shadan, N. B.; Mustafah, S.; Ayyadhury, S.; Fulop, T., The Immune System in the Elderly: a Fair Fight against Diseases? *Aging Health* **2013,** *9* (1), 35-47.

96. Lyczak, J. B.; Cannon, C. L.; Pier, G. B., Establishment of *Pseudomonas aeruginosa* Infection: Lessons from a Versatile Opportunist. *Microbes and Infection* **2000,** *2* (9), 1051-1060.

97. Govan, J. R.; Deretic, V., Microbial Pathogenesis in Cystic Fibrosis: Mucoid *Pseudomonas aeruginosa* and *Burkholderia cepacia*. *Microbiological Reviews* **1996,** *60* (3), 539-574.

98. Bendig, J. W.; Kyle, P. W.; Giangrande, P. L.; Samson, D. M.; Azadian, B. S., Two Neutropenic Patients with Multiple Resistant *Pseudomonas aeruginosa* Septicaemia Treated with Ciprofloxacin. *Journal of the Royal Society of Medicine* **1987,** *80* (5), 316-317.

99. Franzetti, F.; Cernuschi, M.; Esposito, R.; Moroni, M., *Pseudomonas* Infections in Patients with AIDS and AIDS-Related Complex. *Journal of Internal Medicine* **1992,** *231* (4), 437-443.

100. Marcia, K.; Atmar, R. L.; Richard, J. H.; Daniel, M. M., Life-Threatening *Pseudomonas aeruginosa* Infections in Patients with Human Immunodeficiency Virus Infection. *Clinical Infectious Diseases* **1992,** *14* (2), 403-411.

101. Guggenbichler, J. P.; Assadian, O.; Boeswald, M.; Kramer, A., Incidence and Clinical Implication of Nosocomial Infections Associated with Implantable Biomaterials - Catheters, Ventilator-Associated Pneumonia, Urinary Tract Infections. *GMS Krankenhaushygiene interdisziplinar* **2011,** *6* (1), Doc18-Doc18.

102. Consortium, T. C. e. S., Genome Sequence of the Nematode C. elegans: A Platform for Investigating Biology. *Science* **1998,** *282* (5396), 2012-2018.

103. Tjahjono, E.; Kirienko, N. V., A Conserved Mitochondrial Surveillance Pathway is Required for Defense against *Pseudomonas aeruginosa*. *PLOS Genetics* **2017,** *13* (6), e1006876.

104. Krijgsveld, J.; Ketting, R. F.; Mahmoudi, T.; Johansen, J.; Artal-Sanz, M.; Verrijzer, C. P.; Plasterk, R. H. A.; Heck, A. J. R., Metabolic Labeling of *C. elegans* and *D. melanogaster* for Quantitative Proteomics. *Nature Biotechnology* **2003,** *21* (8), 927-931.

105. Gouw, J. W.; Tops, B. B. J.; Mortensen, P.; Heck, A. J. R.; Krijgsveld, J., Optimizing Identification and Quantitation of 15N-Labeled Proteins in Comparative Proteomics. *Analytical Chemistry* **2008,** *80* (20), 7796-7803.

106. Frewen, B. E.; Merrihew, G. E.; Wu, C. C.; Noble, W. S.; MacCoss, M. J., Analysis of Peptide MS/MS Spectra from Large-Scale Proteomics Experiments Using Spectrum Libraries. *Analytical Chemistry* **2006,** *78* (16), 5678-5684.

107. Walther, Dirk M.; Kasturi, P.; Zheng, M.; Pinkert, S.; Vecchi, G.; Ciryam, P.; Morimoto, Richard I.; Dobson, Christopher M.; Vendruscolo, M.; Mann, M.; Hartl, F. U., Widespread Proteome Remodeling and Aggregation in Aging C. elegans. *Cell 161* (4), 919-932.

108. Bogaerts, A.; Temmerman, L.; Boerjan, B.; Husson, S. J.; Schoofs, L.; Verleyen, P., A Differential Proteomics Study of *Caenorhabditis elegans* Infected with *Aeromonas hydrophila*. *Developmental & Comparative Immunology* **2010,** *34* (6), 690-698.

109. Dai, L.-L.; Gao, J.-X.; Zou, C.-G.; Ma, Y.-C.; Zhang, K.-Q., *mir-233* Modulates the Unfolded Protein Response in *C. elegans* during *Pseudomonas aeruginosa* Infection. *PLoS Pathog* **2015,** *11* (1), e1004606.

110. Brenner, S., The Genetics of *Caenorhabditis elegans*. *Genetics* **1974,** *77*, 71 - 94.

111. Mahajan-Miklos, S.; Tan, M. W.; Rahme, L. G.; Ausubel, F. M., Molecular Mechanisms of Bacterial Virulence Elucidated using a *Pseudomonas aeruginosa*-*Caenorhabditis elegans* Pathogenesis Model. *Cell* **1999,** *96* (1), 47-56.

112. Keith, S. A.; Amrit, F. R. G.; Ratnappan, R.; Ghazi, A., The *C. elegans* Healthspan and Stress-Resistance Assay Toolkit. *Methods* **2014,** *68* (3), 476-486.

113. Amrit, F. R. G.; Ratnappan, R.; Keith, S. A.; Ghazi, A., The *C. elegans* Lifespan Assay Toolkit. *Methods* **2014,** *68* (3), 465-475.

114. Yang, J.-S.; Nam, H.-J.; Seo, M.; Han, S. K.; Choi, Y.; Nam, H. G.; Lee, S.-J.; Kim, S., OASIS: Online Application for the Survival Analysis of Lifespan Assays Performed in Aging Research. *PLoS ONE* **2011,** *6* (8), e23525.

115. Cao, Z.; Yende, S.; Kellum, J. A.; Angus, D. C.; Robinson, R. A., Proteomics Reveals Age-Related Differences in the Host Immune Response to Sepsis. *Journal of Proteome Research* **2014,** *13* (2), 422-32.

116. Ting, L.; Rad, R.; Gygi, S. P.; Haas, W., MS3 Eliminates Ratio Distortion in Isobaric Multiplexed Quantitative Proteomics. *Nature Methods* **2011,** *8* (11), 937-940.

117. Wenger, C. D.; Lee, M. V.; Hebert, A. S.; McAlister, G. C.; Phanstiel, D. H.; Westphall, M. S.; Coon, J. J., Gas-Phase Purification Enables Accurate, Multiplexed Proteome Quantification with Isobaric Tagging. *Nature Methods* **2011,** *8* (11), 933-935.

118. Lau, H.-T.; Suh, H. W.; Golkowski, M.; Ong, S.-E., Comparing SILAC- and Stable Isotope Dimethyl-Labeling Approaches for Quantitative Proteomics. *Journal of Proteome Research* **2014,** *13* (9), 4164-4174.

119. Szklarczyk, D.; Morris, J. H.; Cook, H.; Kuhn, M.; Wyder, S.; Simonovic, M.; Santos, A.; Doncheva, N. T.; Roth, A.; Bork, P.; Jensen, L. J.; von Mering, C., The STRING Database in 2017: Quality-Controlled Protein–Protein Association Networks, made Broadly Accessible. *Nucleic Acids Research* **2017,** *45* (D1), D362-D368.

120. Goudeau, J.; Aguilaniu, H., Carbonylated Proteins are Eliminated during Reproduction in *C. elegans*. *Aging Cell* **2010,** *9* (6), 991-1003.

121. Ono, K.; Parast, M.; Alberico, C.; Benian, G. M.; Ono, S., Specific Requirement for Two ADF/Cofilin Isoforms in Distinct Actin-Dependent Processes in *Caenorhabditis elegans*. *Journal of Cell Science* **2003,** *116* (10), 2073-2085.

122. Kashyap, L.; Perera, S.; Fisher, A. L., Identification of Novel Genes Involved in Sarcopenia Through RNAi Screening in Caenorhabditis elegans. *The Journals of Gerontology: Series A* **2012,** *67A* (1), 56-65.

123. Melo, Justine A.; Ruvkun, G., Inactivation of Conserved C. elegans Genes Engages Pathogen- and Xenobiotic-Associated Defenses. *Cell* **2012,** *149* (2), 452-466.

124. Sifri, C. D.; Begun, J.; Ausubel, F. M., The Worm has Turned--Microbial Virulence Modeled in *Caenorhabditis elegans*. *Trends Microbiol* **2005,** *13* (3), 119-27.

125. Marsh, K. E. M., R. C., *Caenorhabditis elegans*, a Model Organism for Investigating Immunity. *Applied and Enviromental Microbiology* **2012,** *78* (7), 2075 - 2081.

126. Gruber, J.; Chen, C.-B.; Fong, S.; Ng, L. F.; Teo, E.; Halliwell, B., Caenorhabditis elegans: What We Can and Cannot Learn from Aging Worms. *Antioxidants & Redox Signaling* **2014**.

127. Hauser, A. R. R., J., *Severe Infections caused by Pseudomonas Aeruginosa*. Kluwer Academic Publishers: Norwell, MA, 2003.

128. Gallagher, L. A.; Manoil, C., *Pseudomonas aeruginosa* PAO1 Kills *Caenorhabditis elegans* by Cyanide Poisoning. *Journal of Bacteriology* **2001,** *183* (21), 6207-14.

129. Pessi, G.; Haas, D., Transcriptional Control of the Hydrogen Cyanide Biosynthetic Genes hcnABC by the Anaerobic Regulator ANR and the Quorum-Sensing Regulators LasR and RhlR inPseudomonas aeruginosa. *Journal of Bacteriology* **2000,** *182* (24), 6940-6949.

130. Whiteley, M.; Lee, K. M.; Greenberg, E. P., Identification of Genes Controlled by Quorum Sensing in *Pseudomonas aeruginosa*. *Proceedings of the National Academy of Sciences* **1999,** *96* (24), 13904-13909.

131. Darby, C.; Cosma, C. L.; Thomas, J. H.; Manoil, C., Lethal Paralysis of *Caenorhabditis elegans* by *Pseudomonas aeruginosa Proceedings of the National Academy of Sciences* **1999,** *96* (26), 15202 - 15207.

132. Vigneshkumar, B.; Pandian, S. K.; Balamurugan, K., Regulation of *Caenorhabditis elegans* and *Pseudomonas aeruginosa* Machinery during Interactions. *Arch Microbiol* **2012,** *194* (4), 229-42.

133. Gething, M.-J.; Sambrook, J., Protein Folding in the Cell. *Nature* **1992,** *355* (6355), 33-45.

134. Parsell, D. A.; Lindquist, S., The Function of Heat-Shock Proteins in Stress Tolerance: Degradation and Reactivation of Damaged Proteins. *Annual Review of Genetics* **1993,** *27* (1), 437-496.

135. Morley, J. F.; Morimoto, R. I., Regulation of Longevity in Caenorhabditis elegans by Heat Shock Factor and Molecular Chaperones. *Molecular Biology of the Cell* **2004,** *15* (2), 657-664.

136. Srivastava, P., Roles of Heat-Shock Proteins in Innate and Adaptive Immunity. *Nature Reviews Immunology* **2002,** *2* (3), 185-194.

137. Stewart, G. R.; Young, D. B., Heat-Shock Proteins and the Host–Pathogen Interaction during Bacterial Infection. *Current Opinion in Immunology* **2004,** *16* (4), 506-510.

138. Njemini, R.; Lambert, M.; Demanet, C.; Kooijman, R.; Mets, T., Basal and Infection-Induced Levels of Heat Shock Proteins in Human Aging. *Biogerontology* **2007,** *8* (3), 353-364.

139. Njemini, R.; Lambert, M.; Demanet, C.; Vanden Abeele, M.; Vandebosch, S.; Mets, T., The Induction of Heat Shock Protein 70 in Peripheral Mononuclear Blood Cells in Elderly Patients: a Role for Inflammatory Markers. *Human Immunology* **2003,** *64* (6), 575-585.

140. Njemini, R.; Lambert, M.; Demanet, C.; Mets, T., Elevated Serum Heat-Shock Protein 70 Levels in Patients with Acute Infection: Use of an Optimized Enzyme-Linked Immunosorbent Assay. *Scandinavian Journal of Immunology* **2003,** *58* (6), 664-669.

141. Herndon, L. A.; Schmeissner, P. J.; Dudaronek, J. M.; Brown, P. A.; Listner, K. M.; Sakano, Y.; Paupard, M. C.; Hall, D. H.; Driscoll, M., Stochastic and Genetic Gactors Influence Tissue-Specific Decline in Ageing *C. elegans*. *Nature* **2002,** *419* (6909), 808-814.

142. Ono, S.; Baillie, D. L.; Benian, G. M., UNC-60B, an ADF/Cofilin Family Protein, Is Required for Proper Assembly of Actin into Myofibrils in *Caenorhabditis elegans* Body Wall Muscle. *The Journal of Cell Biology* **1999,** *145* (3), 491-502.

143. Levine, R. L.; Stadtman, E. R., Oxidative Modification of Proteins during Aging. *Experimental Gerontology* **2001,** *36* (9), 1495-1502.

144. Portal-Celhay, C.; Bradley, E.; Blaser, M., Control of Intestinal Bacterial Proliferation in Regulation of Lifespan in *Caenorhabditis elegans*. *BMC Microbiology* **2012,** *12* (1), 49.

145. Chávez, V.; Mohri-Shiomi, A.; Maadani, A.; Vega, L. A.; Garsin, D. A., Oxidative Stress Enzymes Are Required for DAF-16-Mediated Immunity Due to Generation of Reactive Oxygen Species by Caenorhabditis elegans. *Genetics* **2007,** *176* (3), 1567-1577.

146. Minniti, A. N.; Cataldo, R.; Trigo, C.; Vasquez, L.; Mujica, P.; Leighton, F.; Inestrosa, N. C.; Aldunate, R., Methionine Sulfoxide Reductase A Expression is Regulated by the DAF-16/FOXO Pathway in *Caenorhabditis elegans*. *Aging Cell* **2009,** *8* (6), 690-705.

147. King, C. D.; Singh, D.; Holden, K.; Govan, A. B.; Keith, S.; Ghazi, A.; Robinson, R. A. S., Dataset of Proteomics Analysis of Aging *C. elegans* Exposed to *Pseudomonas aeruginosa* Strain PA01. *Data in brief* **2017,** *11*, 245-251.

148. Olsen, J. V.; Schwartz, J. C.; Griep-Raming, J.; Nielsen, M. L.; Damoc, E.; Denisov, E.; Lange, O.; Remes, P.; Taylor, D.; Splendore, M.; Wouters, E. R.; Senko, M.; Makarov, A.; Mann, M.; Horning, S., A Dual Pressure Linear Ion Trap Orbitrap Instrument with Very High Sequencing Speed. *Molecular & Cellular Proteomics* **2009,** *8* (12), 2759-2769.

149. de la Monte, S. M.; Tong, M., Brain Metabolic Dysfunction at the Core of Alzheimer's Disease. *Biochemical pharmacology* **2014,** *88* (4), 548-559.

150. Steen, E.; Terry, B. M.; Rivera, E. J.; Cannon, J. L.; Neely, T. R.; Tavares, R.; Xu, X. J.; Wands, J. R.; de la Monte, S. M., Impaired Insulin and Insulin-Like Growth Factor Expression and Signaling Mechanisms in Alzheimer's Disease--is this Type 3 Diabetes? *Journal of Alzheimer's Disease* **2005,** *7* (1), 63-80.

151. Talbot, K.; Wang, H.-Y.; Kazi, H.; Han, L.-Y.; Bakshi, K. P.; Stucky, A.; Fuino, R. L.; Kawaguchi, K. R.; Samoyedny, A. J.; Wilson, R. S.; Arvanitakis, Z.; Schneider, J. A.; Wolf, B. A.; Bennett, D. A.; Trojanowski, J. Q.; Arnold, S. E., Demonstrated Brain Insulin Resistance in Alzheimer's Disease Patients is Associated with IGF-1 Resistance, IRS-1 Dysregulation, and Cognitive Decline. *The Journal of Clinical Investigation* **2012,** *122* (4), 1316-1338.

152. Furst, A. J.; Rabinovici, G. D.; Rostomian, A. H.; Steed, T.; Alkalay, A.; Racine, C.; Miller, B. L.; Jagust, W. J., Cognition, Glucose Metabolism and Amyloid Burden in Alzheimer's Disease. *Neurobiology of Aging* **2012,** *33* (2), 215-225.

153. Valenti, R.; Pantoni, L.; Markus, H. S., Treatment of Vascular Risk Factors in Patients with a Diagnosis of Alzheimer's Disease: a Systematic Review. *BMC Medicine* **2014,** *12* (1), 160.

154. de Bruijn, R. F.; Ikram, M. A., Cardiovascular Risk Factors and Future Risk of Alzheimer's Disease. *BMC Medicine* **2014,** *12* (1), 130.

155. Attems, J.; Jellinger, K. A., The Overlap between Vascular Disease and Alzheimer's Disease - Lessons from Pathology. *BMC Medicine* **2014,** *12* (1), 206.

156. Savonenko, A.; Xu, G. M.; Melnikova, T.; Morton, J. L.; Gonzales, V.; Wong, M. P. F.; Price, D. L.; Tang, F.; Markowska, A. L.; Borchelt, D. R., Episodic-Like Memory Deficits in the

APPswe/PS1dE9 Mouse Model of Alzheimer's Disease: Relationships to β-amyloid Deposition and Neurotransmitter Abnormalities. *Neurobiology of Disease* **2005,** *18* (3), 602-617.

157. Reaume, A. G.; Howland, D. S.; Trusko, S. P.; Savage, M. J.; Lang, D. M.; Greenberg, B. D.; Siman, R.; Scott, R. W., Enhanced Amyloidogenic Processing of the β-Amyloid Precursor Protein in Gene-targeted Mice Bearing the Swedish Familial Alzheimer's Disease Mutations and a "Humanized" Aβ Sequence. *Journal of Biological Chemistry* **1996,** *271* (38), 23380-23388.

158. Sultana, R.; Robinson, R. A. S.; Di Domenico, F.; Abdul, H. M.; Clair, D. K. S.; Markesbery, W. R.; Cai, J.; Pierce, W. M.; Butterfield, D. A., Proteomic Identification of Specifically Carbonylated Brain Proteins in APPNLh/APPNLh×PS-1P264L/PS-1P264L Human Double Mutant Knock-in Mice Model of Alzheimer Disease as a Gunction of Age. *Journal of Proteomics* **2011,** *74* (11), 2430-2440.

159. Kempf, S. J.; Metaxas, A.; Ibáñez-Vea, M.; Darvesh, S.; Finsen, B.; Larsen, M. R., An Integrated Proteomics Approach Shows Synaptic Plasticity Changes in an APP/PS1 Alzheimer's Mouse Model. *Oncotarget* **2016,** *7* (23), 33627-33648.

160. Völgyi, K.; Badics, K.; Sialana, F. J.; Gulyássy, P.; Udvari, E. B.; Kis, V.; Drahos, L.; Lubec, G.; Kékesi, K. A.; Juhász, G., Early Presymptomatic Changes in the Proteome of Mitochondria-Associated Membrane in the APP/PS1 Mouse Model of Alzheimer's Disease. *Molecular Neurobiology* **2018,** *55* (10), 7839-7857.

161. LaBaer, J.; Ramachandran, N., Protein Microarrays as Tools for Functional Proteomics. *Current Opinion in Chemical Biology* **2005,** *9* (1), 14-19.

162. Ünlü, M.; Morgan, M. E.; Minden, J. S., Difference Gel Electrophoresis. A Single Gel Method for Detecting Changes in Protein Extracts. *ELECTROPHORESIS* **1997,** *18* (11), 2071-2077.

163. Kellermann, J., ICPL—Isotope-Coded Protein Label. In *2D PAGE: Sample Preparation and Fractionation*, Posch, A., Ed. Humana Press: Totowa, NJ, 2008; pp 113-123.

164. Yao, X.; Freas, A.; Ramirez, J.; Demirev, P. A.; Fenselau, C., Proteolytic 18O Labeling for Comparative Proteomics: Model Studies with Two Serotypes of Adenovirus. *Analytical Chemistry* **2001,** *73* (13), 2836-2842.

165. Ghesquiere, B.; Goethals, M.; Van Damme, J.; Staes, A.; Timmerman, E.; Vandekerckhove, J.; Gevaert, K., Improved Tandem Mass Spectrometric Characterization of 3-nitrotyrosine Sites in Peptides. *Rapid Communications in Mass Spectrometry* **2006,** *20* (19), 2885-93.

166. Wiese, S.; Reidegeld, K. A.; Meyer, H. E.; Warscheid, B., Protein Labeling by iTRAQ: A New Tool for Quantitative Mass Spectrometry in Proteome Research. *PROTEOMICS* **2007,** *7* (3), 340-350.

167. McAlister, G. C.; Huttlin, E. L.; Haas, W.; Ting, L.; Jedrychowski, M. P.; Rogers, J. C.; Kuhn, K.; Pike, I.; Grothe, R. A.; Blethrow, J. D.; Gygi, S. P., Increasing the Multiplexing Capacity of TMTs Using Reporter Ion Isotopologues with Isobaric Masses. *Analytical Chemistry* **2012,** *84* (17), 7469-7478.

168. Frost, D. C.; Greer, T.; Li, L., High-Resolution Enabled 12-Plex DiLeu Isobaric Tags for Quantitative Proteomics. *Analytical Chemistry* **2015,** *87* (3), 1646-1654.

169. Senko, M. W.; Remes, P. M.; Canterbury, J. D.; Mathur, R.; Song, Q.; Eliuk, S. M.; Mullen, C.; Earley, L.; Hardman, M.; Blethrow, J. D.; Bui, H.; Specht, A.; Lange, O.; Denisov, E.; Makarov, A.; Horning, S.; Zabrouskov, V., Novel Parallelized Quadrupole/Linear Ion Trap/Orbitrap Tribrid Mass Spectrometer Improving Proteome Coverage and Peptide Identification Rates. *Analytical Chemistry* **2013,** *85* (24), 11710-11714.

170. Eliuk, S.; Makarov, A., Evolution of Orbitrap Mass Spectrometry Instrumentation. *Annual Review of Analytical Chemistry* **2015,** *8* (1), 61-80.

171. McAlister, G. C.; Nusinow, D. P.; Jedrychowski, M. P.; Wühr, M.; Huttlin, E. L.; Erickson, B. K.; Rad, R.; Haas, W.; Gygi, S. P., MultiNotch MS3 Enables Accurate, Sensitive, and Multiplexed Detection of Differential Expression across Cancer Cell Line Proteomes. *Analytical Chemistry* **2014,** *86* (14), 7150-7158.

172. Plubell, D. L.; Wilmarth, P. A.; Zhao, Y.; Fenton, A. M.; Minnier, J.; Reddy, A. P.; Klimek, J.; Yang, X.; David, L. L.; Pamir, N., Extended Multiplexing of Tandem Mass Tags (TMT) Labeling Reveals Age and High Fat Diet Specific Proteome Changes in Mouse Epididymal Adipose Tissue. *Molecular & Cellular Proteomics* **2017,** *16* (5), 873-890.

173. Tyanova, S.; Temu, T.; Sinitcyn, P.; Carlson, A.; Hein, M. Y.; Geiger, T.; Mann, M.; Cox, J., The Perseus Computational Platform for Comprehensive Analysis of (Prote)omics Data. *Nature Methods* **2016,** *13*, 731.

174. Suzuki, T.; Araki, Y.; Yamamoto, T.; Nakaya, T., Trafficking of Alzheimer's Disease–Related Membrane Proteins and Its Participation in Disease Pathogenesis. *The Journal of Biochemistry* **2006,** *139* (6), 949-955.

175. Di Paolo, G.; Kim, T.-W., Linking Lipids to Alzheimer's Disease: Cholesterol and Beyond. *Nature Reviews Neuroscience* **2011,** *12* (5), 284-296.

176. Martins, I. J.; Berger, T.; Sharman, M. J.; Verdile, G.; Fuller, S. J.; Martins, R. N., Cholesterol Metabolism and Transport in the Pathogenesis of Alzheimer's Disease. *Journal of Neurochemistry* **2009,** *111* (6), 1275-1308.

177. Mahley, R. W., Apolipoprotein E: from Cardiovascular Disease to Neurodegenerative Disorders. *Journal of Molecular Medicine* **2016,** *94* (7), 739-746.

178. Poirier, J.; Bertrand, P.; Poirier, J.; Kogan, S.; Gauthier, S.; Poirier, J.; Gauthier, S.; Davignon, J.; Bouthillier, D.; Davignon, J., Apolipoprotein E Polymorphism and Alzheimer's Disease. *The Lancet* **1993,** *342* (8873), 697-699.

179. Kamino, K.; Nagasaka, K.; Imagawa, M.; Yamamoto, H.; Yoneda, H.; Ueki, A.; Kitamura, S.; Namekata, K.; Miki, T.; Ohta, S., Deficiency in Mitochondrial Aldehyde Dehydrogenase Increases the Risk for Late-Onset Alzheimer's Disease in the Japanese Population. *Biochemical and Biophysical Research Communications* **2000,** *273* (1), 192-196.

180. Grünblatt, E.; Riederer, P., Aldehyde Dehydrogenase (ALDH) in Alzheimer's and Parkinson's Disease. *Journal of Neural Transmission* **2016,** *123* (2), 83-90.

181. Taguchi, H.; Planque, S.; Sapparapu, G.; Boivin, S.; Hara, M.; Nishiyama, Y.; Paul, S., Exceptional Amyloid Beta Peptide Hydrolyzing Activity of Nonphysiological Immunoglobulin Variable Domain Scaffolds. *The Journal of biological chemistry* **2008,** *283* (52), 36724-36733.

182. Cadonic, C.; Sabbir, M. G.; Albensi, B. C., Mechanisms of Mitochondrial Dysfunction in Alzheimer's Disease. *Molecular Neurobiology* **2016,** *53* (9), 6078-6090.

183. Chen, Z.; Zhong, C., Decoding Alzheimer's Disease from Perturbed Cerebral Glucose Metabolism: Implications for Diagnostic and Therapeutic Strategies. *Progress in Neurobiology* **2013,** *108*, 21-43.

184. Calsolaro, V.; Edison, P., Alterations in Glucose Metabolism in Alzheimer's Disease. *Recent Patents on Endocrine, Metabolic & Immune Drug Discovery* **2016,** *10* (1), 31-39.

185. Cisternas, P.; Inestrosa, N. C., Brain Glucose Metabolism: Role of Wnt Signaling in the Metabolic Impairment in Alzheimer's Disease. *Neuroscience & Biobehavioral Reviews* **2017,** *80*, 316-328.

186. Grimm, M. O. W.; Rothhaar, T. L.; Hartmann, T., The Role of APP Proteolytic Processing in Lipid Metabolism. *Experimental Brain Research* **2012,** *217* (3), 365-375.

187. Chan, R. B.; Oliveira, T. G.; Cortes, E. P.; Honig, L. S.; Duff, K. E.; Small, S. A.; Wenk, M. R.; Shui, G.; Di Paolo, G., Comparative Lipidomic Analysis of Mouse and Human Brain with Alzheimer Disease. *The Journal of biological chemistry* **2012,** *287* (4), 2678-2688.

188. Steculorum, S. M.; Solas, M.; Brüning, J. C., The Paradox of Neuronal Insulin Action and Resistance in the Development of Aging-Associated Diseases. *Alzheimer's & Dementia* **2014,** *10* (1, Supplement), S3-S11.

189. Neth, B. J.; Craft, S., Insulin Resistance and Alzheimer's Disease: Bioenergetic Linkages. *Frontiers in aging neuroscience* **2017,** *9*, 345-345.

190. Diehl, T.; Mullins, R.; Kapogiannis, D., Insulin Resistance in Alzheimer's Disease. *Translational Research* **2017,** *183*, 26-40.

191. Morris, J. K.; Honea, R. A.; Vidoni, E. D.; Swerdlow, R. H.; Burns, J. M., Is Alzheimer's Disease a Systemic Disease? *Biochimica et biophysica acta* **2014,** *1842* (9), 1340-1349.

192. Tramutola, A.; Abate, G.; Lanzillotta, C.; Triani, F.; Barone, E.; Iavarone, F.; Vincenzoni, F.; Castagnola, M.; Marziano, M.; Memo, M.; Garrafa, E.; Butterfield, D. A.; Perluigi, M.; Di Domenico, F.; Uberti, D., Protein Nitration profile of CD3+ Lymphocytes from Alzheimer Disease Patients: Novel Hints on Immunosenescence and Biomarker Detection. *Free Radical Biology and Medicine* **2018,** *129*, 430-439.

193. Tamaki, C.; Ohtsuki, S.; Iwatsubo, T.; Hashimoto, T.; Yamada, K.; Yabuki, C.; Terasaki, T., Major Involvement of Low-Density Lipoprotein Receptor-Related Protein 1 in the Clearance of Plasma Free Amyloid β-Peptide by the Liver. *Pharmaceutical Research* **2006,** *23* (7), 1407-1416.

194. Sagare, A.; Deane, R.; Bell, R. D.; Johnson, B.; Hamm, K.; Pendu, R.; Marky, A.; Lenting, P. J.; Wu, Z.; Zarcone, T.; Goate, A.; Mayo, K.; Perlmutter, D.; Coma, M.; Zhong, Z.; Zlokovic, B. V., Clearance of Amyloid-Beta by Circulating Lipoprotein Receptors. *Nature medicine* **2007,** *13* (9), 1029-1031.

195. Maarouf, C. L.; Walker, J. E.; Sue, L. I.; Dugger, B. N.; Beach, T. G.; Serrano, G. E., Impaired Hepatic Amyloid-Beta Degradation in Alzheimer's Disease. *PLoS ONE* **2018,** *13* (9), e0203659.

196. Wendell, C. R.; Waldstein, S. R.; Ferrucci, L.; O'Brien, R. J.; Strait, J. B.; Zonderman, A. B., Carotid Atherosclerosis and Prospective Risk of Dementia. *Stroke* **2012,** *43* (12), 3319-3324.

197. Silvestrini, M.; Gobbi, B.; Pasqualetti, P.; Bartolini, M.; Baruffaldi, R.; Lanciotti, C.; Cerqua, R.; Altamura, C.; Provinciali, L.; Vernieri, F., Carotid Atherosclerosis and Cognitive Decline in Patients with Alzheimer's Disease. *Neurobiology of Aging* **2009,** *30* (8), 1177-1183.

198. Vermeer, S. E.; Prins, N. D.; den Heijer, T.; Hofman, A.; Koudstaal, P. J.; Breteler, M. M. B., Silent Brain Infarcts and the Risk of Dementia and Cognitive Decline. *New England Journal of Medicine* **2003,** *348* (13), 1215-1222.

199. Troncoso, J. C.; Zonderman, A. B.; Resnick, S. M.; Crain, B.; Pletnikova, O.; O'Brien, R. J., Effect of Infarcts on Dementia in the Baltimore Longitudinal Study of Aging. *Annals of neurology* **2008,** *64* (2), 168-176.

200. Prins, N. D.; van Dijk, E. J.; den Heijer, T., Cerebral White Matter Lesions and the Risk of Dementia. *Archives of Neurology* **2004,** *61* (10), 1531-1534.

201. Inaba, M.; White, L.; Bell, C.; Chen, R.; Petrovitch, H.; Launer, L.; Abbott, R. D.; Ross, G. W.; Masaki, K., White Matter Lesions on Brain Magnetic Resonance Imaging Scan and 5-

year Cognitive Decline: the Honolulu-Asia Aging study. *Journal of the American Geriatrics Society* **2011,** *59* (8), 1484-1489.

202. de la Torre, J. C., Cardiovascular Risk Factors Promote Brain Hypoperfusion Leading to Cognitive Decline and Dementia. *Cardiovascular psychiatry and neurology* **2012,** *2012*, 367516-367516.

203. Epstein, N. U.; Xie, H.; Ruland, S. D.; Pandey, D. K., Vascular Risk Factors and Cardiovascular Outcomes in the Alzheimer's Disease Neuroimaging Initiative. *American Journal of Alzheimer's Disease & Other Dementias* **2012,** *27* (4), 275-279.

204. Liu, G.; Yao, L.; Liu, J.; Jiang, Y.; Ma, G.; Chen, Z.; Zhao, B.; Li, K., Cardiovascular Disease Contributes to Alzheimer's Disease: Evidence from Large-Scale Genome-Wide Association Studies. *Neurobiology of Aging* **2014,** *35* (4), 786-792.

205. Rosano, C.; Newman, A. B., Cardiovascular Disease and Risk of Alzheimer's Disease. *Neurological Research* **2006,** *28* (6), 612-620.

206. Liao, P.-C.; Yu, L.; Kuo, C.-C.; Lin, C.; Kuo, Y.-M., Proteomics Analysis of Plasma for Potential Biomarkers in the Diagnosis of Alzheimer's Disease. *PROTEOMICS – Clinical Applications* **2007,** *1* (5), 506-512.

207. Dayon, L.; Núñez Galindo, A.; Wojcik, J.; Cominetti, O.; Corthésy, J.; Oikonomidi, A.; Henry, H.; Kussmann, M.; Migliavacca, E.; Severin, I.; Bowman, G. L.; Popp, J., Alzheimer Disease Pathology and the Cerebrospinal Fluid Proteome. *Alzheimer's research & therapy* **2018,** *10* (1), 66.

208. Begcevic, I.; Kosanam, H.; Martínez-Morillo, E.; Dimitromanolakis, A.; Diamandis, P.; Kuzmanov, U.; Hazrati, L.-N.; Diamandis, E. P., Semiquantitative Proteomic Analysis of Human

Hippocampal Tissues from Alzheimer's Disease and Age-Matched Control Brains. *Clinical proteomics* **2013,** *10* (1), 5.

209. Andreev, V. P.; Petyuk, V. A.; Brewer, H. M.; Karpievitch, Y. V.; Xie, F.; Clarke, J.; Camp, D.; Smith, R. D.; Lieberman, A. P.; Albin, R. L.; Nawaz, Z.; El Hokayem, J.; Myers, A. J., Label-Free Quantitative LC-MS Proteomics of Alzheimer's Disease and Normally Aged Human Brains. *Journal of Proteome Research* **2012,** *11* (6), 3053-3067.

210. Lachén-Montes, M.; González-Morales, A.; Zelaya, M. V.; Pérez-Valderrama, E.; Ausín, K.; Ferrer, I.; Fernández-Irigoyen, J.; Santamaría, E., Olfactory Bulb Neuroproteomics Reveals a Chronological Perturbation of Survival Routes and a Disruption of Prohibitin Complex during Alzheimer's Disease Progression. *Scientific reports* **2017,** *7* (1), 9115.

211. Garranzo-Asensio, M.; San Segundo-Acosta, P.; Martínez-Useros, J.; Montero-Calle, A.; Fernández-Aceñero, M. J.; Häggmark-Månberg, A.; Pelaez-Garcia, A.; Villalba, M.; Rabano, A.; Nilsson, P.; Barderas, R., Identification of Prefrontal Cortex Protein Alterations in Alzheimer's Disease. *Oncotarget* **2018,** *9* (13), 10847-10867.

212. Musunuri, S.; Wetterhall, M.; Ingelsson, M.; Lannfelt, L.; Artemenko, K.; Bergquist, J.; Kultima, K.; Shevchenko, G., Quantification of the Brain Proteome in Alzheimer's Disease Using Multiplexed Mass Spectrometry. *Journal of Proteome Research* **2014,** *13* (4), 2056-2068.

213. Cao, Z.; Robinson, R. A. S., Proteome Characterization of Splenocytes from an Aβpp/ps-1 Alzheimer's Disease Model. *PROTEOMICS* **2014,** *14* (2-3), 291-297.

214. Boisgueheneuc, F. d.; Levy, R.; Volle, E.; Seassau, M.; Duffau, H.; Kinkingnehun, S.; Samson, Y.; Zhang, S.; Dubois, B., Functions of the left superior frontal gyrus in humans: a lesion study. *Brain* **2006,** *129* (12), 3315-3328.

215. Hu, S.; Ide, J. S.; Zhang, S.; Li, C.-S. R., The Right Superior Frontal Gyrus and Individual Variation in Proactive Control of Impulsive Response. *The Journal of Neuroscience* **2016,** *36* (50), 12688-12696.

216. Metsalu, T.; Vilo, J., ClustVis: a Web Tool for Visualizing Clustering of Multivariate Data using Principal Component Analysis and Heatmap. *Nucleic Acids Research* **2015,** *43* (W1), W566-W570.

217. Ding, Q.; Markesbery, W. R.; Chen, Q.; Li, F.; Keller, J. N., Ribosome Dysfunction Is an Early Event in Alzheimer's Disease. *The Journal of Neuroscience* **2005,** *25* (40), 9171-9175.

218. Hernández-Ortega, K.; Garcia-Esparcia, P.; Gil, L.; Lucas, J. J.; Ferrer, I., Altered Machinery of Protein Synthesis in Alzheimer's: From the Nucleolus to the Ribosome. *Brain Pathology* **2016,** *26* (5), 593-605.

219. Silva, D. F.; Selfridge, J. E.; Lu, J.; E, L.; Cardoso, S. M.; Swerdlow, R. H., Mitochondrial Abnormalities in Alzheimer's Disease: Possible Targets for Therapeutic Intervention. *Advances in pharmacology (San Diego, Calif.)* **2012,** *64*, 83-126.

220. Novick, P.; Zerial, M., The Diversity of Rab Proteins in Vesicle Transport. *Current Opinion in Cell Biology* **1997,** *9* (4), 496-504.

221. Jiang, S.; Li, Y.; Zhang, X.; Bu, G.; Xu, H.; Zhang, Y.-w., Trafficking Regulation of Proteins in Alzheimer's Disease. *Molecular neurodegeneration* **2014,** *9*, 6.

222. Adriaanse, S. M.; Binnewijzend, M. A. A.; Ossenkoppele, R.; Tijms, B. M.; van der Flier, W. M.; Koene, T.; Smits, L. L.; Wink, A. M.; Scheltens, P.; van Berckel, B. N. M.; Barkhof, F., Widespread disruption of functional brain organization in early-onset Alzheimer's disease. *PLoS ONE* **2014,** *9* (7), e102995.

223. Senanarong, V.; Cummings, J. L.; Fairbanks, L.; Mega, M.; Masterman, D. M.; O'Connor, S. M.; Strickland, T. L., Agitation in Alzheimer's Disease Is a Manifestation of Frontal Lobe Dysfunction. *Dementia and Geriatric Cognitive Disorders* **2004,** *17* (1-2), 14-20.

224. Johnson, J. K.; Head, E.; Kim, R.; Starr, A.; Cotman, C. W., Clinical and Pathological Evidence for a Frontal Variant of Alzheimer Disease. *Archives of Neurology* **1999,** *56* (10), 1233-1239.

225. Woodward, M.; Jacova, C.; Black, S. E.; Kertesz, A.; Mackenzie, I. R.; Feldman, H., Differentiating the Frontal Variant of Alzheimer's Disease. *International Journal of Geriatric Psychiatry* **2010,** *25* (7), 732-738.

226. Casademont, J.; Miró, Ò., Electron Transport Chain Defects in Heart Failure. *Heart Failure Reviews* **2002,** *7* (2), 131-139.

227. Roth, K. A., Caspases, Apoptosis, and Alzheimer Disease: Causation, Correlation, and Confusion. *Journal of Neuropathology & Experimental Neurology* **2001,** *60* (9), 829-838.

228. Tampellini, D.; Capetillo-Zarate, E.; Dumont, M.; Huang, Z.; Yu, F.; Lin, M. T.; Gouras, G. K., Effects of Synaptic Modulation on Beta-Amyloid, Synaptophysin, and Memory Performance in Alzheimer's Disease Transgenic Mice. *The Journal of Neuroscience* **2010,** *30* (43), 14299-14304.

229. Rohn, T. T.; Head, E., Caspases as Therapeutic Targets in Alzheimer's Disease: Is it Time to "Cut" to the Chase? *International journal of clinical and experimental pathology* **2008,** *2* (2), 108-118.

230. Bredesen, D. E., Neurodegeneration in Alzheimer's Disease: Caspases and Synaptic Element Interdependence. *Molecular neurodegeneration* **2009,** *4*, 27-27.

231. Hambly, D. M.; Gross, M. L., Laser Flash Photolysis of Hydrogen Peroxide to Oxidize Protein Solvent-Accessible Residues on the Microsecond Timescale. *Journal of The American Society for Mass Spectrometry* **2005,** *16* (12), 2057-2063.

232. Espino, J. A.; Mali, V. S.; Jones, L. M., In Cell Footprinting Coupled with Mass Spectrometry for the Structural Analysis of Proteins in Live Cells. *Analytical Chemistry* **2015,** *87* (15), 7971-7978.

233. Rinas, A.; Mali, V. S.; Espino, J. A.; Jones, L. M., Development of a Microflow System for In-Cell Footprinting Coupled with Mass Spectrometry. *Analytical Chemistry* **2016,** *88* (20), 10052-10058.